LEACHING OF SECONDARY ZINC OXIDES USING SULPHURIC ACID

by

Catherine Lottering

Thesis presented in partial fulfilment
of the requirements for the Degree

of

MASTER OF ENGINEERING
(EXTRACTIVE METALLURGICAL ENGINEERING)

in the Faculty of Engineering
at Stellenbosch University

Supervisor
Dr Christie Dorfling

March 2016

Declaration

By submitting this thesis electronically, I declare that the entirety of the work contained therein is my own, original work, that I am the sole author thereof (save to the extent explicitly otherwise stated), that reproduction and publication thereof by Stellenbosch University will not infringe any third party rights and that I have not previously in its entirety or in part submitted it for obtaining any qualification.

Date: March 2016

Summary

Located in the south-western Spergebiet region in Namibia, Skorpion Zinc is one of the few mines in the world with an economically viable oxide zinc deposit. The ore is processed in a sulphuric acid atmospheric leaching circuit, followed by solvent extraction and electrowinning. Zinc casting is used to obtain the 99.995% SHG zinc final product.

With Skorpion Zinc's predicted mine closure date of 2017 approaching, the company is investigating various possibilities for maximizing zinc throughput. The possibility of using secondary zinc oxides, such as electric arc furnace dust (EAFD), galvanizing dross and flue dusts was investigated during the course of this project.

This investigation was aimed at determining whether it would be possible to process these oxide sources in conjunction with the feed ore, to make up for the zinc deficit from the pit. To this end, the project had two main goals: determine whether it would be possible to process the various zinc oxide samples provided in Skorpion's plant, and determine the maximum potential feed quantities of the different materials tested to the refinery, from both a production and profitability perspective. Optimum processing conditions for these materials were also briefly investigated.

Leaching test work showed that it would be possible to obtain recoveries in excess of 93% on the EAF dust, 96.9% from the zinc dross and 98% from the flue dust samples in the Skorpion process, using the normal process conditions of 50°C, a pH of between 1.8 and 1.85 and a slurry feed containing 20% solids.

Literature suggested that increasing temperature and decreasing pH would result in faster zinc recovery and potentially better zinc recovery, depending on whether or not equilibrium was attained. To determine the effect of these factors on the zinc recovery and kinetics, a full factorial experimental design for temperature and pH was developed, using temperatures ranging from 40°C to 70°C in increments of 10°C, with pH's ranging from 1.2-2.1 in increments of 0.3. Results from these experiments showed that the system reached equilibrium by the end of the 120 minutes residence. Thus, there was little improvement in overall zinc recovery (less than 5% overall change in recovery across all experimental conditions).

Kinetics of leaching from EAFD seemed unaffected by changes in pH and temperature. Contrary to expectations from literature, all samples seemed to experience slower kinetics at 70°C than at lower temperatures. This may be due to the fact that all reactions occurring in the system were exothermic, and increasing the temperature to this point limited the reaction kinetics. There was little consistency in the pH and temperature trends for the rest of the samples. It was therefore not possible to draw conclusions about the relationship between leaching kinetics, temperature and pH. However, it was clear from these results that it would be possible to process the different samples in the Skorpion refinery, from a technical point of view.

Using the data obtained from the experimental work, a mass balance was performed over the Skorpion refinery. Blends of the different secondaries with the Skorpion ore were tested in ratios of 10, 20, 30, 40 and 50% oxide in this mass balance to determine which secondary source could provide the greatest zinc return, without causing impurity accumulation in the refinery. The results of this

mass balance indicated that, under the normal Skorpion operating conditions, the flue dust would allow for maximal zinc production per annum.

Base case conditions, using only Skorpion ore, allowed for a maximum production of 151 kt/y. EAF dust provided a maximum zinc production of 220 kt/y, using a blend of 20% EAFD with 80% ore. This particular scenario was limited by the maximum feed throughput for the Skorpion refinery (limited to 230 t/h) and experienced no impurity accumulation. Higher ratios of this particular oxide experienced accumulation of copper, magnesium and manganese. Zinc dross zinc production was limited by the amount of nickel in this sample. The maximum zinc production for this particular oxide was at 10% zinc dross, 90% ore blend and resulted in a total zinc production of approximately 183 kt/y. The scenario which resulted in the greatest zinc production involved using zinc fume oxide in a 50:50 blend with Skorpion ore. Although the throughput was limited to a total of 152 t/h feed by the amount of copper contained in the source, the large amount of zinc contained in this sample meant that a total of 495 kt/y of zinc production was theoretically possible from this scenario.

The results of the different mass balance scenarios were used to construct a simplistic financial feasibility model. Considering only zinc contained in the oxide, the profit obtained from the zinc for each of the scenarios was determined. A certain %LME (London Metal Exchange) zinc price for the zinc contained in the oxide sources was assumed to determine the oxide purchase price. The profit for the oxide supplier was calculated, based on this price, and assuming that the supplier would be responsible for covering the cost of transport to site.

Using an assumed oxide price of 20% of LME zinc price for zinc in the oxide, all three samples resulted in a profit for Skorpion, with the total profit increasing as the blending ratios increased. Scaled profit per ton for the zinc produced from each was as follows: EAFD – 28.1, zinc fume – 37 and zinc dross – 32.5. However, at this purchase price, the suppliers experienced losses of 3.2 on the EAFD and 6.8 on the zinc dross, while the zinc fume oxide supplier made a profit of 10.8. Under these conditions, only the zinc fume oxide could feasibly be processed, as it was the only sample which provided a profitable situation for both parties.

Increasing the assumed oxide price to 30% increased the suppliers' profits to 6.6, 20.5 and 3 for the EAFD, zinc fume oxide and zinc dross suppliers respectively. However, this lowered the Skorpion profit to 17.5, 27.1 and 22.5 for the EAFD, zinc fume oxide and dross respectively. This translated to a decrease in profit of 38%, 27% and 31% respectively. Thus, with the highest Skorpion and supplier profit of the three, the zinc fume sample was still the best option for processing.

Opsomming

Skorpion Zinc, geleë in suid westerlike Spergebiet streek in Namibië, is een van die min myne in die wêreld wat ‘n ekonomies lewensvatbare sinkoksied bron besit. Hier word die erts verwerk deur dit in ‘n atmosferiese swaelsuur logingsproses op te los. Daarna word dit verder verwerk deur oplosmiddel ekstraksie, elektroplatering en gieting van die sink om die finale produk van 99.995% suiwer SHG sink te maak.

Met die Skorpion mynsluitingsdatum van 2017 wat nader kom, begin die maatskappy ondersoek instel na moontlike maniere om die sink produksie te vermeerder. Die moontlikheid om sekondêre sinkoksied bronne soos staaloond afval, metaalskuim en skoorsteen stof te gebruik is tydens hierdie projek ondersoek.

Die hoofdoel van hierdie projek was om te bevestig of dit moontlik sou wees om hierdie sekondêre sink bronne saam met die Skorpion erts as voer te gebruik om die sink produksie te vermeerder. Om hierdie doelwit te bereik het die projek uit twee primêre ondersoek bestaan: bepaal of dit moontlik sou wees om die sekondêre sink bronne in die Skorpion aanleg te behandel, en bepaal die maksimum hoeveelhede van die verskillende tipes materiaal wat in die aanleg hanteer kan word – uit beide ’n produksie en ’n finansiële oogpunt. Optimale bedryfstoestande vir hierdie materiaal is ook kortliks ondersoek.

Logingstoetse het getoon dat dit moontlik sal wees om herwinnings van meer as 93% vanaf staaloond afval, 96.9% vanaf metaalskuim en 98% vanaf skoorsteen stof te behaal deur van Skorpion se standaard bedryfstoestande van 50°C, ’n pH van 1.8 tot 1.85 en 20% vastestowwe in die voer gebruik te maak.

Die literatuurstudie het aangetoon dat ’n verhoging in temperatuur en verlaging in pH vinniger logingskinetika en hoër sink herwinning sou teweegbring, indien ewewig nie bereik word nie. Om die effek van temperatuur en pH op die logingsproses te bepaal was ’n volledige eksperimentele skedule opgestel. Temperatuur was volgens hierdie skedule in inkremente van 10°C verhoog vanaf 40°C na 70°C. Die pH was in inkremente van 0.3 verander van 1.2 na 2.1. Resultate van hierdie toetse het bewys dat die proses chemiese ewewig bereik binne die 120 minute eksperimentele tydperk. Dus was daar baie min verandering in die sink herwinning (minder as 5% verandering oor die hele stel toetse).

Kinetika van die loging van staaloond afval het nie gelyk asof dit beïnvloed word deur verandering in temperatuur en pH nie. Al die bronne het stadiger kinetika teen 70°C ervaar, teenoor laer temperature – moontlik as gevolg van die feit dat die reaksies in die stelsel eksotermies was. Daar was nie ’n duidelike verhouding tussen die temperatuur en pH vir die res van die monsters nie. Dus was dit onmoontlik om die verhouding tussen temperatuur, pH en loging vas te stel. Hierdie toetse het wel gewys dat dit uit ’n tegniese oogpunt moontlik is om die drie verskillende bronne in die Skorpion proses te behandel.

Die resultate van die logingstoetse was gebruik om ‘n massabalans uit te voer. Dit massabalans het verskillende mengsels van Skorpion erts en sekondêre sink oksied (mengsels van 10, 20, 30, 40 en 50% oksied) gebruik om te bereken wat die maksimum sink produksie sou wees onder verskillende omstandighede, sonder om enige opeenhoping van onsuiwerhede in die proses te veroorsaak. Hierdie

massabalans resultate het gewys dat die skoorsteen stof die hoogste produksie sou lewer teen die standaard bedryfstoestande in die Skorpion aanleg.

Die basis, met net Skorpion erts, het 151 kt/jaar sink opbrengs gelewer. Die maksimum staaloond afval sink produksie van 220 kt/jaar was bereken deur ’n 20% staaloond afval en 80% erts mengsel te gebruik. In hierdie geval was die produksie beperk deur die aanleg se voer deurset (beperk tot 230 t/uur) en daar was geen opeenhoping van onsuiwerhede in die proses nie. Hoër staaloond afval persentasies het opeenhoping van koper, magnesium en mangaan veroorsaak. Die hoeveelheid nikkel in die metaalskuim het die sink produksie vanaf hierdie bron beperk. Teen ’n 10% metaalskuim, 90% erts mengsel was die maksimum sink produksie vir hierdie bron 183 kt/jaar. Skoorsteen stof in ’n 50:50 mengsel met erts het die maksimum sink produksie veroorsaak. Hierdie situasie was beperk deur die hoeveelheid koper in die skoorsteen stof (152 t/uur voer), maar die hoë sink konsentrasie in hierdie bron het veroorsaak dat sink teen 495kt/jaar geproduseer kan word.

Resultate van die massabalans was gebruik om ’n basiese finansiële studie te doen. Die wins vanaf die sink in die oksied was bepaal vir elkeen van die mengsels in die massabalans. Om die prys vir die oksied te bepaal was ’n aanname van ’n sekere persentasie van die LME sink prys gebruik vir die sink in die oksied. Die verskaffer se wins was bereken, met die aanname dat die verskaffer sou verantwoordelik wees vir die vervoer van die oksied na Skorpion se aanleg.

Teen 20% van die LME sink prys, het Skorpion ’n wins gemaak met al drie oksied bronne: staaloond afval – 28.1, skoorsteen stof – 37 en metaal skuim – 32.5. Die staaloond afval en metaalskuim verskaffers het egter elk een ’n verlies van 3.2 en 6.8 gely, terwyl die skoorsteen stof verskaffer ‘n wins van 10.8 getoon het. Onder hierdie omstandighede was die skoorsteen stof die enigste lonende opsie, aangesien dit die enigste bron was wat vir beide partye ’n wins getoon het.

’n Verhoging van die sink prys in die oksied na 30% het ’n wins vir al drie verskaffers veroorsaak: 6.6 vir die staaloond afval 20.5 vir die skoorsteen stof en 3 vir die metaalskuim. Aan die ander kant het hierdie verandering die Skorpion wins verlaag na 17.5 vir staaloond afval, 27.1 vir skoorsteen stof en 22.5 vir die metaalskuim. Hierdie is ‘n verlaging van 38%, 27% en 31% onderskeidelik. Dus is die skoorsteen stof bron nog steeds die beste, aangesien dit die hoogste wins vir Skorpion voorsien.

Acknowledgements

The author wishes to thank the following individuals and companies for their significant contribution to the completion of this project:

Skorpion Zinc/Namzinc, which provided funding this project and made available all the resources required for completing the technical investigations.

The Skorpion Zinc laboratory operations team for the many long hours spent on performing all the analyses on the samples for this project, over and above their normal plant samples.

Herman Fuls whose knowledge and expertise proved to be invaluable in gaining an understanding of the Skorpion leaching process.

Christie Dorfling for the technical support and guidance provided throughout the course of this project. The insights and guidance you provided were instrumental in the completion of this project.

Table of contents

List of figures

List of tables

1. Introduction and background

1.1. Skorpion Zinc life of mine

For the past 10 years, Skorpion Zinc has managed to achieve its target production each year. However, since the start of the mining project, it was estimated that the existing oxide ore body would be depleted by 2017. As this year approaches, the ore body is being depleted, and it is becoming increasingly difficult to maintain targeted production. Having made a significant capital investment in purchasing the Skorpion refinery and mine, Vedanta Resources Ltd hopes to maintain production levels until mine closure and has considered several options to do so.

One such option is the possibility of processing zinc secondaries, such as EAFD, galvanizer dross and natural state zinc oxide, as alternative sources of zinc oxides. The idea is to blend the remaining Skorpion ore with these secondaries in a ratio that will allow the remaining ore to be processed over a longer time period and ensure good feed grades into the refinery. This will allow the refinery to continue to produce at its maximum capacity, despite lower ore zinc feed to the process.

Since the existing plant is optimized for the processing of the Skorpion ore, which differs significantly from the zinc secondaries in terms of composition and elemental matrices, it was necessary to determine whether the Skorpion refinery would be able to process these sources and produce zinc from them profitably.

To this end, this project aimed to determine whether the existing Skorpion process was capable of recovering zinc from these alternative sources profitably, without causing any problems in the process. The amount of each source that could be fed and the potential zinc production from each had to be determined; so that the potential ore feed reduction could be seen.

Several laboratory-scale leaching tests were performed to determine whether it would be possible to process these alternative sources from a technical point of view. This involved using the typical Skorpion processing conditions. Thereafter, optimization of the process conditions for maximum zinc recovery from the various alternative sources was briefly investigated by varying temperature and pH over a range of set points.

To determine the maximum theoretically achievable zinc production from each source, a high-level mass balance over the Skorpion refinery was necessary. Finally, this project was aimed at determining whether the treatment of these oxides would be financially feasible. Thus, a basic financial model was required, based on the experimental and mass balance results.

1.2. Processing alternative zinc oxides

The key to Skorpion's success in the processing of its oxide ores lies in the solvent extraction (SX) circuit. This circuit lies between the leach-neutralization and electrowinning circuits and serves as a barrier against impurities in PLS, which may be harmful to the electrowinning process. SX also serves as a zinc concentrator, increasing the zinc concentration in solution from 30 g/l to approximately 120 g/l. With electrowinning being so sensitive to impurities, it is vital to ensure that the impurities introduced with the zinc secondaries can be dealt with in the SX circuit.

It is also important to be aware of the behaviour of the impurity elements in the leaching process and the potential effects that these could have on the downstream processes. Since many of the impurities introduced with the zinc secondaries are impurities not commonly associated with zinc ore deposits, it is likely that it will be difficult to predict the behaviour of these impurities in the circuit prior to test work.

1.2.1. Electric arc furnace dust

Currently, many of the steel producers in the world are turning to steel scrap as a source of iron, instead of using iron ore. The steel scrap is molten and then reprocessed into steel. During the melting down of the steel scrap, volatile components fume off and form vapour, which is then condensed as a fine dust in the off-gas cleaning system (Barrett, *et al.*, 1992). This dust is known as Electric Arc Furnace Dust (EAFD).

Temperatures in the electric arc furnace can reach in excess of 1600˚C, allowing the impurity components in the scrap charged to be volatilized. When the vapour generated from the volatilization is cooled, fine particles are formed. These particles are known as EAF dust. With much of the steel scrap nowadays coming from galvanized steel, zinc is one of the major components of the EAFD- present in concentrations between 7 and 40%, depending on how much of the feed scrap is galvanized (Pereira, *et al.*, 2007). This zinc forms part of the vapour phase during the metal fusing process because of its low solubility in molten steel and slag, and because of its high vapour pressure relative to the iron vapour pressure at the steelmaking temperature (Oustadakis, *et al.*, 2010).

On average, between 15 and 20 kg of EAFD is generated for every ton of recycled steel. In addition to zinc, some of the other major volatile components in the charge include lead, cadmium and some of the iron. Due to the presence of heavy metals such as lead and cadmium, EAFD is classified as a hazardous waste, according to the European Waste Catalogue (European Waste Catalogue, 2002), as well as by the United States Environmental Protection Agency (EPA) (Sofilic, *et al.*, 2004), when dangerous substances exceed the threshold concentrations.

This hazardous waste classification makes the disposal process a complex one, as the waste cannot be landfilled. For this reason, there is a drive towards finding methods to reprocess this dust to remove hazardous elements and produce a saleable product. Hydrometallurgical methods have proven to be favourable, since they can be used to separate chemically similar compounds. One method of reprocessing waste products like EAFD is to produce zinc by a leach-solvent extraction-electrowinning process. This processing method requires control of iron dissolution or removal of some of the dissolved iron prior to electrowinning. Skorpion makes use of a neutralization stage to remove excess iron and so, should be capable of handling an EAFD feed.

1.2.2. Zinc dross

Zinc dross is formed during the process of melting zinc ingots to create a zinc bath that is used for hot-dip galvanizing. The dross is a layer of slag that is formed on the surface of the molten zinc and on the inside surfaces of the bath, due to oxidation and entrapment of foreign particles in the molten metal. Due to the lower purity of this slag, it cannot be recycled directly to the furnaces for recovery, and is therefore often treated by alternative pyro- or hydrometallurgical processes. In addition, the high

impurity content prevents this material from being dissolved in acid and directly electrowon, as the zinc electrowinning process is very sensitive to impurities.

This material generally consists of metallic zinc, zinc oxide, zinc chloride, some copper, iron, lead and other impurity elements (in both oxide and metallic forms) (Bahram, *et al.*, 2013). In addition, because aluminium is added to the zinc in the bath for a better galvanized coating, the dross normally contains significant quantities (greater than 0.6%) of this metal. Iron can also form part of this dross (a small amount of iron can be released during the hot galvanizing process, as the steel pieces are dipped in the zinc bath).

The majority of the metallic zinc typically reports to the coarser size fractions, while the fine size fractions normally contain the oxidized metals.

1.2.3. Zinc oxide from smelting furnace fumes

Zinc oxide can be collected as a waste product from smelting activities – most commonly lead and zinc smelters. These fuming furnace zinc oxide powders typically contain large amounts of zinc and lead, along with some other metals such as aluminium and cadmium. These zinc oxides also normally contain large quantities of chlorides and fluorides, which can cause downstream processing issues (Li, *et al.*, 2015).

During the synthetic production of zinc oxide, Jandová, *et al.* (1999) found that it was unlikely that Zn^{2+} was substituted by impurity elements. Instead, the outcomes of this study suggested that impurities in ZnO powder were in the form of their own oxides or spinels. In addition, this study showed that all zinc oxide particles synthesised, regardless of the method used for synthesis, were non-porous, like-spherical particles.

Jandová, *et al.* (1999) found that ZnO powder dissolved easily and rapidly under all experimental conditions tested, including low acid and low temperature conditions.

1.3. Objectives

This project primarily aimed to determine whether it would be possible to process the selected alternative zinc oxide sources in the Skorpion Zinc refinery and how to obtain maximal zinc from blending the ore feed with the alternative zinc oxide sources.

To achieve this primary aim, the following objectives were defined:

- Evaluate the leaching of zinc from different oxide sources at the standard Skorpion plant conditions
- Determine the effect of temperature, pH, particle size and feed slurry density on the leaching performance for each of the oxide sources
- Perform mass balances using the leaching test results and different ore to alternative oxide blends to determine which combination would provide the highest zinc recovery without impurity accumulation
- Perform a preliminary financial assessment for processing of the secondary zinc oxides

1.4. Research approach

First, leaching experimental work was performed in the laboratory to determine possible recoveries obtainable from the various oxides sources under the normal Skorpion operating conditions of 50 ˚C and a pH of 1.8-1.85 with a slurry feed of 20% solids and an 80% passing particle size of 180 microns. Next, optimization of the leaching of each of these sources was investigated by varying the temperature and pH according to a full factorial design. The effects of feed slurry density and particle size were also briefly investigated.

Hereafter, a basic mass balance on the Skorpion refinery process was used to determine the maximum obtainable zinc production for different blends of secondary oxides with Skorpion's ore. This was done by determining the maximum amount of a particular source that could be fed, within Skorpion's maximum design throughput range, without impurity accumulation occurring.

These sets of results were then used for a concept study for how to feed the oxides to the refinery. Based on this concept study, a basic financial feasibility model was constructed and is briefly discussed.

2. Literature review

2.1. Skorpion Zinc process overview

The Skorpion Zinc process to produce SHG zinc consists of three major steps. These steps include atmospheric leach, solvent extraction and electrowinning processes (Gnoinski, 2007). Figure 1 shows an overview of the Skorpion process, as given by Gnoinski (2007).

Skorpion's oxide zinc ore is produced from an open pit mine and is dissolved in sulphuric acid, in the leaching section. This produces Pregnant Liquor Solution (PLS), containing approximately 30 g/l zinc and high impurity concentrations. For this reason, the leaching step is followed by a neutralization step, where the pH is raised to 4 by adding calcium carbonate. This allows agglomeration and precipitation of some of the major impurities, such as iron, aluminium and silica (Gnoinski, 2007).

Atmospheric leaching of the Skorpion ore takes place in a continuous operation consisting of five agitated leaching tanks arranged in series (Gnoinski, 2007). Slurry from the ball mill flows into the first tank, where it is mixed with raffinate from the solvent extraction (SX) section. A small amount of pure acid is then added to adjust the pH to the level set for this tank.

Residence time across the leaching section is approximately 2 hours, and as the slurry flows into each subsequent leach tank, raffinate and pure acid are added to adjust the pH to the desired level. Temperature is controlled in each tank at approximately 50˚C and the final pH at the end of the leaching section is maintained between 1.8 and 2 to maximise colloidal silica stability (Gnoinski, 2007). pH is progressively lowered over the course of the leaching step, as rapid pH decrease also enhances the risk of colloidal silica formation. Table 1 shows the operating parameters in the Skorpion leaching section.

Table 1. Operating conditions in Skorpion Zinc leaching circuit.

Temperature (°C)	pH range	Residence time (h)	% Solids	D80 Passing (µm)
50	1.8-2	2	20	180

Formation of colloidal silica is caused by a dehydration reaction and is irreversible (Gnoinski, 2007):

$$nSi(OH)_4 \rightarrow (SiO(OH)_2)n.H_2O + (n-1)H_2O \qquad \text{Reaction 1}$$

Colloidal silica can cause major problems in the solvent extraction step, since the dissolved siliceous species (in the form of monosilicic acid ($Si(OH)_4$) do not precipitate in the neutralization step. These species then tend to polymerize to form colloidal silica. Colloidal silica has a massive surface area, but the polymers are small enough that they remain unaffected by gravity (Gnoinski, 2007). Thus, the siliceous polymers do not settle out of solution during the solvent extraction step, but rather form silica gel in the organic phase, which inhibits separation of the organic and aqueous phases. The main leaching reactions taking place in the leaching section are as follows (Gnoinski, 2007):

$$ZnO.SiO_2 + H_2SO_4 + H_2O \rightarrow ZnSO_4 + H_4SiO_4 \qquad \text{Reaction 2}$$
$$Zn_2SiO_4 + 2H_2SO_4 \rightarrow 2ZnSO_4 + Si(OH)_4 \qquad \text{Reaction 3}$$
$$Zn_4Si_2O_7(OH)_2.H_2O + 4H_2SO_4 \rightarrow 4ZnSO_4 + 2Si(OH)_4 + 2H_2O \qquad \text{Reaction 4}$$

Solvent extraction is employed to increase the zinc tenor, enabling electrowinning, as well as to remove many of the impurities in the PLS. Removal of the dissolved halides from the solution is of key interest in this section (Gnoinski, 2007). These impurities cause major corrosion of the lead anodes used in the electrowinning section of the process. Anode dissolution causes high lead levels in the electrolyte solution, which causes the lead concentration in the plated zinc to exceed the desired limit.

During solvent extraction, the aqueous PLS is contacted with the organic solvent di-2-ethyl hexyl phosphoric acid (D2EHPA) at 40˚C (Gnoinski, 2007). D2EHPA is dissolved in a 40:60 ratio in ESCAID 100, a kerosene diluent. Extraction, the first stage of the solvent extraction process, involves extracting the zinc (along with some of the impurities) by cationic substitution (Reaction 5) from the PLS into the organic phase (Gnoinski, 2007). Extraction takes place over 3 stages and operates at an O/A ratio of between 1 and 1.5. Raffinate is the aqueous product of the extraction step.

$$Zn^{2+}{}_{(aq)} + 2RH_{(org)} \rightarrow 2H^{+}{}_{(aq)} + ZnR_{2\,(org)}$$ **Reaction 5**

The reverse of this reaction takes place during the stripping stage, where zinc is stripped from the organic phase into the aqueous spent electrolyte from cell house. This stage produces loaded electrolyte for use in the electrowinning circuit.

Impurities are also extracted by the organic. The selectivity of the organic with increasing pH is as follows: Fe(III)<Zn<Ca<Al(III)<Mn<Cd~Cu<Mg<Co<Ni (Gnoinski, 2007).

Between the extraction and the stripping stages, impurities are removed from the organic by a washing stage. This involves both physical washing, with demineralised water, and chemical washing, with spent electrolyte. Physical washing removes impurities that may have been carried over into the organic by PLS entrainment in the organic. Chemical washing, on the other hand will remove impurities that were co-extracted by the organic (Gnoinski, 2007).

Iron and aluminium are co-extracted with the zinc but, unlike the other impurities, are not easily stripped off the organic. A 6 M HCl solution is used to strip the iron and aluminium off a small bleed stream of organic, so that the organic is regenerated (Gnoinski, 2007).

Finally, the loaded electrolyte from the SX section can be passed to the electrowinning section, where zinc is electroplated onto aluminium cathodes according to Reaction 6 (Gnoinski, 2007):

$$2Zn^{2+} + 2H_2O \rightarrow 2Zn + 4H^{+} + O_2$$ **Reaction 6**

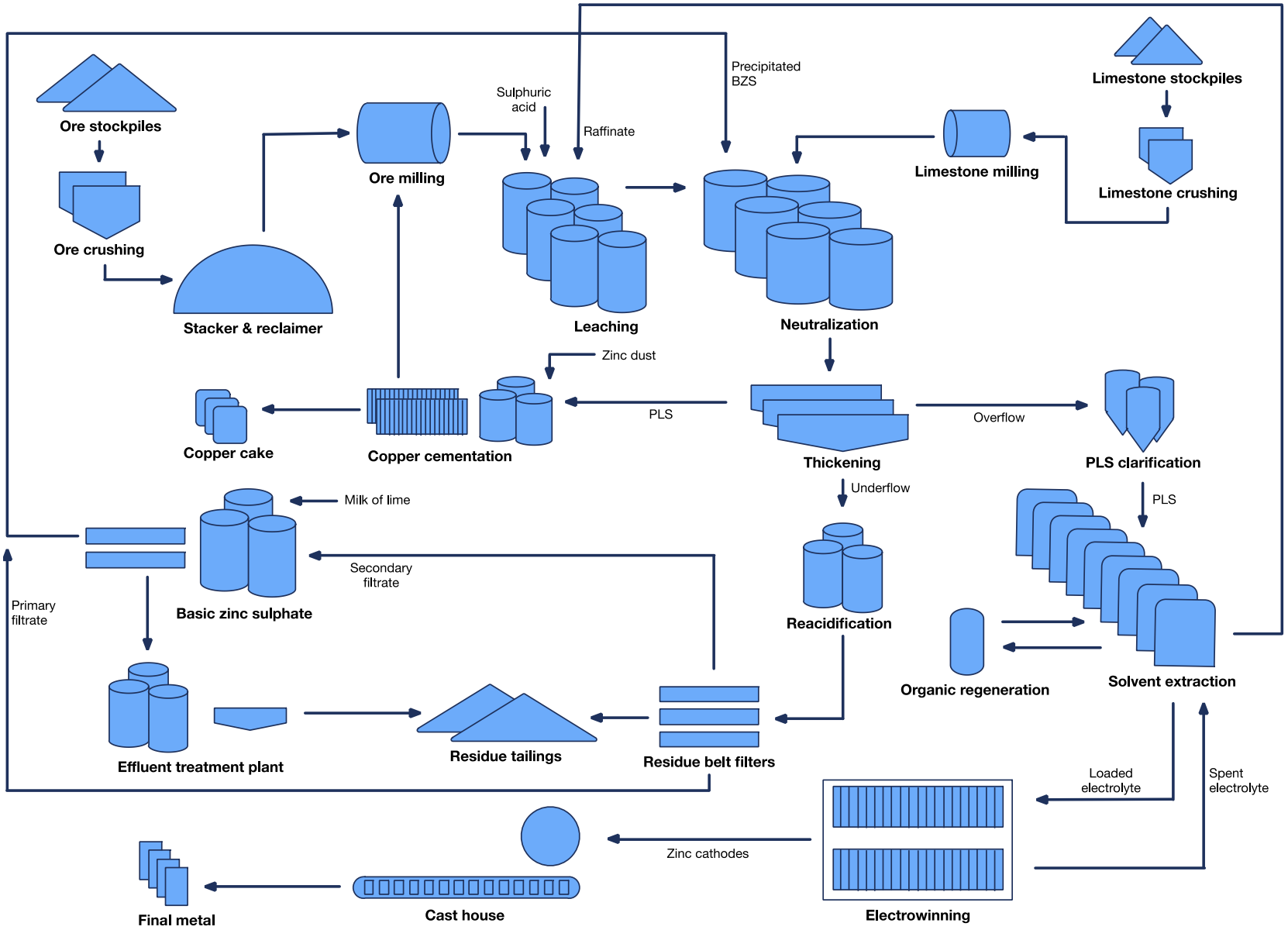

2.2. Leaching theory

In general, the study of a leaching system will involve investigating the best lixiviant for the specific purpose and the best type of operation (batch, continuous, counter-current, co-current, etc.). However, in the current study, modifications are being made to an existing leaching process. Since sulphuric acid has been determined to be the best lixiviant for the Skorpion ore and all equipment has been designed around the continuous co-current operation of the leaching section, these factors will not be investigated. Making modifications to the design parameters of the leaching equipment would require capital investments that would be excessive.

2.2.1. Leaching description

Leaching can be defined as the process by which a certain valuable soluble fraction is removed from the solid phase with which it is associated, into a solution (Green and Perry, 2008). Thus, leaching aims at removing the component of interest from the solid phase particle into the solution, which can then be used for further processing.

The solid phase must be insoluble and is generally permeable, most often in the form of a particle with a porous surface or permeable cell walls (Green and Perry, 2008). This allows the leachant to enter into the particle, increasing the chemical reaction surface area. Selective dissolution is key to the leaching process, while diffusion may or may not be involved.

Several leaching mechanisms exist. In general, leaching can take place by one of two general types of mechanisms. The first of these types is merely a result of the solubility of the desired solid substance in a liquid. Chemical reactions are involved in the second type of leaching (Green and Perry, 2008).

There are several factors which influence the rate at which leaching takes place. These factors may include the chemical reaction rate (which is, in turn, influenced by a number of factors), the rate at which the solvent is transported to the site at which the substance of interest is located, the rate at which the substance of interest is leached into the solvent, and interfacial resistance (Green and Perry, 2008), to name but a few.

Leaching reactions are heterogeneous reactions that take place at the interface between different phases. All three phases may be involved, but all hydrometallurgical reactions involve the contact of a solid phase (containing the substance of interest that is to be leached into solution) and a liquid phase (the lixiviant) (Web book in Hydrometallurgy, 2012).

The leaching process can be summarized in several steps. First, diffusion of the lixiviant through the diffusion layer to surface of the solid particle occurs (step 1). At the solid surface, this reactant is adsorbed onto the solid (step 2) and the chemical reaction between the solid and the leachant takes place, forming the product (step 3). Hereafter, the product must first desorb from the solid surface (step 4) and then diffuse from the solid surface through the diffusion layer (step 5) and into the surrounding liquid (Web book in Hydrometallurgy, 2012). A diagram illustrating the leaching process can be seen in Figure 2.

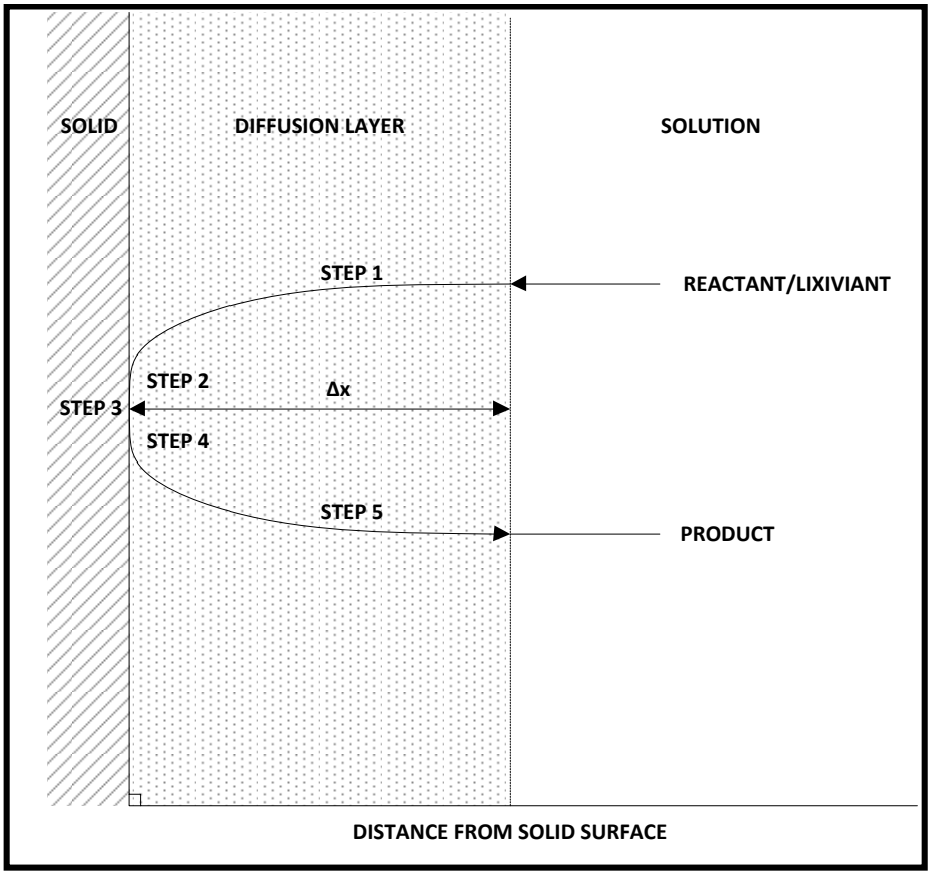

Figure 2. Summary of the steps involved in the leaching process (redrawn from the Web book of hydrometallurgy).

Fick's law can describe the diffusion rate in a solution:

$$J = \frac{dn}{dt} = -A \cdot D \cdot \frac{dC}{dx} \qquad \text{Equation 1}$$

In this equation, A refers to the surface area of the reacting particle, D to the diffusion constant and $\frac{dC}{dx}$ to the concentration gradient. This concentration gradient is a factor of the thickness of the diffusion layer. It can thus be concluded that each of these factors will have an effect on the speed at which leaching takes place (Web book in Hydrometallurgy, 2012).

2.2.2. Rate controlling step

The overall speed at which the leaching reaction takes place is determined by the step which takes the longest in the leaching process. This is called the rate-controlling step.

When the chemical reaction rate is much slower than the speed at which transport through the diffusion layer takes place, leaching is said to be chemical reaction controlled. However, if the chemical reaction is much faster than the rate of diffusion, the leaching is diffusion controlled. Intermediate controlled leaching occurs when the rates of diffusion and the chemical reaction are approximately equal (Web book in Hydrometallurgy, 2012).

In general, when a porous layer of the product forms on the particle surface during the leaching process, the mechanism becomes diffusion controlled (Web book in Hydrometallurgy, 2012). This is

due to the collection of the product layer on the surface of the particle increasing the thickness of the layer though which the reagent and product must travel between the particle surface and bulk solution.

A general guideline for determining which rate-controlling step is present in the system is shown in Table 2. This table assumes that the experiments are performed at a constant temperature. L represents the initial particle size, while E_a is the activation energy required for the reaction to take place.

Table 2. Guidelines to identify the rate controlling step in leaching systems.

Mechanism	E_a (kJ/mol)	Reaction order	Stirring impact	Effect of L
Surface reaction	>40	Any	None	Rate α1/L
Product layer diffusion	<20	First	None	Rate α $1/L^2$
Film layer diffusion	<20	First	Yes	Rate α 1/L

2.2.3. The Shrinking Core Model

Many oxide ores follow the common leaching model, the shrinking core model, when leached in sulphuric acid. This model can be illustrated as shown in Figure 3.

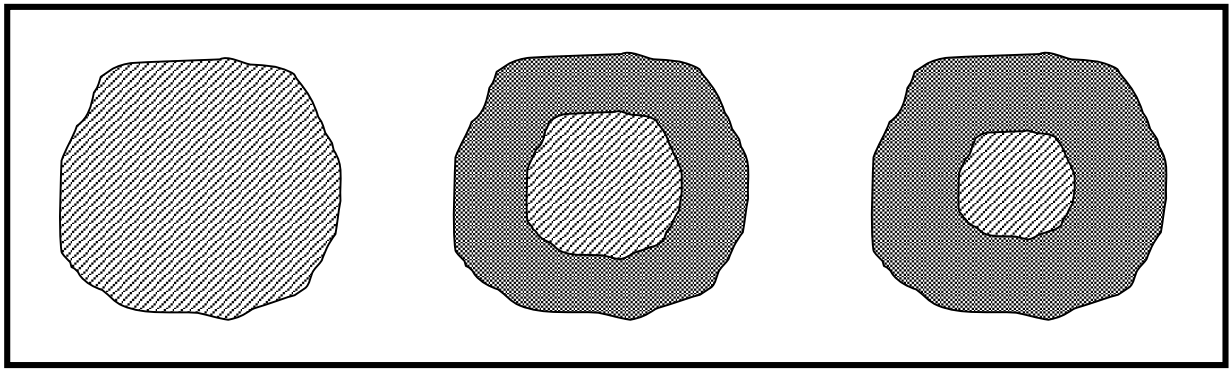

Figure 3. Illustration of the shrinking core model for leaching (Redrawn from Safari, *et al.*, 2009).

The shrinking core model suggests that, as the solid particle is leached, a layer of the product species is built up on the surface of the particle. This may occur by adsorption of the product compounds onto the surface of the reagent particle. By building a layer around the original particle, the initial particle size is maintained by the growing layer of product compounds around the original core particle. However, the size of the original particle decreases as leaching proceeds (Safari, *et al.*, 2009).

Figure 4 illustrates leaching according to the shrinking core model. Leaching of oxides with sulphuric acid follows the basic reaction:

$$A_l + bB_s \rightarrow products$$ Reaction 7

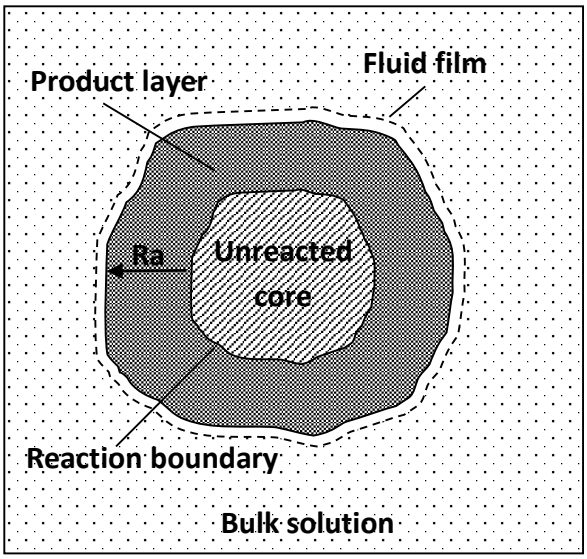

Figure 4. Illustration of a particle topo-chemically reacted according to the SCM (Redrawn from Pecina, et al., 2008).

2.2.4. Factors affecting leaching

Depending on which is the rate-controlling step in the leaching process, several process parameters and physical factors may have an effect on the rate of leaching.

If the process is chemical reaction controlled, one can infer from reaction rate of a heterogeneous reaction (at constant acid concentration) (Equation 2) which factors will affect the chemical reaction rate (Web book in Hydrometallurgy, 2012):

$$-\frac{dW}{dt} = k \cdot A \cdot C \qquad \text{Equation 2}$$

Here, W is the weight of the particle at time t, with k representing the rate constant and A the particle surface area. C is the concentration of the reactant. Since the rate constant, k is dependent on temperature; it stands to reason that changing the temperature will affect the reaction rate. In addition, it is evident that alterations to the surface area of the particle will also affect the reaction rate.

On the other hand, if the process is diffusion controlled, the Equation 3 describes the rate of diffusion:

$$D = \frac{RT}{6 \cdot \pi \cdot r \cdot \eta \cdot N} \qquad \text{Equation 3}$$

Diffusion, D, is equal to the product of temperature and the universal gas constant, divided by the product of the particle radius (r), Avogadro's number (N) and the viscosity of the substance (η). Thus, diffusion controlled systems will be affected by the temperature and size of the solid particles.

Pressure

The Skorpion process does not make provision for high pressure leaching, as the existing leaching circuit is designed to operate at atmospheric pressure. For this reason, pressure will not be considered as one of the factors in the experimental design.

Temperature

Increasing the temperature in a leaching system will result in faster leaching kinetics. This is due to the relationship between the rate constant and the temperature, as described by the Arrhenius equation for chemical reaction rate controlled systems. For diffusion-controlled leaching, the dependence of the diffusion coefficient on temperature causes this trend (Equation 3) (Web book in Hydrometallurgy, 2012).

Particle size

As a rule of thumb, smaller particle size will increase the kinetics of leaching. However, the extent of this effect will vary depending on the rate-controlling step.

By considering the dependence of the diffusion rate on the particle surface area, the relationship between the particle size and leaching kinetics becomes clear. From Equation 1 it is evident that the diffusion rate is directly related to the surface area. Thus, if the leaching process is diffusion controlled, surface area (and therefore particle size) will have a significant impact on the leaching rate.

Porous particles may experience very little or no change in recovery when the particle size is reduced. This is due to the large surface area of the original particle, caused by the particle's porosity. Reducing the particle size may therefore have a negligible effect on the exposed surface area of the solids (Souza, *et al.*, 2007).

Reagent concentration

Lixiviant concentration generally does affect the leaching kinetics. However, increasing the concentration will only increase the kinetics up to a point. In addition, changing the reagent concentration may lead to a change in the leaching mechanism and therefore, a change in the rate-controlling step (Web book in Hydrometallurgy, 2012).

Agitation rate

Agitating the leaching slurry allows the solid particles and liquid to mix effectively, maximising the contact between the different phases and facilitating the leaching reaction (Leaching and absorption resource book, 2012).

Diffusion layer thickness may be affected by the stirring speed in a system, and generally decreases with increased stirring speed. Due to this decrease in diffusion layer thickness, the leaching kinetics for a diffusion-controlled system will increase with increasing agitation speed. However, a chemical reaction controlled leaching system will be unaffected by the agitation rate (Web book in Hydrometallurgy, 2012).

Miller (2005) suggested that transfer of acidic solution to the particle surface initially affected leaching of copper oxide ore (and the leaching was hence limited by the amount of acid being supplied to the particle surface). This was affected by the rate of diffusion of the lixiviant through the particle's surface boundary layer. Increasing agitation caused the boundary layers to thin and therefore allowed for faster diffusion rates. This study also found that higher-grade materials created thicker concentration boundary layers, which caused comparatively slower leaching. Since this process is unaffected by the chemistry of the solid particle, it should also be applicable to zinc oxide particles.

pH

In general, the pH in a system is a function of the concentration of the lixiviant. Thus, pH will normally have an effect on both the leaching kinetics and the extent of extraction. The relationship between pH and hydronium concentration (related to acid concentration) can be seen in Equation 4.

$$pH = -\log[H^+] \qquad \text{Equation 4}$$

Low pH's imply that the H^+ concentration in solution is higher. On the other hand, high pH values imply low H^+ concentrations. When the H^+ concentration in solution is high, the OH^- concentration will be low and vice versa. The implications of this will be further discussed in section 2.3.2 (pH).

Solid-liquid ratio

By optimising the pulp density or solid-liquid ratio, one can minimize the lixiviant consumption by ensuring that there is no excess, unnecessary reagent that is not being used for leaching in the tank (Leaching and absorption resource book, 2012). With reagent consumption being one of the major expenses in leaching processes, it is important to optimize this factor.

In general, increasing the solid-liquid ratio will mean that there is less lixiviant per unit of solid. This means that there is a potential that there will be particles that do not come into contact with the lixiviant and do not leach properly. On the other hand, while decreasing the pulp density will ensure that all of the particles leach simultaneously; increasing the leaching rate, using too much liquid will drive leaching costs up. It is also important to remember that increasing the amount of liquid used for slurrying will dilute the lixiviant.

Residence time

In leaching operations, residence time refers to the amount of time it takes for the leach slurry to flow through all of the leach tanks. This means that there is an amount of time that each volume of slurry spends in each leach tank, called the residence time. In general, the longer the solid particles are in contact with the lixiviant, the greater the total amount leached, until the point at which equilibrium is reached (Leaching and absorption resource book, 2012).

This is however, very dependent on a number of factors and sometimes, precipitation may start to take place after a certain amount of time. There is also a potential for chemical reactions between dissolved species, with these reactions taking place to a greater extent as the residence time is increased. It is therefore important to understand the chemistry of the leaching process, as well as the leaching mechanism to determine the effect that residence time will have on the extent of reaction.

Mineralogy

The composition of the solids being leached may also have a severe impact on the leaching extent and kinetics. Mineralogical effects will be discussed in greater detail in the next section.

2.3. Leaching alternative zinc oxides

Several different zinc secondaries have been used as sources of zinc for processing. Depending on the origin of the zinc secondaries and their composition, there are numerous methods that can be used to recover the zinc.

Hydro- and pyrometallurgical processes have been investigated, but past experience has shown that hydrometallurgical processes not only produce fewer wastes and have less environmental impact, but also are also less energy intensive. For these reasons, hydrometallurgical methods are generally favoured for zinc secondaries processing.

Studies have shown that during the leaching of EAFD specimens, Zn oxides (such as zincite) tend to dissolve with relative ease, while zinc ferrites are more difficult to dissolve. The reason behind the differences in the leaching characteristics of these two different phases is the fact that ferrite is very stable. To liberate the zinc, the ferrite must first be decomposed, making it difficult to recover the zinc from franklinite (zinc ferrite) (Jandová, *et al*, 1999).

During acid leaching of solids, the adsorption of protons onto the solid surface at the solid liquid interface plays a major role. It weakens the metal-oxygen bonds that allow the metal oxide structure and ultimately causes the metal protons to be released into the solution (Jandová, *et al*., 1999).

In addition, Jandová, *et al*, (1999) found that the presence of impurities in the zinc oxides does not generally affect the reaction rate of zinc dissolution. This is due to the fact that the Zn^{2+} ions are not substituted by impurity ions. These impurity ions tend to rather form their own oxides. However, the extent of zinc dissolution may be affected by the presence of impurities, since the zinc may be caught up in complexes or spinels with the impurities, which cannot be easily dissolved by the weak acid used for leaching.

2.3.1. Composition of alternative zinc oxides

Electric arc furnace dust

During the oxidative smelting process that takes place inside an electric arc furnace, many of the zinc compounds contained in the recycled steel are oxidized to form zinc oxides in various forms. However, due to the large amount of iron present in the system, some of the zinc is also transformed into zinc ferrites (Jandová, *et al*., 1999).

Zinc in the EAFD is present chiefly in the form of zincite (ZnO) or franklinite ($ZnFe_2O_4$), while iron presents itself mainly in the form of magnetite (Fe_3O_4) or haematite (Fe_2O_3) (in addition to franklinite). Zinc may also be present in the form of complex ferrites, for example $(ZnMnFe)_2O_4$ (Havlik, *et al.*, 2004). Trace elements may also be present in the form of franklinite with isomorphously substituted metals, $(Zn_x,Me_y)Fe_2O_4$, where Me refers to other metals, such as manganese, cobalt, calcium, nickel, and so forth (Havlik, *et al.*, 2004). The typical mineralogy of EAF dust samples is shown in Table 3.

Table 3. Mineralogy present in typical EAF dust from steel recycling processes.

Element	Phase
Zn	ZnO (zincite), $ZnFe_2O_4$ (franklinite/zinc ferrite)
Fe	Fe_3O_4 (magnetite), Fe_2O_3 (haematite), $ZnFe_2O_4$ (franklinite/zinc ferrite)
Al	Al_2O_3, $Al_2O{\cdot}SiO_2$, $Al_2O{\cdot}2SiO_2{\cdot}2H_2O$
Si	SiO_2 (silica, as cristobalite and tridymite)
Ca	CaO (lime), $Ca(OH)_2$ (slaked lime), $CaCO_3$ (calcite)
Cu	$Cu_{1,96}S$, $Cu_2O{\cdot}2Fe_2O_3$
Cr	$FeCr_2O_4$ (ferrous chromite)
Pb	Pb(OH)Cl (laurionite), PbO (lead oxide)
Mn	MnO_2, Mn_3O_4

Oustadakis, *et al.* (2010) found that the zincite in EAF dust is generally present as finer particles, while the franklinite presents itself as larger spherical particles. Further characterization studies performed by Su and Shen (2009) found that the ZnO particles contained in the dust were generally smaller and irregular in shape, while the franklinite tended to appear as larger, spherical particles, to which the smaller zincite particles were attached.

While ZnO is leached with relative ease in both acid and alkaline leaching systems, zinc ferrite (franklinite and complex ferrite) is relatively refractory against leaching and requires either a concentrated medium or high temperatures to be extracted. This allows for co-extraction of iron in the leaching process (Oustadakis, *et al.*, 2010).

Leaching EAFD with sulphuric acid allows a significant portion of the highly reactive zinc species (up to 78% of the total zinc in the fumes) to be leached, while limiting iron dissolution, but zinc ferrite remains essentially unreacted (Oustadakis, *et al.*, 2010). Jandová, *et al.* (2002) found that this form of zinc is sparingly soluble and required a 3M sulphuric acid leaching system at elevated temperatures to yield good zinc recoveries of roughly 80%. At lower acid concentrations, only about 20-40% of the zinc can be realistically expected to be extracted (Langová, *et al.*, 2007).

There is great difficulty in predicting the precise forms in which zinc is present in the EAFD (Havlik, *et al.*, 2004) and how much of the zinc is present in each form. This is often not controllable, as the composition is heavily dependent on the composition of the charge. This would seem to imply that each EAFD with a very different chemical and mineralogical composition would require a unique set of optimum leaching parameters. However, many studies have been done to try and determine a standardized leaching procedure and process conditions (Shawabkeh, 2010).

In addition, there are some general characteristics of EAFD composition, which remain fairly consistent. For example, Oustadakis, *et al.* (2010) found that the major components constituting EAFD included iron, zinc and calcium, with some less prevalent, but still significant elements including aluminium, arsenic, silicon, magnesium, potassium, sodium, sulphur, chromium, lead, manganese, cobalt, copper, fluorine and chlorine.

This corresponds well with studies performed by other authors (Havlik, *et al.*, 2005), which show that the main elements that are present in EAFD include zinc, iron, lead, calcium, copper, cadmium, chromium and silicon. In general, the presence of the large amounts of calcium oxide can be attributed

to the lime that is added to the furnace during steel scrap meltdown that serves as an impurity removal agent (Oustadakis, *et al.*, 2010).

Calcium is also present in relatively large quantities as calcium oxide. This is due to lime, which is added to the metal during the smelting process, used to make steel. Wustite, periclase, pyolusite, lead oxide and quartz may also be present in varying amounts (Oustadakis, *et al.*, 2010).

Approximately 90% of the EAFD is composed of oxide minerals species. Iron occurs predominantly in the form of magnetite (Fe_3O_4), but the Fe iron in this phase may be replaced with Zn, Mg, Ca, Cr, Mn and so on to create metal ferrites in the form $MeFe_2O_4$. Some of the iron may also be present as Fe_2O_3. Zinc presents mainly as zincite and zinc ferrite, as well as a small amount of $ZnCO_3$. Very small amounts of zinc may be present as sulphides, silicates or aluminates. Although cadmium has not been well investigated, it can be assumed that, due to the similarities in the metal properties, cadmium is distributed in a similar way to zinc (i.e. CdO, $CdFe_2O_4$ and $CdCO_3$) (Dreissinger, *et al.*, 1990; Nyirenda, 1991).

Lead is present mostly in oxide forms, but small amounts of $PbCl_2$ and $PbSO_4$, as well as some carbonates can also be found in EAFD. Chromium and nickel replace iron in the magnetite phase, while some Cr may be present as Cr_2O_3. Calcium oxide and calcium carbonate are the dominant forms of calcium in EAFD, but some calcium may present as fluoride, ferrite or silicate compounds. Chloride in the dust is probably present as NaCl, KCl, $CaCl_2$ and other metal chlorides (Dreissinger, *et al.*, 1990; Nyirenda, 1991).

Unlike the zinc dross and zinc ash, where zinc is associated mainly with the coarser particles, zinc is found mainly in the fines in EAF dusts. Here, the zinc is suspected to be present largely in the form of zincite. However, significant quantities of zinc and iron are also present in the coarser particles, leading to the conclusion that these particles contain the bulk of the franklinite (zinc ferrite) (Oustadakis, *et al.*, 2010). In general, the grains of the EAFD are spherical in shape and porous (Shawabkeh, 2010).

A study performed by Suetens, *et al.* (2015) defined the mineralogy of the EAF dust over the different size fractions of the EAFD. The outcomes of this characterization are as follows: The submicron fraction (less than 0.5 microns in size) made up approximately 50% of the total dust volume, while particle clusters were found to contribute to roughly 28% of the total dust volume. The distribution of mineralogy across different particles sizes is shown in Table 4.

Table 4. A summary of the mineralogy of EAFD as distributed across different size fractions in the raw EAFD.

Size fraction	Mineralogy
<1 µm	Almost entirely ZnO
1-40 µm	Iron oxide and slag
40-250 µm	Clusters of small particles

This study also noted that this cluster formation is typical in all forms and compositions of EAF dust and it suggested that the mechanism for the formation of zinc ferrite is as follows (Figure 5):

In the first mechanism, the outer shell of a pure iron particle is oxidised. ZnO particles then precipitate on the oxidised layer surrounding the iron particle to form franklinite (zinc ferrite). The zinc oxide and iron oxide then react to form an oxidised particle surrounded by a ring of spinel, which is the final product.

The second mechanism suggests that gaseous zinc reacts directly with a solid pure iron particle, forming the spinel phase. This spinel particle continues to react with oxygen, resulting in particle which has a zinc concentration gradient through the particle, with the highest zinc concentration at the edge, and the lowest at the centre (Suetens, *et al.*, 2015). The study by Suetens, *et al.* (2015) suggested that the second mechanism was more likely, as they observed a zinc concentration gradient within the franklinite particles, but both mechanisms are possible.

The slag phases contained in the EAFD were found by Suetens, *et al.* (2015) to contain large amounts of chromium, calcium and silica, but no zinc whatsoever.

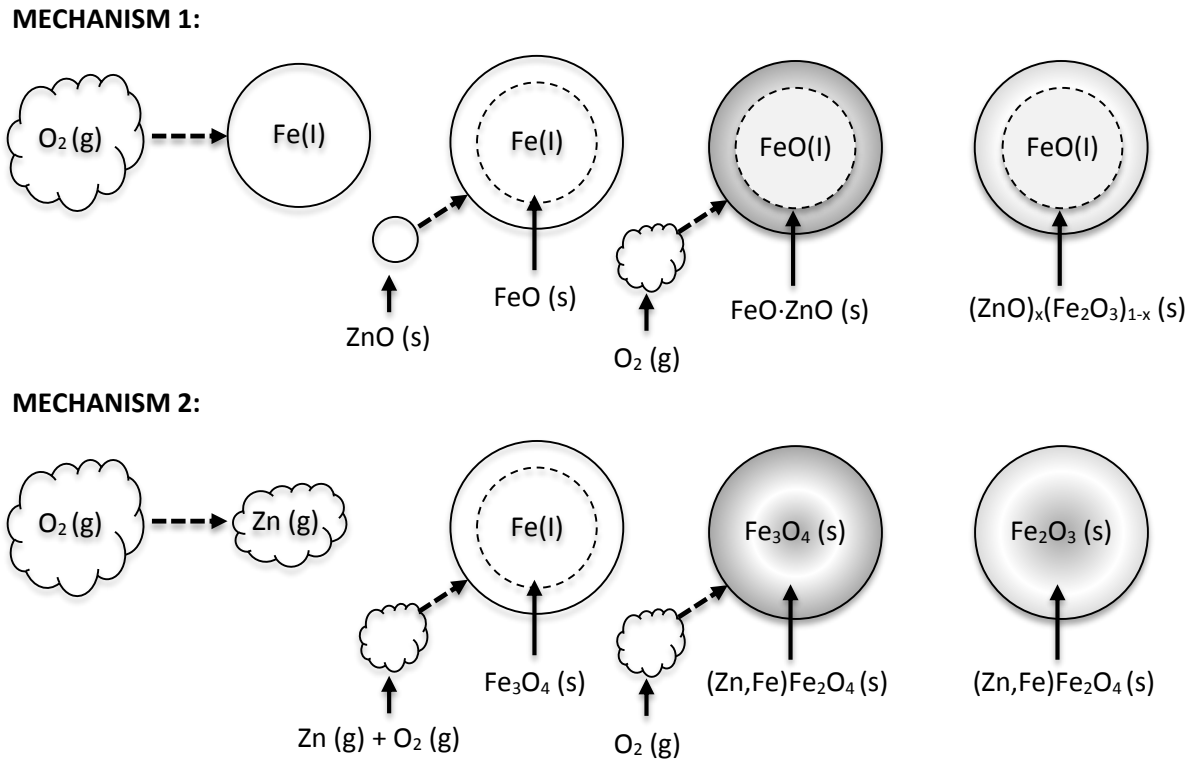

Figure 5. Diagram showing the mechanism of franklinite formation in EAF dusts (Redrawn from Suetens, *et al.*, 2015)

Zinc dross and zinc ash

The waste sample obtained from an overseas galvanizer for test work was composed of a mixture of zinc ash and zinc dross. Thus, the composition and characteristics of both of these waste products were reviewed.

During the hot dip galvanizing process, zinc is molten in a bath. The surface of the molten zinc metal, which is exposed to the atmosphere, reacts with oxygen, forming an oxidized zinc layer. This top dross, which is often called zinc ash, must occasionally be removed to ensure good galvanizing coatings.

Shitov, *et al.* (2005) stated that this zinc dross consists of approximately equal portions of oxidized and metallic zinc.

Zinc dross, as it is defined in the galvanizing industry, refers to the layer formed at the bottom of the zinc bath by intermetallic reactions taking place inside the molten zinc. This layer, called “hard zinc” is typically removed less often than the ash and has a higher density, causing it to settle to the bottom of the bath (Trpčevská, *et al.*, 2010).

Characterization of zinc ash from zinc dross was performed by Dvořák and Jandová (2005) and this characterization found that the samples contained simonkolleite ($Zn_5(OH)_8Cl_2{\cdot}H_2O$) in majority, zincite (ZnO) and metallic zinc (in minority). However, the dross composition varies greatly, as the different stable phases formed in the dross are dependent on the temperature and bath chemistry in the galvanizing process.

Rabah and El-Sayeh (1995) found, in their study of the leaching of zinc dross and zinc ash, that the zinc ash, with a higher percentage of fines, contained less zinc. They concluded that this was due to the fact that finer particles have a greater percentage non-metallic inclusions than the coarser powder cuts. This leads to the suggestion that it may be possible to recover more zinc from coarser particles than fines, albeit at a slower rate of recovery. The slower recovery rate would be related to the smaller total surface area available for reaction in coarser particles. This study found that the zinc content is highest at particle sizes in excess of 400 microns, for both dross and ash.

Zinc ash formation particle size is influenced by the temperature of the zinc bath and by the amount of iron super-saturation in the bath. Iron is slowly dissolved into the bath as it is dipped into the molten zinc during galvanising.

These leach residues mostly contain varying amounts of the following major components: lead sulphate, iron silicate, zinc ferrite and zinc silicate, zinc sulphate heptahydrate, iron oxide, calcium silicate, quartz and calcium sulphate hemihydrate (Ruşen, *et al.*, 2008).

Top dross, formed on the surface of the zinc bath, is generally composed of iron-aluminium intermetallic components containing some zinc, and are in the form $Fe_2Al_5Zn_x$ (Koutsaris, 2011). Zinc dross typically consists of a mixture of different intermetallic particles of Fe_2Al_5 and $FeZn_{10}$, zinc oxides and areas of metallic oxides in a zinc matrix (Koutsaris, 2011).

In addition to the other impurities, zinc dross and zinc ash from galvanizing processes generally contain significant quantities of chlorides due to the flux added to the zinc bath during galvanizing. This means that the dross typically contains chloride compounds (Dvořák and Jandová, 2005).

Zinc oxide obtained from zinc smelter fumes

Jandová, *et al.* (1999) found that leaching of zinc oxide at elevated temperatures (greater than 20 ˚C) in dilute sulphuric acid solutions was diffusion controlled and the reaction was completed relatively quickly.

This study also reported that, because impurities did not substitute the zinc, but instead formed separate spinels and oxides, the presence of impurities did not slow down the zinc dissolution rate. However, zinc oxides containing contaminants did not experience recoveries as high as purer forms of zinc oxides, because the impurity spinels remained unreacted and reported to the residue solids.

Table 5. Mineralogy present in typical zinc oxide from fuming processes.

Element	Phase
Zn	ZnO (zincite), $ZnSiO_4$
Fe	Fe_2O_3
Al	Al_2O_3
Si	SiO_2
Ca	CaO
Cu	CuO
Cr	Cr_2O_3
Pb	PbO
Mn	MnO
Mg	MgO
Ni	NiO

Jandová, *et al.* (1999) also found that the oxides contained within the ZnO samples were all spherical, non-porous particles. This study also found that the dissolution of the various elements was directly related to the actual surface area of the particles.

Contaminated sources of zinc oxide generally contain a spinel, in which some of the zinc particles are bound. This spinel can be represented as $Mn_{1-x}(Zn,Mg,Ni)_x(Al,Cr)_2O_4$ and is an insoluble spinel (Jandová, *et al.*, 1999). More detail on the mineralogy contained in typical zinc smelter furnace zinc oxides can be found in Table 5.

2.3.2. Factors affecting leaching

Temperature

For zinc dross and zinc ash dissolution, it has been found that increasing the temperature at a constant acid molarity will increase the zinc dissolution by increasing acid attack, up to a temperature of 80˚C, above which the temperature seems to have insignificant effects (Rabah and El-Sayeh, 1995). Dvořák and Jandová (2005) performed leaching experiments at 40˚C and found that despite the comparatively low temperature 98% of the zinc had been extracted from zinc dross within 30 minutes of reacting with 10% acid in a stirred vessel at atmospheric pressure. However, increasing the temperature to 80˚C did result in faster reaction kinetics.

In increasing the leaching temperature from 30-95˚C for leaching of leach residues, an increase in the extent of zinc extraction was experienced from 63.7-71.9%, indicating the temperature dependence of the leaching process. Jha, *et al.* (2001) also observed this increase in zinc extraction from zinc ferrite. Iron dissolution is also a function of temperature, having shown a similar trend to zinc. Optimum temperature in this study was thus determined to be 95˚C (Ruşen, *et al.*, 2008).

Havlik, *et al.* (2006) found that the optimum temperatures for extracting zinc from EAFD lay in the range from 70-90˚C. Within this range, significant zinc dissolution was achieved (up to roughly 72%)

and varying the temperature affected the iron extraction achieved. However, it was reported that the iron dissolution was somewhat negatively affected by increasing temperature, with zinc recoveries dropping roughly 1-5% over the temperature range from 30 to 90˚C. Similarly, lower temperatures resulted in greater iron extraction, although the iron extraction was initially high and reduced with time under constant operating conditions.

The inverse relationship between iron extraction and temperature can potentially be explained by the assumption that some of the iron starts to precipitate out of the solution with time. This precipitation of iron was a result of the fact that the system pH increased as the residence time increased. No acid addition was performed to keep the pH at a desired set point. Thus, the pH increased with time, to the point where iron started to precipitate out of the solution.

In the study of leaching EAFD at atmospheric pressure, Havlik, *et al.* (2005) found that the temperature had a marked effect on the amount of zinc leached, regardless of the solid/liquid ratio used.

San Lorenzo, *et al.* (2005) suggest that a temperature between 45 and 65˚C is sufficient to cause zinc dissolution in EAFD and Waelz oxides, when operating in a pH range from 0-3 with a residence time of between 0.5 and 2 hours.

As expected, Shawabkeh (2010) also found that increasing the reaction temperature from 4-50˚C increased the zinc extraction rate. This was due to the increased rate constant, diffusivity and mass transfer coefficient.

On the other hand, in the temperature range of 18 to 51˚C, Cruells, *et al.* (1992), found that iron dissolution was directly proportional to temperature, while zinc dissolution was virtually independent. It is thus recommended that working at lower temperatures would be of greater benefit.

The rate constant for the dissolution of zinc ferrite in sulphuric acid was found to vary considerably with temperature in the temperature range from 75 to 95˚C. This rate constant increased from 0.0043g/m^2.min to 0.0174 g/m^2.min over the given temperature range (Elgersma, *et al.*, 1992).

It was observed that during the first 20 minutes of leaching of a zincite sample, the temperature had a significant effect on the dissolution rate of the sample, when the temperature was varied between 30 and 60˚C. However, the effect decreased with time beyond the 20-minute mark and continued to decrease (Moradi and Monhemius, 2011). Possible reasons for this decrease in impact of the temperature may be the pore blocking by solid products, which would cause a barrier for diffusion of reagent into the particles, as well as a barrier for diffusion of products away from the particle (Moradi and Monhemius, 2011). This theory suggests that although chemical reaction control occurs initially, the leaching process may later become diffusion controlled (ash layer diffusion controlled), because of the barrier of solid products that builds up around the particle.

A study performed by Jandová, *et al.* (1999) on zinc oxide powder leaching, showed that increasing temperatures had little to no effect on reaction kinetics of zinc dissolution.

Particle size

Jandová, *et al*. (1999) found that dissolution of the zinc oxides proceeded with essentially linear kinetics, since both the reagent and product concentrations remained almost constant, while the products were highly soluble. They concluded from their ZnO leaching study that zinc oxide dissolution proceeded relatively fast and was unaffected by the sample preparation techniques used. This could be concluded from the fact that the linear rate constant was affected only by temperature and was hence independent of grain size.

Ramachandra Sarma, *et al.* (1976) found that the dissolution of zinc ferrite particles from zinc leach residue was dependent on the size of the interfacial surface area. Similarly, Moradi and Monhemius (2011) found that the dissolution of a zinc silicate ore, composed of a significant amount of zincite, was dependent on the particle size. This effect could be expected, as decreasing particle size increases the interfacial surface area, and therefore the surface on which reaction can take place. It may be that the findings of this study differ from those studies involving zinc secondaries, because the leaching of zinc secondaries involves leaching zinc that has been bound in different matrices. It has been suggested by Suetens, *et al.* (2015) that the zinc ferrite in EAFD is formed via a solid-gas reaction. This results in a particle with a zinc concentration gradient from the edge of the particle to the centre. Zinc ferrite contained in leach residue would probably not have the same structure, because

Reagent concentration

In the extraction of zinc from EAFD, as studied by Havlik, *et al.* (2006), it was determined that a sulphuric acid concentration of 0.5 M provided optimal zinc extraction (up to roughly 72%) with minimal iron extraction at a temperature between 70 and 90˚C. An alternative study conducted by Langová, *et al.* (2007) found that using 3M H_2SO_4 in a similar temperature range and solid/liquid ratio of 5 could produce almost 100% zinc extraction, with iron recoveries in the region of 90%, after 6 hours. This process does have a downstream iron precipitation section, though. This study also found that good zinc selectivity was obtained when 0.1-0.3M H_2SO_4 was used. This study thus supports the theory that an increased reagent concentration will result in increased metal recovery. Pecina, *et al.* (2008) reported results that support this trend.

Oustadakis, *et al*, (2010) found that acid concentration played the greatest role in the leaching of zinc from EAFD, over a range of temperatures from 30-60˚C and a solid/liquid ratio between 10 and 20%. Here, acid concentration was varied between 1 and 1.5M. This study found that up to 80% of the total zinc could be leached from the EAFD, with only 45% of the iron being leached.

A study by Havlik, *et al.* (2004) also found that the acid concentration had the greatest effect on zinc extraction when leaching at atmospheric pressures, with the optimal acid concentration being 0.4 M at an elevated temperature of 150˚C. This study also suggested that acid concentration is the limiting factor in zinc dissolution from EAFD, since the process seems to be relatively independent of temperature. A similar study conducted by the same authors in 2006 found that within the acid concentration range from 0.1-1 M, acid concentration also heavily affected overall zinc recoveries, allowing a maximum recovery of 75% to be achieved at 1M (Havlik, *et al.*, 2006).

Cruells, *et al.* (1992) on the other hand, found that within the range of 18-61˚C and 0.1-2M H_2SO_4, acid concentration had a negligible effect on zinc extraction. The reason for this apparent discrepancy may

lie in the composition of the EAF dust treated. Samples studied by Cruells, *et al.* (1992) contained 22% total zinc of which the majority was zincite, zinc ferrite and $Ca[Zn(OH)_3]_2 \cdot 2H_2O$. This study did however correspond well with the others (Havlik, *et al.*, 2005; Havlik, *et al*., 2006; Langová, *et al.*, 2007 and Oustadakis, *et al.*, 2010) in terms of iron dissolution, with the amount of iron extracted being proportional to the acid concentration and temperature of the system.

Rabah and El-Sayeh (1995) found that, in leaching zinc dross and zinc ash, increasing the sulphuric acid concentration gradually increased the amount of zinc extracted up to an acid concentration of 2M. Cruells, *et al.* (1992) performed a leaching study with EAFD in a similar range of acid concentrations (between 0.1 and 2 M acid) and found that the amount of iron leached increased with the sulphuric acid concentration, while zinc leaching was essentially unaffected by acid concentration. In this study, the residence time was 24 hours; long enough for maximum zinc extraction to be achieved. Thus, it seems that in this case, the extent of reaction is also relatively unaffected by acid concentration.

Ruşen, *et al.* (2008) found that, when the reaction time, temperature and solid/liquid ratio were kept constant, the amount of metal extracted increased with increasing acid concentration. It is however, important to note that, while iron extraction continued to increase with increasing reagent concentration, zinc extraction achieved a maximum extraction of 75%, beyond which the extraction was independent of the reagent concentration. This may be because of the high acid concentrations used for the tests (acid concentration varied from 0 M to 3.5M). Nonetheless, these findings show the importance of optimizing the acid concentration. It is desirable to minimize iron extraction while maximizing zinc extraction, as iron may lead to overloading of the SX circuit and, ultimately to the production of off-spec zinc. In addition, leaching of iron instead of zinc leads to higher acid consumption figures, which is a major focal point for cost optimization in any leaching process.

It was found that increasing the sulphuric acid concentration from 0.1 to 2 mol/L increased the amount of zinc leached from EAFD, but this effect was reduced as the acid concentration increased beyond 2 mol/L (Shawabkeh, 2010). This corresponds well with the results from other resources, which suggest that acid concentration has a notable effect on zinc dissolution, but only up to a certain point. Increasing acid concentration increases the flux of hydrogen ions across the boundary layer (diffusion layer) to the solid surface of the particle, as there are more hydrogen ions present in solution. This increases the reaction rate (Shawabkeh, 2010).

Overall, it is important to note that the amount of acid added to the system will depend on the stoichiometry of the system reactions. It should be kept in mind that the solid/liquid ratio will therefore affect the amount of acid that should be added. In addition, the tendency of iron dissolution to increase with increasing acid concentration should be considered (Cruells, *et al.*, 1992).

At low acid concentrations, the amount of zinc extracted was found to decrease slightly with time over a 2 hour residence time period. This may be due to the fact that iron precipitates as FeO.OH, and some zinc may be adsorbed onto the surface of this precipitate (Hoang Trung, *et al.*, 2007).

Zinc oxide powder dissolution, studied by Jandová, *et al.* (1999), seemed to be unaffected by acid concentrations higher than 0.5 M.

Dvořák and Jandová (2005) developed a method for zinc recovery from zinc galvanizing dross, which used 10% acid solution at a temperature of 40 ˚C. The fact that 98% zinc extraction was obtained within the first 30 minutes of reaction time, despite many sources which suggest that low temperature is detrimental to leaching, suggests that the acid does have an impact on leaching of zinc from galvanizing dross.

The optimum acid concentration was found by Xu, *et al*. (2010) to be 0.44 mol/L, as an increase in concentration beyond this had little or no impact on the zinc dissolution, but higher acid concentrations did result in an increase in the amount of iron and silica leached.

Agitation rate

Increasing the agitation rate from 100 to 900 rpm was found to increase the zinc dissolution rate significantly, from 5% to almost 20% in the first 5 minutes of reaction time. This is due to the thinning of the boundary layer that is experienced, as agitation speed is increased (Shawabkeh, 2010).

Increasing stirrer speed from 100 to 1000 rpm was found to increase zinc dissolution rate slightly, while increasing agitation speed above 100 rpm was found to have little impact on dissolution rate (Ramachandra Sarma, *et al.*, 1976). This is probably due to the fact that the dissolution of zinc ferrite, as studied in this paper, was chemical reaction controlled and therefore not affected by the thinning of the boundary layer.

pH

pH within the leaching system is highly dependent on the quantity of solids charged at the start of the experiment (Havlik, *et al.*, 2005). Increasing the slurry density (i.e. adding more solid charge) resulted in a higher final pH, since acid consumption during leaching was significantly increased (Havlik, *et al.*, 2005). The acid consumption increased in this case, because of the larger amount of solids available for leaching relative to the amount of acid available.

Herrero, *et al.* (2010) performed a study to theoretically determine the optimum pH for leaching zinc (II) compounds in sulphuric acid, by considering the maximum solubility of the zinc compounds in the sulphuric media (Reaction 8 to Reaction 11).

$$Zn^{2+} + 2OH^- \leftrightarrow Zn(OH)_2 \downarrow \quad K_{PS} = 1.58 \times 10^{-15} \qquad \text{Reaction 8}$$

$$Zn^{2+} + OH^- \leftrightarrow ZnOH^+ \quad K_1 = 2.50 \times 10^4 \qquad \text{Reaction 9}$$

$$Zn^{2+} + 3OH^- \leftrightarrow Zn(OH)_3^- \quad K_2 = 3.00 \times 10^{15} \qquad \text{Reaction 10}$$

$$Zn^{2+} + 4OH^- \leftrightarrow Zn(OH)_4^{2-} \quad K_3 = 3.77 \times 10^{15} \qquad \text{Reaction 11}$$

Low pH values (where more H^+ was present in the solution) theoretically provided higher leached zinc quantities, as the presence of more H^+ ions drives the leaching reactions (discussed in section 2.3.3) forward. In addition, lower pH values imply that the amount of OH^- contained in the solution will be lower than at high pH values. Thus, the OH^- concentration was not high enough to facilitate the precipitation of zinc as $Zn(OH)_2$ (Reaction 8). On the other hand, as the pH increases, so does the OH^- concentration relative to the H^+ concentration (as the H^+ is consumed during leaching), allowing $Zn(OH)_2$ precipitation and reducing the lixiviant performance (Herrero, *et al.*, 2010). Once the pH has exceeded 12, Reaction 9, Reaction 10 and Reaction 11 will start to take place.

Since zinc seems to leach best at lower pH values, based on theory, it is recommended that the lowest practicably possible and economically feasible pH be used for leaching. Herrero, *et al.* (2010) found that between a pH of 2-3.5, zinc extraction of between 82.7 and 80.1 % respectively could be achieved. Since these extraction values were relatively close, a pH of 3.5 was selected for their pH values, as this was more feasible in a large-scale leaching plant. This factor was found to have a major impact on the dissolution of zincite by Moradi and Monhemius (2011).

It should be noted that the pH has a major impact on the dissolution of iron, the major impurity associated with zinc secondaries from steel dust processing. A lower pH will result in increased iron dissolution. Thus, the pH should be limited to between 2 and 3.5 to ensure that iron levels in the leaching product solution are not excessive. During the leaching process, the consumption of acid and the associated rise in pH may lead to the precipitation of some of the iron in the solution (Duyvesteyn and Jha, 1986). In addition, the iron leached will cause an increase in the ionic concentration of the resultant solution, which will decrease the solubility of the components contained in the solution and remaining in the solids. Under these conditions, with a temperature of 75˚C, about 70% of the iron was recovered, according to Duyvesteyn and Jha (1986).

Maintaining a high pH between 2 and 3.5 is however, impractical if atmospheric leaching at lower temperatures is used, as zinc recovery is then low. As such, an optimum pH for zinc recovery with minimum iron dissolution under atmospheric leaching conditions has yet to be determined.

Solid-liquid ratio

Increasing the solid-liquid ratio typically increases the total amount of zinc leached, because there is more zinc present in the system. However, the percentage of the zinc leached was found to generally decrease at higher solid-liquid ratios because, at higher solid-liquid ratios, all particles may not be completely surrounded by the solution. In addition, the amount of acid available for leaching would likely be in excess at lower solid-liquid ratios, while the limited acid available per unit of solid at higher S-L ratios may limit the dissolution reactions.

Since higher quantities of zinc are leached at higher S-L ratios, the ionic strength (concentration of total ions in the solution) of the resultant solution increases. Solubility is affected by the ionic strength of the solution in that, as the solution's ionic strength increases, the solubility will be decreased (if the ions are like ions). Thus, in the case of higher solid to liquid ratios, the solubility decreases as the ions are leached from the solids. Since there are more ions to be leached (due to the presence of more solids), a lower percentage of the ions can be leached, because the ionic strength of the solution will increase as more ions are leached.

Herrero, *et al.* (2010) found that decreasing the solid-liquid ratio increased the percentage of metal leached, due to the presence of a greater amount of lixiviant per unit of solids and therefore, a greater chance of solid-liquid contact. In addition, at higher solid:liquid ratios, this study suggested that, because of the high zinc quantities leached for the amount of solution available, the solution became saturated with zinc, preventing more zinc from being leached, and limiting the overall zinc recovery. Studies involving the leaching of EAFD have shown that increasing the solution density decreases the percentage of the zinc that is dissolved (Havlik, *et al.*, 2006).

Havlik, *et al.* (2004) found that increasing the amount of solids added to the system decreased the overall zinc recovery. This corresponds well to other literature (Herrero, *et al.*, 2010) and follows the expected trend. This study also found that decreasing the acid-to-dust ratio resulted in better selectivity of the leaching reaction towards zinc. In 2006, Havlik, *et al.* (2006) once again found that using higher L:S values increased the absolute zinc and iron recoveries.

Zinc extraction was found to be inversely proportional to the solid/liquid ratio (Havlik, *et al.*, 2005) in the leaching of EAFD at 80˚C. Herrero, *et al.* (2010) reported similar results in their study of leaching ZnO and zinc ferrites from Waelz oxide, theorizing that, since zinc is leached Zn^{2+} at the low pH values involved in acid leaching, the solution would become saturated with zinc ions, if the solid/liquid ratio were too high. This study found that 75kg/m^3 was the optimum S/L ratio for leaching, as lower ratios did not provide higher extraction values. However, such a low S/L ratio would be difficult to maintain in industry, due to the high acid consumption costs, so a compromise was made to use a S/L ratio value of 150 kg/m^3.

Ruşen, *et al.* (2008), on the other hand found that decreasing slurry density had little effect on zinc extraction, resulting in only about 3% increase in zinc extraction, when the density was lowered by 100 g/l. Minimum pulp density investigated in this study was 50 g/l, while the maximum was 250 g/l. This limited dependence on pulp density may be due to the fact that the sample used for this study contained predominantly zinc sulphate heptahydrate and zinc ferrite, which typically requires high acid and high temperature to recover (Leclerc, *et al.*, 2003). It may be that too little of the overall zinc was recovered to cause the solution to become saturated in the first place. Thus, the ability of the zinc ferrite to be leached under the selected operating conditions would limit the recovery more than the solid-to-liquid ratio.

Contrary to the other studies discussed thus far, Shawabkeh (2010) found that increasing the mass of dust per unit solution increased the zinc extraction. It was suggested that this was due to the increased surface area of solids available for contact with the solution and therefore, the larger amount of zinc available for potential extraction.

The reason for this divergence from the other studies probably has to do with the acid concentration in the solution. At the concentration studied by Shawabkeh (2010) the amount of hydrogen ions was probably sufficient to dissolve the increasing amounts of zinc presented in the larger quantities of dust. However, once a certain the amount of dust added exceeds the limit of the hydrogen ions in the solution, the trend is likely to be reversed, with increasing S/L ratio resulting in reduced Zn recoveries.

Langová, *et al.* (2007) suggested that for a maximum zinc recovery, a solid liquid ratio of at least 5 is necessary. Duyvesteyn and Jha (1986) found that a pulp density of about 5-40% provided reasonable recoveries, with pH values not exceeding 3.5. However, when greater amounts of solids were used, the pH was increased up to 5%. Although this resulted in very low iron concentrations in solution, with the majority of the iron precipitated out, zinc recoveries remained below 50%.

Based on the stoichiometry of the major reactions taking place in the system, in conjunction with the solid/liquid ratio, it was found that a minimum acid concentration of 1M was necessary to leach the zinc species completely (Cruells, *et al.*, 1992). This study also found that the dissolution of both iron

and zinc was almost independent of the solid/liquid ratio. This is possibly due to the very long residence time of 24 hours used for these experiments. However, solid/liquid separation was negatively affected by solid/liquid ratios that were too low. Cruells, *et al.* (1992) therefore suggest that a ratio of 1:10 should be used.

Little impact was noticed in varying the solid/liquid ratio for the dissolution of a zinc oxide ore, containing zincite as a primary component. A slight inverse relationship was however noticed between the extraction rate and pulp density (Moradi and Monhemius, 2011), because of the effects of the ionic strength and viscosity of the solution.

A study by Xu, *et al.* (2010) noted that zinc dissolution was only mildly affected by the solid:liquid ratio (less than 1% difference in recoveries), while silica and iron dissolution were heavily affected, with recoveries decreasing as the solid:liquid ratio increased by 13% and 8% respectively. This study focussed only on dissolution of zinc silicates, such as hemimorphite and willemite. These can be found in zinc secondaries, but are more common in leaching residues than EAF dusts, drosses and fume dusts.

Hoang Trung, *et al.* (2007) found that the zinc extraction rate from steel furnace dusts was unaffected by the solid/liquid ratio. This study did however find that at high S/L ratios, the amount of free acid in the system decreased significantly with time (as the acid reacted with the solids) until the pH started increasing. The pH did not increase enough to allow for zinc precipitation, but it was found that iron started to precipitate at the higher pH values experienced after longer residence times at higher S:L ratios. Iron precipitated hydrolytically to form iron oxides, hydroxides and oxysulphates.

For the leaching of zinc from brass slag fume, Ahmed, *et al.* (2012) found that decreasing the solid-to-liquid ratio (or increasing the liquid-to-solid ratio) also had an inverse effect on the recovery of zinc and copper from the material. This corresponds with the majority of the research (Havlik, *et al.*, 2004; Langová, *et al.*, 2007; Herrero, *et al.*, 2010) available regarding the effect of changing solid-to-liquid ratio on the recovery of zinc from EAFD and zinc dross. However, this study also found that the increase in recovery with increasing liquid-to-solid ratio reached a plateau. Beyond a certain point, reducing the amount of solids no longer had any effect on the recovery. For this study, the maximum zinc recovery was reached at a liquid-to-solid ratio of 5:1 (17% solids), while the maximum copper recovery was attained at a ratio of 6:1 (14% solids).

Kukurugya, *et al.* (2015) found that increasing solid-to-liquid ratios had different effects on the leaching of different elements. Zinc was found to experience higher recoveries at lower solids concentrations. Iron, on the other hand, showed lower dissolution at lower slurry densities. It was proposed that this may be due to selective leaching of zinc. In this study, the greatest calcium leaching was observed at the highest solid-to-liquid ratio. This may be due to the tendency of calcium to precipitate from the solution, as gypsum, while the experiment is on-going, once the solution becomes saturated with calcium.

Residence time

Rabah and El-Sayeh (1995) found that dissolution of zinc at room temperature in a 2M sulphuric acid solution was at 98% within 30 minutes of the start of the experiment. Increasing the residence time

beyond this up to 24 hours did result in a slight increase (2% overall) in the amount of zinc leached and total dissolution of zinc was achieved after 20 hours. It is probable, based on the findings of this study, that (at higher temperatures) less residence time will be required to achieve complete dissolution (see "temperature" section on page 19).

In the leaching of leach residues, it was found that zinc and iron extraction follow similar trends, with the extraction extent increasing with increasing time up to 1440 minutes, at which point approximately 83% of the zinc had been extracted (Ruşen, *et al.*, 2008).

An optimum leaching time of 120 minutes was thus selected to maintain reasonable zinc extraction, while limiting iron dissolution. This corresponds well with the study by San Lorenzo, *et al.* (2005) that suggests that an optimal residence time for zinc extraction from secondary resources is between 0.5 and 2 hours, at a temperature between 45 and 65˚C. This result also corresponds well with the findings reported by Langová, *et al.* (2007), which states that maximum zinc recovery had been obtained after 1 hour of leaching.

Jandová, *et al.* (1999) showed that ZnO could be essentially completely leached in 10-15 minutes., while Leclerc, *et al.* (2003) found that dissolution of zinc ferrites required far longer residence times (up to 24 hours, depending on the temperature used) and elevated temperatures (up to 150˚C), as well as multiple extraction steps. Yet this method is regarded as undesirable due to the large amount of iron dissolution that takes place in parallel (Cruells, *et al.*, 1992).

Shawabkeh (2010) also found that a large zinc recovery (approximately 70% of the total zinc) could be obtained in a short time period- under 5 minutes. This result was attributed to a combination of the fine particle size used in the study (1-5µm) and the fast solubility of the zincite (Nagib and Inoue, 2000). The result corresponds well with the finding by Jandová, *et al.* (1999).

The study conducted by Havlik, *et al.* (2006) suggested that at the same acid concentration and temperature, the residence time had little impact on the amount of zinc leached. However, at higher temperatures, it was found that the overall recovery decreased as the residence time increased. This may be because of the higher temperatures initially causing increased reaction rates. Since no acid was added to this system to maintain a constant pH, the leaching reactions consumed acid, causing the pH to rise, potentially allowing for zinc precipitation.

Havlik, *et al.* (2006) also found that leaching zinc from EAFD using a sulphuric acid lixiviant was a very fast process. Almost all zinc was dissolved almost immediately after combining the solids with the lixiviant. This study also found that the amount of zinc extracted reduced with reaction time, as the experiment progressed. This is suggested to be a result of the system attempting to achieve dynamic equilibrium.

A residence time of 2 hours was found to be sufficient to provide recovery values of 70%, provided the temperature used was in the range of 30-90˚C, according to Duyvesteyn and Jha (1986). However, this residence time will depend not only on the temperature, but also on the pulp density. Residence time may therefore have to be extended for higher pulp density values.

Mineralogy

EAFD is predominantly made up of ZnO and zinc ferrites, which generally make up roughly 50% of the zinc contained in EAFD (Leclerc, *et al.* 2003). Overall zinc content varies widely, but is generally in the region of 20% total zinc by weight (Leclerc, *et al.*, 2003). ZnO leaches easily, but ferric zinc oxide is difficult to leach at pH values above 1.

Zinc furnace dross – consists of ZnO and metallic zinc. Both should be easy to leach; has the potential for a higher recovery than EAFD or Waelz oxides.

Jandová, *et al.* (1999) found that all zinc oxides produced in their study formed spherical, non-porous particles, regardless of the preparation method used.

2.3.3. Reaction chemistry

Electric arc furnace dust

Havlik, *et al.* (2004) suggested the following reaction takes place between zincite and sulphuric acid (Reaction 12). This reaction is a reductive leaching reaction (Crundwell, 2003).

$$ZnO + H_2SO_{4\,(aq)} \rightarrow ZnSO_{4\,(aq)} + H_2O \qquad \text{Reaction 12}$$

Zinc ferrite reacts with sulphuric acid to form zinc sulphate and iron(III) sulphate, according to Reaction 13 (Turan, *et al.*, 2004). This reaction has slow kinetics at low temperature and the reaction rate increases significantly with temperature (Havlik, *et al.*, 2004).

$$ZnFe_2O_4 + 4H_2SO_{4\,(aq)} \rightarrow ZnSO_{4\,(aq)} + Fe_2(SO_4)_{3\,(aq)} + 4H_2O \qquad \text{Reaction 13}$$

Havlik, *et al.* (2004) suggested an alternative reaction that may take place in leaching of zinc ferrite in addition to Reaction 13 (Reaction 14):

$$ZnFe_2O_4 + H_2SO_{4\,(aq)} \rightarrow ZnSO_{4\,(aq)} + Fe_2O_3 + H_2O \qquad \text{Reaction 14}$$

Havlik, *et al* (2006) suggested an alternative zinc ferrite leaching reaction, as shown below (Reaction 15).

$$ZnFe_2O_4 + H_2SO_{4\,(aq)} + H_2O \rightarrow ZnSO_{4\,(aq)} + 2Fe(OH)_3 \qquad \text{Reaction 15}$$

According to Havlik, *et al.* (2004), based on the EH-pH diagrams presented in Figure 6 and Figure 7, Reaction 13 takes place preferentially over Reaction 14 and Reaction 15 for the leaching of zinc ferrite, in the temperature range from 25 to 100˚C. (also reported by Hoang Trung, *et al.*, 2007). Increasing pH and decreasing potential will result in the precipitation of ferrous from the Zn^{2+} and Fe^{2+} stability zone. Zinc, on the other hand, will remain in solution. On the EH-pH diagrams, there is an area of ferric stability in the very low pH (pH close to 0), high potential region. Havlik, *et al.* (2004) suggested that, during leaching, the ferric ions would act as an oxidative agent. When the pH starts to increase, as leaching progresses, the Fe^{3+} will start to precipitate as FeO·OH. By increasing the system temperature, the ferric stability zone is enlarged.

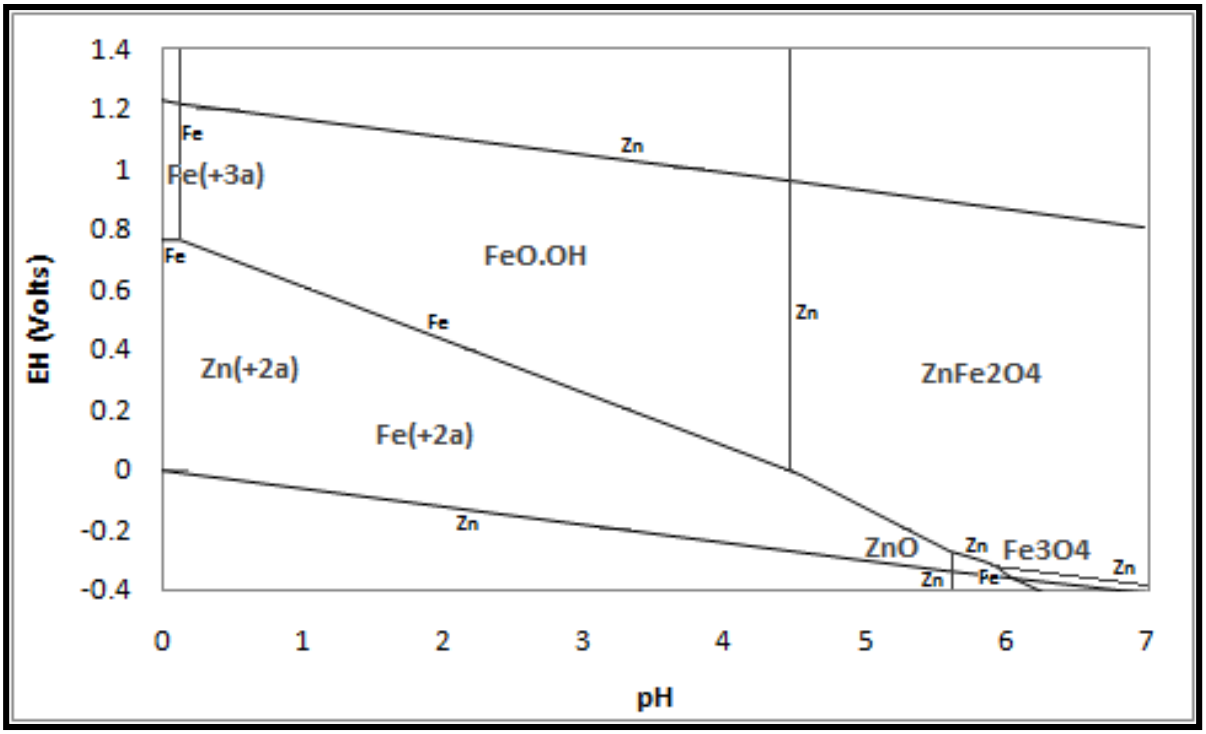

Figure 6. Zn-Fe-H2O System at 25 ˚C (redrawn from Havlik, *et al.*, 1992).

In both these diagrams, an area of stability is evident for the Fe^{2+} and Zn^{2+} ions in solution. However, increasing the pH while lowering the potential causes the ferrous ions to precipitate out of solution. The zinc ions, on the other hand, remain in solution (Havlik, *et al.*, 2006).

By increasing the temperature, the Fe^{3+} stability region is increased in size, making it more unlikely that the iron will precipitate out of solution. An additional change that results from a temperature increase is the shifting of the Fe^{3+}/Fe^{2+} potential limit towards higher redox potential values (Havlik, *et al.*, 2006).

In addition to the zinc ferrite in the system, leach residues and EAFD are likely to contain significant quantities of iron in the form of haematite. This compound is also leached easily with sulphuric acid under the experimental conditions considered for zinc ferrite leaching.

The reaction of haematite with sulphuric acid is as follows (Reaction 16) (Turan, *et al.*, 2004).

$$Fe_2O_3 + 3H_2SO_{4\,(aq)} \rightarrow Fe_2(SO_4)_{3\,(aq)} + 3H_2O \qquad \text{Reaction 16}$$

This haematite leaching reaction suggest that even if zinc ferrite reacts according to Reaction 14 to form haematite, the haematite will react with sulphuric acid in the solution to form $Fe_2(SO_4)_3$.

Some magnetite may also be present in the sample, reacting with the sulphuric acid in the following way (Reaction 17) (Cruells, *et al.*, 1992):

$$Fe_3O_4 + 4H_2SO_{4\,(aq)} \rightarrow FeSO_{4\,(aq)} + Fe_2(SO_4)_{3\,(aq)} + 4H_2O \qquad \text{Reaction 17}$$

Magnetite, when reacting in the presence of atmospheric oxygen, may also react as shown in Reaction 18 (Kukurugya, *et al.*, 2015):

$$4Fe_3O_4 + 18H_2SO_{4\,(aq)} + O_{2(g)} \rightarrow 6Fe_2(SO_4)_{3\,(aq)} + 18H_2O \qquad \text{Reaction 18}$$

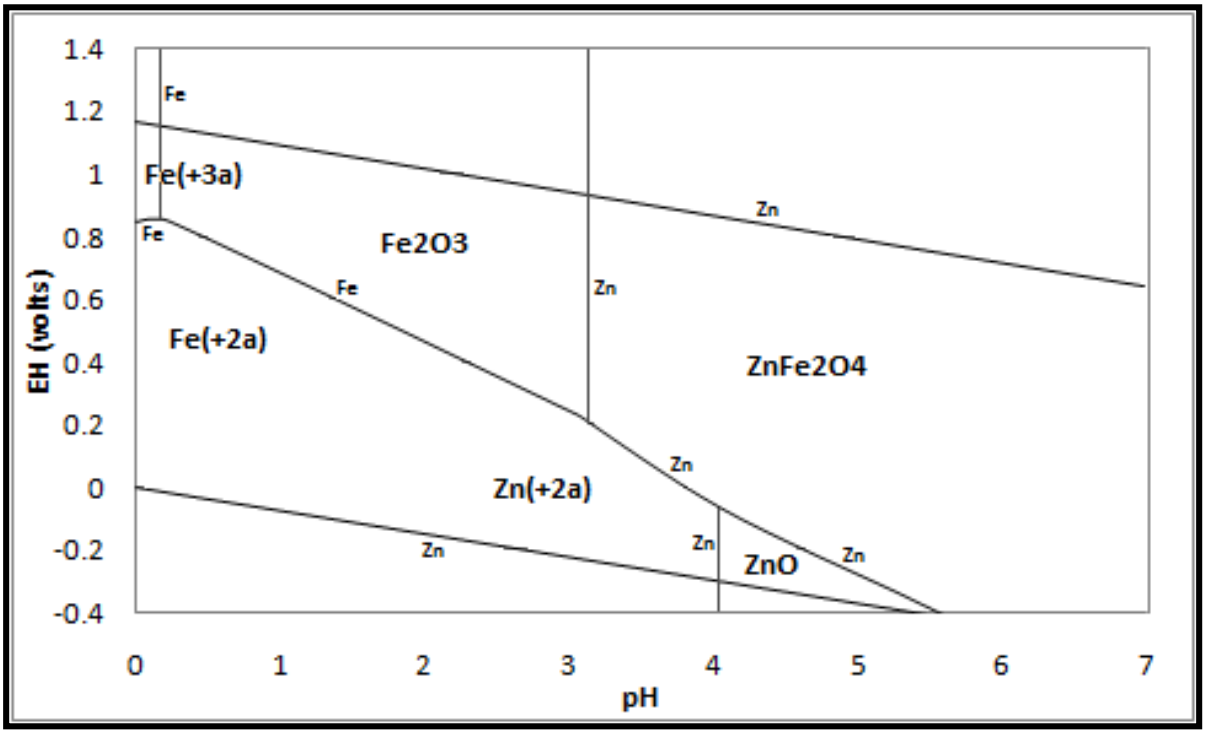

Figure 7. Zn-Fe-H2O System at 100 ˚C (redrawn from Havlik, *et al.*, 1992).

It is difficult to predict the precise form in which calcium compounds will be present in an alternative ZnO source, but Havlik, *et al.* (2004) suggest that calcium may be present in EAFD as CaO, $CaCO_3$, (Dreissinger, *et al.*, 1990; Lupi, *et al.*, 1996) or even $CaFe_2O_4$ and $Ca_2Fe_2O_5$. Potential side reactions that could occur for each of these compounds include (Reaction 19 to Reaction 22):

$$CaCO_3 + H_2SO_{4\,(aq)} \rightarrow CaSO_4 + CO_2 + H_2O \qquad \text{Reaction 19}$$
$$CaO + H_2SO_{4\,(aq)} \rightarrow CaSO_4 + H_2O \qquad \text{Reaction 20}$$
$$CaFe_2O_4 + 4H_2SO_{4\,(aq)} \rightarrow CaSO_4 + Fe_2(SO_4)_{3\,(aq)} + 4H_2O \qquad \text{Reaction 21}$$
$$Ca_2Fe_2O_5 + 5H_2SO_{4\,(aq)} \rightarrow 2CaSO_4 + Fe_2(SO_4)_{3\,(aq)} + 5H_2O \qquad \text{Reaction 22}$$

Reaction 19 and Reaction 20 occur at all sulphuric acid concentrations, increasing the acid consumption of the leaching process (Havlik, *et al.*, 2004). Calcium may also be present in a form bound with zinc, resulting in zinc sulphate and calcium sulphate, as shown in Reaction 23 (Jha, *et al.*, 2001).

$$Ca[Zn(OH)_3]_2 \cdot 2H_2O + 3H_2SO_4 \rightarrow CaSO_4 + 2ZnSO_4 + 8H_2O \qquad \text{Reaction 23}$$

Calcium sulphate formed by the reaction of calcium with the sulphuric acid, is sparingly soluble and is therefore mostly removed with the solid residue.

Calcium hydroxide contained in the EAFD will react with the acid according to Reaction 24 below:

$$Ca(OH)_2 + H_2SO_{4\,(aq)} \rightarrow CaSO_4 + 2H_2O \qquad \text{Reaction 24}$$

Zinc ferrite dissolution is described by Elgersma, *et al.* (1992) as the potential difference between the solid surface and the bulk solution. This potential difference is directly influenced by the presence of iron(II) and iron(III) ions, thereby influencing the dissolution rate of the zinc ferrite. High Fe^{3+} concentrations negatively impact the dissolution rate of the zinc ferrite. However, in the dissolution process, Fe(III) ions are released into solution. It is therefore necessary to consider the impacts that these ions will have on the leaching process.

Zinc dross and zinc ash

Zincite contained in the dross/ash mixture will leach according to Reaction 12. The zinc-iron-aluminium complex reactions are more complicated to describe and very little research is available for the leaching of these complexes.

Zinc oxide fume dust

Zinc oxides were found to leach in a diffusion-controlled process by Jandová, *et al.* (1999), when dilute sulphuric acid solutions (<0.5M) and elevated temperatures (>50 ˚C) were used. Yoshida (2003) expanded on this finding and determined that the transfer through the liquid boundary layer surrounding the particle was the limiting factor in leaching. However, it was not conclusively determined which chemicals diffusion rates controlled the reaction rate.

Pure ZnO samples completely dissolved in the experiment by Jandová, *et al.* (1999), while the contaminated samples contained a portion of insoluble spinel, in which some of the zinc was trapped – preventing complete zinc dissolution in these samples.

Since this particular sample consists of predominantly zinc oxides in the form of zincite (due to the manufacturing process used) it can be assumed that the zinc will react according to Reaction 12.

Jandová, *et al.* (1999) suggested that the iron contained in this particular zinc oxide source will be predominantly in the form of haematite, which will react according to Reaction 16. Calcium should be present as CaO, which reacts as per Reaction 20. This sample contains more lead than the other two samples. Due to the manufacturing technique used, literature suggests that this lead will be present as PbO, which will react with sulphuric acid (Jandová, *et al.*, 1999).

2.3.4. Rate controlling step

With the rate determining step being a major indication of the kinetics of leaching, it is very important to understand the mechanism by which leaching of different compounds takes place. Investigations into dissolution and leaching of zinc oxides have shown that leaching of these compounds tends to be dissolution controlled (the mass transfer of dissolved reactants from the bulk solution to the solid surface is the slowest step), while zinc ferrites have been found to experience chemically reaction controlled leaching (Jandová, *et al*., 1999), which is dependent on the acidity of the experiment.

The acidity of the lixiviant is deemed to be the variable with the most significant influence on the leaching rate of zinc ferrites. However, it is important to note that the rate-controlling step can be significantly influenced by the surface of the solid particle being leached. This may, in turn be affected by sample preparation (Jandová, *et al*., 1999).

Guspiel and Riesenkampf (1993) found that ZnO dissolution was mass transfer controlled over a wide range of acid concentrations (from 0.0005-0.1 mol/dm^3) and temperatures (from 0 to 55°C). Such a wide range of diffusion controlled leaching suggests the formation of a layer around the solid particle. This will most likely be due to formation of anions, not reaction products, which then adsorb onto the surface of the solid oxide, forming surface complexes and increasing the thickness of the diffusion layer (Jandová, *et al*., 1999).

Surface complexes formed in this way will contain hydroxide groups, which will affect the hydrogen concentration in the solution. This will, in turn, decrease the effect of the hydrogen ion concentration in the solution on the leaching kinetics (dissolution rate) (Jandová, *et al*., 1999). Ultimately then, Jandová, *et al*. (1999) determined that the dissolution of zinc oxides in dilute sulphuric acid at elevated temperatures (above 40 ˚C) was a diffusion-controlled process.

Ramachandra Sarma, *et al.*, (1976) studied the leaching of zinc leach residues, composed predominantly of zinc ferrite. This study found that between 70 and 99˚C and 0.5-2.5 M, a chemical reaction controlled shrinking core model provided a good fit for the leaching reaction data. This conclusion is supported by the fact that high activation energy was obtained for the dissolution of iron from zinc ferrite (15 kcal/mol). Similar results were yielded by the study done by Elgersma, *et al.* (1992), which investigated the dissolution of zinc ferrite over a temperature range of 75-95˚C. Apparent activation energy was found to be 74±2 kJ/mol.

The model used by Elgersma, *et al.* (1992) is given below (Equation 5). This model was found to provide a close match to the experimental data, provided the conversion increased with time.

$$1-(1-x)^{1/3}=\frac{1}{3}kS_o t \qquad \text{Equation 5}$$

In this equation, x represents the conversion (defined as the ratio of dissolved iron per gram zinc ferrite in a sample over the dissolved iron per gram zinc ferrite in the solution from the total leach), k the rate constant and S_o the specific surface area of the solids being leached. In deriving this equation, it was assumed that the particle dissolution takes place isomorphically (i.e. in such a way that the crystal structure remained the same) and the dissolution rate per unit surface area remains the same, throughout the course of the leaching. It was additionally assumed that the number of particles remained constant.

Kukurugya, *et al.* (2015) found that the leaching of EAF dust took place in two steps. The first step involved the leaching of zincite and was diffusion controlled, while the second step, the leaching of the zinc ferrites, was chemical reaction controlled.

2.3.5. Potential problems and suggested solutions

EAFD

Although large amounts of EAFD are generated around the world on a daily basis, it must be noted that the quantity produced by each individual steel manufacturer is relatively small. In addition, due to the large percentage of hazardous material in the dust, processing the dust can potentially cause pollution. One must thus ensure that processing the dust presents less of a hazard than disposing the hazardous dust directly (Cruells, *et al.*, 1992).

Finally, because of the high variation in the composition of the scrap used to feed the electric arc furnaces, the composition of the EAFD varies widely. This may present a problem in the refining of these materials, as it will be difficult to control the feed grade and impurity levels in the operation (Cruells, *et al.*, 1992).

Zinc dross and zinc ash

The aluminium added to the zinc bath for better galvanizing forms part of the zinc dross composition. During the galvanizing process, some iron also dissolves in the zinc bath, and becomes part of the molten zinc. This means that the zinc dross will typically contain high levels of aluminium and iron – potentially so high that the Skorpion impurity removal circuit will not be capable of removing large enough quantities. If this is the case, it may be necessary to consider alternative designs for the neutralization circuit, if this is the sample chosen. However, if these impurities are too high for the circuit to handle, it is more likely that an alternative source will be chosen. With the short life of mine remaining for Skorpion, it is not desirable to make changes to existing processes, as these changes will incur potentially unnecessary and excessive costs.

Ammonium chloride is often added to zinc baths as a fluxing agent in the galvanizing industry. The chloride contained in this compound may report to the dross or ash phases, contaminating them. Skorpion's EW is extremely sensitive to chloride. Thus, to reduce the risk of chloride carry-over, it may be necessary to consider a small pre-washing stage for this material.

Zinc oxide obtained from zinc smelter fumes

Jandová, *et al.* (1999) suggested that it should be relatively easy to recover zinc from zinc oxides, as they consist predominantly of ZnO, which is easy to leach, without requiring excessive temperature and extreme pH values. It should therefore be possible to leach this sample in the Skorpion process without any problems.

However, previous studies have shown that contaminated zinc oxide samples do not leach completely, as some of the zinc in the sample is trapped in an insoluble spinel phase. Since the ZnO sample that will be tested is by-product from a fuming process, it is an impure zinc oxide source. Therefore, some of the zinc may remain undissolved. The extent of this problem will be determined by the experimental test work, and the recoveries obtained will be the determining factor which will classify this as being a problem for the process or not.

Since the impurity content of the zinc oxide sample is low (as is typical in the samples studied in the literature), it is unlikely that impurities will cause trouble with the leaching or downstream processes.

One possible problem with the processing of this material is the inconsistency of the supply. Since this is a by-product, only small amounts of this material are manufactured. This can limit the potential production from this source. To resolve this, blends with the Skorpion ore may have to contain larger quantities of the ore. Alternatively, it may be possible to blend multiple alternative feed stocks together with the ore to obtain the desired production.

2.4. Acid consumption

Skorpion's acid consumption is considered in a number of different ways. First, the total acid consumption for the leaching circuit is considered to determine the acid consumption of the overall leaching process. Next, the gangue acid consumption is determined, so that the amount of the total leaching acid consumed by the gangue elements can be quantified. Since the SX circuit regenerates all zinc-related acid consumed in leach, this zinc acid is the acid which is really consumed and will need to be replaced to maintain an acid concentration high enough to dissolve the zinc in the ore.

Finally, the net acid consumption is considered. This takes into account the acid which is consumed for gangue leaching as well as the acid consumed during the filtration of the residue on the residue belt filters (RBF's). Residue on the filters is washed with an acidic solution to recover all remaining soluble zinc from the residue. In the process, some of the acid remains behind in the residue.

Based on the model constructed for the Skorpion feasibility project, the main acid consuming elements in the Skorpion circuit are calcium (as calcite), iron and manganese (de Wet, 2000). These elements are found in their oxide forms in the calcium ore, and exist in similar forms in the secondary zinc oxides. Thus, it will be assumed that the elements existing in similar phases will have similar effects on the acid consumption. One of the main reactions that takes place during leaching is the reaction of calcite with sulphuric acid (Reaction 25):

$$CaCO_{3(s)} + H_2SO_{4(aq)} \rightarrow CaSO_{4(aq)} + CO_{2(g)} + H_2O \qquad \text{Reaction 25}$$

Reaction 25 takes place at all temperatures and sulphuric acid concentrations, increasing the acid consumption (Cruells, *et al.*, 1992). In addition, this reaction takes place preferentially over the other leaching reactions associated with EAFD, dross or ash and zinc oxides, so it will be the main acid consumer (Kukurugya, *et al.*, 2015). Sometimes, zinc secondaries may contain calcium compounds, such as $Ca[Zn(OH)_3]_2{\cdot}2H_2O$, which will also react with the acid and increase acid consumption (Reaction 26) (Cruells, *et al.*, 1992):

$$Ca[Zn(OH_3)]_2 \cdot 2H_2O_{(s)} + H_2SO_{4(aq)} \rightarrow CaSO_{4(aq)} + 2ZnSO_{4(aq)} + 8H_2O \qquad \text{Reaction 26}$$

Gangue acid consumption will be affected by all non-zinc elements contained in the secondary oxide. Due to the nature of the process that EAF dust is manufactured from, this dust contains a considerable amount of iron, often in the form of haematite and magnetite, which will react with the acid as follows (Reaction 27 and Reaction 28) (de Wet, 2000):

$$Fe_2O_{3(s)} + 3H_2SO_{4(aq)} \rightarrow Fe_2(SO_4)_{3(aq)} + 3H_2O \qquad \text{Reaction 27}$$
$$Fe_3O_{4(s)} + 4H_2SO_{4(aq)} \rightarrow FeSO_{4(aq)} + Fe_2(SO_4)_{3(aq)} + 4H_2O \qquad \text{Reaction 28}$$

Some manganese is present in an oxide form in some of the secondary oxides. The reaction of manganese with acid can be seen in Reaction 31:

$$MnO_{(s)} + H_2SO_{4(aq)} \rightarrow MnSO_{4(aq)} + H_2O$$ Reaction 29

Since the gangue acid has the greatest impact on the overall acid consumption, the amount of gangue contained in the solid feed to circuit, and the solubility of the gangue element phases, will have a significant impact on the acid consumption in the Skorpion refinery. Factors that increase the amount of gangue dissolved will drive up the acid consumption in the circuit as well.

2.5. Impurity effects on leaching and downstream processes

The electrowinning process used by Skorpion Zinc to recover elemental zinc from electrolyte is a very sensitive process. Solvent extraction is used as a barrier against impurities from the leaching section. It is therefore very important to ensure that the SZ SX section can treat the leach solution generated using alternative zinc oxides. At this stage, Skorpion aims to obtain a PLS solution, after neutralization, containing the following concentrations of impurity elements (Table 6):

Table 6. PLS specifications for solvent extraction stage.

Element	Concentration unit	Average concentration	Concentration range
Zinc	g/L	30	38-35
Aluminium	g/L	0.3	<0.5
Iron	ppm	5	<10
Silicon	ppm	40	<60
Magnesium	g/L	2	<3
Manganese	g/L	0.5	<2
Potassium	g/L	0.3	<0.5
Copper	g/L	0.7	<1
Cobalt	g/L	0.1	<0.2
Nickel	g/L	0.8	<1
Cadmium	g/L	0.1	<0.5
Chlorine	g/L	0.5	<10
Fluorine	g/L	0.2	<0.5
TSS	mg/L	<10	<25
Sulphates	g/L	50	40-60

Certain elements associated with secondary zinc oxides have never been found with the Skorpion ore. For this reason, there are no limits set on the concentrations of these impurities, which the solvent extraction and electrowinning sections are capable of coping with. To demonstrate the importance of impurity concentration limits, the effects of the different impurities on SX and EW (the downstream processes) have been investigated. The following sections give a brief overview of the potential effects that these impurities could have in the downstream sections.

2.5.1. Aluminium

Aluminium in electrolyte causes changes to the morphology of the zinc cathode, causing larger grain sizes and therefore a coarser cathode deposit (Fukubayashi, 1972). In addition, aluminium can form

complexes with fluorides, allowing these ions to be transported through the SX circuit, so that they enter electrowinning, where they do damage to the surface of the aluminium cathodes.

2.5.2. Calcium

Significant calcium concentrations (>500 ppm) in the PLS can lead to scaling of process equipment. This can be particularly detrimental in solvent extraction and EW sections, where equipment units must be taken offline to be cleaned. With the sensitivity of both these sections to process upsets, it is undesirable, but not unmanageable to have high calcium concentrations (Sinclair, 2005).

More importantly, high calcium content in the PLS is an indication of large amounts calcium having been leached. This causes excessive acid consumption in the leaching section, but cannot really be controlled other than by monitoring the ore feed. Large amounts of calcium (>4%) in the leach feed solids stock has caused the Skorpion leaching tanks to overflow in the past. This is due to the large amount of gas generation caused by the reaction of the large amount of calcium with sulphuric acid in the leachant:

$$Ca + H_2SO_{4\,(aq)} \rightarrow CaSO_4 + H_2 \qquad \text{Reaction 30}$$

Most of the calcium in process solutions is removed in the neutralization step, so that the calcium can be removed from the circuit via the residue solids or tailings, and by the ETP bleed stream.

2.5.3. Copper and Nickel

The presence of nickel in the cell house electrolyte in quantities exceeding 200 ppb can cause dissolution of the plated zinc and decrease the current efficiency (Fukubayashi, 1972). Dissolution can cause large quantities of hydrogen to be emitted. This presents an extreme fire and explosion risk in a zinc tank house.

$$Zn + H_2SO_{4\,(aq)} \rightarrow ZnSO_4 + H_2 \qquad \text{Reaction 31}$$

Copper has a lower overpotential than zinc and therefore plates preferentially to zinc. In addition, because copper lowers the hydrogen overpotential, hydrogen is released and the current efficiency will be slightly reduced (Sinclair, 2005).

Carryover of these elements to the electrolyte is via physical transfer (entrainment of PLS in organic) across SX. Both elements are removed by their respective impurity cementation plants, by treating a constant bleed stream of PLS. This prevents impurity build-up in the leaching circuit.

2.5.4. Iron

During the SX extraction stage, iron is preferentially extracted, along with zinc, but unlike the zinc, it cannot be easily stripped off by the spent electrolyte. This means that the iron accumulates in the organic, limiting the amount of molecules available for zinc to bind onto. For this reason, an organic stream is bled from the storage tank and contacted with 6M HCl, which strips the iron from the organic (Skorpion Zinc Solvent Extraction Operational Manual, 2003). During this process, the HCl becomes deactivated and must be regenerated in Skorpion's HCl plant. Iron from the HCl plant is bled from the process via a small bleed to the effluent treatment plant.

In addition, any iron that enters the electrolyte en route to EW will cause reduced current efficiency by continuously being oxidised to ferric iron at the anode, and then being reduced to ferrous iron at the cathode (Sinclair, 2005). With electricity being one of Skorpion's major expenses, it is detrimental to the process for the iron in EW to increase above 1.5 g/l in solution.

2.5.5. Lead

Although the electrolyte entering the electrowinning circuit seldom contains large quantities of lead, lead-silver anodes are used for the electroplating process. Corrosion of these anodes by the highly acidic electrolyte solution introduces significant quantities of lead into the electrolyte in the form of $PbSO_4$. This lead phase is very sparingly soluble, forming a fine precipitate that remains in suspension in the solution.

During the plating process, the movement of zinc ions to the aluminium cathode traps the lead sulphate particles in the plated zinc matrix. The zinc that Skorpion aims to produce is classified as Special High Grade (SHG), with the specification that the zinc product should contain no more than 50 ppm total impurities, consisting of no more than 30 ppm lead, 10 ppm copper and 20 ppm iron, as well as small quantities of other metal impurities. Thus, the entrapment of lead in the plated zinc matrix results in zinc that does not conform to the SHG specifications. This results in reduced profit for the company.

Lead content in the feed solids to the leaching process should however not be a concern for electrowinning, as the lead should not be transferred across the SX circuit, and will therefore be removed from the process in the residue tailings and the ETP bleed.

2.5.6. Magnesium and manganese

Although neither of these impurity elements participates in the chemistry of the SX and EW sections (they cannot be extracted by the extractant in SX, nor do they plate in EW) they do have a detrimental effect on the performance of the EW section.

Magnesium increases electrolyte viscosity and density, limiting the maximum attainable zinc concentration and raising the cell voltage. Manganese on the other hand, although beneficial because it helps form a protective layer on the lead anode, also limits the maximum zinc content in the electrolyte (Sinclair, 2005).

These elements are removed from the process via the tailings or residue stream, in both the solids and the liquids, as well as via the effluent treatment bleed (ETP).

2.5.7. Silica

When silica is dissolved during leaching, the silica in solution may lead to problems in the solvent extraction circuit. During the leaching process, if sudden pH changes are experienced, silica may leach as orthosilicic silica (H_4SiO_4). This form of silica is unstable in aqueous solutions and will decompose in aqueous solutions (Moradi and Monhemius, 2011), if the pH is extremely acidic (as is the case in weak acid leaching), to form silica:

$$H_4SiO_4 \leftrightarrow 2H_2O + SiO_2 \qquad \text{Reaction 32}$$

Silica will then precipitate as a polymer which can, under the right conditions, form hydrated gels, which cause problems with phase separation in the solvent extraction circuit (Sinclair, 2005).

2.6. Summary

Temperature and pH

Most of the literature regarding secondary zinc oxides suggests that increasing temperature will increase zinc recovery from the solid, while decreasing pH will have a similar effect. However, some sources suggest that it may be possible to obtain reasonable zinc recoveries from temperatures lower than 50 ˚C, and pH values higher than 1.8-1.85, which Skorpion uses as its current leach set points.

For these reasons, a lower temperature set point of 40 ˚C was selected. Zinc ferrites do not, based on the literature, seem to leach well at temperatures below 80 ˚C. Due to the difficulty in practically testing this high temperature set point, 70 ˚C was chosen as the upper temperature limit for the test work. To obtain a clear trend of the effect of temperature on leaching efficiency, a set point of 60 ˚C was also tested.

Most literature suggests that lower pH values would have a positive effect on the leaching efficiencies of secondary zinc oxides. For this reason, two lower pH set points (1.2-1.25 and 1.5-1.55) were chosen for testing. To see whether there would be any possibility of saving on acid costs, while maintaining good recoveries, a high set point of 2.1-2.15 was also chosen for testing.

To ascertain whether leaching at the standard Skorpion set points would be possible, all samples were also tested at a temperature of 50 ˚C and pH of 1.8-1.85. The temperature and pH factors were tested according to a full factorial experimental design.

Particle size

There is some difference between the different literature sources regarding the impact of particle size on the leaching efficiencies of the different oxide samples. Some sources reported that leaching efficiency improved at lower particle sizes, while others reported that there was no appreciable difference in the leaching recovery for different particle sizes.

Due to the practical fact that the alternative oxides were all already relatively fine, and the fact that there was no way to practically reduce the particle size of the samples to within a controlled size fraction, only three different groups of particle sizes were chosen for testing.

The first group was the “as received” particle size of the samples, where no changes were made to the sample. This sample was regarded as the “coarse” sample. Next, the sample was sieved to a size of 180 microns and all the oversize particles were pulverized. This was labelled as the “normal” size fraction sample. Finally, pulverizing the entire sample generated the “fine” sample. (More detail regarding the definitions of the relative particle sizes can be found in section 4.2, Table 15)

The results of the leaching of each of these three samples under the normal Skorpion operating parameters would allow for some assessment of the effects of particle size on the leaching efficiency of the various samples.

Solid/liquid ratio

Skorpion uses slurry containing 20% solids to feed the leaching process. It is possible to vary the solids content in the feed slurry, but it is impractical to feed a lower percentage solids into the circuit due to the hydraulic capacity of the circuit and the required residence time. For this reason, feed slurry solids content was only tested at 20, 30 and 40% solids content. This would allow for an understanding of the effect of feed slurry solids content on the leaching efficiency of each oxide.

Residence time

It is important to note that, although studies suggest that longer residence times will increase the zinc extraction, many studies also indicate that such long residence times will increase impurity extractions. In addition, in order to maximize leach throughput in the Skorpion plant, residence time cannot be extended significantly. For this reason, it suggested that the residence time remain fixed at the current operational value of 120 minutes.

3. Materials and methods

3.1. Experimental design

All experiments were performed using an Anaconda leach test procedure, based on Skorpion Zinc's actual process. Synthetic leach solutions were generated in the laboratory, to ensure that the composition of the lixiviant could be controlled.

3.1.1. Solid source

At the beginning of the project, several different potential material sources were identified as supplementary feeds to the Skorpion process. Based on many different economic factors, 3 different sources, with different mineralogies, were selected. The main factors used to screen the different sources included: location of supplier (i.e. transport distance to get the material to site), cost of material (waste materials are cheaper than by-products), additional processing required to make it possible to treat the material at the Skorpion site, zinc concentration in the material (higher concentrations require smaller volumes to be transported for the same amount of zinc) and impurity content (the Skorpion process has not been designed to handle certain impurities).

A mass balance was performed, using the average compositions of each of these sources (see Table 7), and combining the sources with different amounts of Skorpion ore. This allowed for the determination of the impurity limits on each of the different secondaries. In addition, this step was critical in determining the best way in which each of the chosen sources should be fed to the refinery. This mass balance will be addressed in Section 0.

Table 7. Solid compositions of the Skorpion ore and the three different alternative oxide samples tested.

	Skorpion ore	Zinc dross	EAFD	Zinc fume
Zn	9.0%	60%	30%	78%
Fe	2.0%	2.5%	13%	0.70%
Al	5.5%	6.6%	1.5%	0.10%
Ca	4.0%	1.0%	2.5%	0.15%
Cu	0.05%	0.10%	0.20%	0.15%
Ni	0.01%	0.15%	0.02%	0.00%
Si	26%	0.90%	1.8%	1.7%
Mn	0.32%	0.10%	1.0%	0.06%
Mg	0.61%	0.17%	1.3%	0.01%

The three different types of sources chosen were: an electric arc furnace dust, zinc dross (from a hot-dip galvanizer, which did not have the facilities to recycle this material within their own circuit, as Skorpion does with its zinc dross) and a natural state zinc oxide produced from a zinc smelter's furnace fumes.

3.1.2. Experimental strategy

Based on the literature reviewed, five factors were identified as having a potentially significant effect on the dissolution of the alternative zinc oxide sources consisting predominantly of zincite and zinc ferrite. These five factors were temperature, acid concentration (pH), particle size, agitation rate and solid-liquid ratio (pulp density). Due to the complexity of performing a full factorial design on a project with so many factors, some factors were only included on a partial factorial basis.

Since there are many factors that can impact on leaching kinetics with relation to agitation rate (e.g. the dimensions and shape of the container, the shape of the agitator blades, etc.), it was decided that this would not be one of the factors that would be varied during the experimental process. However, it was necessary to determine whether the agitation rate would have an impact on the leaching rate. For this reason, agitation rate was tested on its own, using a fixed temperature, pH, solid-liquid ratio and particle size. Several tests runs were performed and the results compared to determine whether there was an agitation rate beyond which agitation no longer affected the dissolution kinetics of the system. Factor settings for these experiments are shown in Table 8.

Table 8. Specifications for initial agitation rate tests.

Temperature (˚C)	pH	Stirrer rate (rpm)	% Solids
50	1.80-1.85	500	20
50	1.80-1.85	600	20
50	1.80-1.85	700	20
50	1.80-1.85	800	20

By varying the agitation rate, it would theoretically be possible to determine whether or not the process is diffusion controlled. If the rate of leaching continued to increase as the rate of agitation was increased, it could be speculated that diffusion is the rate-limiting step for the leaching reaction. In addition, using the results from these initial tests, the agitation rate that would be used for the rest of tests could be decided.

To see what impact particle size had on dissolution kinetics, 3 experiments were performed on the material – each with different particle size criteria. There was very little control over the particle size of the material received from the various suppliers and Skorpion did not have the facility to mill the material down to within a very narrow band of particle sizes. For this reason, the material was sorted into 3 large categories for the particle size tests: coarse, normal and large.

The particle size required for the leaching equipment at Skorpion's site is 180 um. For this reason, the particle sizes were defined around a P80 of 180 um. Thus, the coarse material band involved using the material as received from the supplier. Different materials had different particle sizes and this will be addressed in more detail in the sections dealing with the individual materials. For the normal particle size, the material was sifted to a 180 µm passing size. All oversized material was placed in a pulveriser for 10 seconds and the process was repeated until 80% of the total material had a 180 µm top size.

To obtain the fine material, all material was placed in the pulveriser for 10 seconds. After each 10 seconds, the coarse material (>180 um) was placed into the pulveriser again, while the fine fraction was removed. This process was repeated until all the material had a 180 µm top size. The tests performed are summarized in the table below:

Table 9. Summary of tests performed with different particle sizes.

Temperature (˚C)	pH	Stirrer rate (rpm)	% Solids	Particle size
50	1.80-1.85	700	20	Coarse
50	1.80-1.85	700	20	Fine
50	1.80-1.85	700	20	Normal

The intermediate or normal sample would be used for further test work, as Skorpion requires a D80 of no greater than 180 µm. Different solids contents were then tested at fixed temperature, pH, and agitation rates and with the normal size fraction. Table 10 shows the experimental conditions chosen for these tests.

Table 10. Summary of tests performed with different solids contents.

Temperature (˚C)	pH	Stirrer rate (rpm)	% Solids
50	1.80-1.85	700	20
50	1.80-1.85	700	30
50	1.80-1.85	700	40

20% solids was selected for the rest of the tests because of the fact that all equipment on the Skorpion site has been designed to operate with 20% solids. Massive re-design would be required to change the solids concentration at which the equipment would operate, and the company had elected to avoid incurring this expenditure, if possible.

A full factorial design was performed on the remaining factors: pH (acid concentration), temperature. These experiments were performed using the optimum agitation rate determined in the agitation tests, with a "normal" material size fraction and using 20 % solids. Temperature and pH were both varied at 4 different levels, according to a full factorial design. The 4 levels are represented as a low (L), intermediate (I), high (H) and extreme (E). The intermediate level set points correspond to Skorpion's operating conditions. These levels are shown in Table 11.

Table 11. Definitions of the 4 different levels chosen for experimental test work.

Level	Temperature (˚C)	pH	% Solids
Low	40	1.60-1.65	20
Intermediate	50	1.80-1.85	20
High	60	2.10-2.15	20
Extreme	70	1.20-1.25	20

The full factorial design for this project can be seen in Table 12. These experiments were repeated for each of the three different samples chosen for the test work. This was done in order to try and establish the differences in the response of the different materials that resulted from individual mineralogies. The mineralogical study was not performed in great detail, as there was no equipment available to examine the mineralogies closely. However, an attempt was made to understand some of the major differences in the reactions for the different samples.

This design is based on a four-level-two-factor factorial layout. All experiments- both screening and further experiments- were performed according to the experimental procedure discussed in section 3.4 (detailed experimental procedure can be found in Appendix C: Experimental procedure).

Table 12. Preliminary factorial design for experiments to be performed.

Experiment	Temperature (˚C)	pH	Experiment	Temperature (˚C)	pH
1	I	I	**25**	H	I
2	I	I	**26**	H	I
3	I	I	**27**	H	I
4	I	L	**28**	H	L
5	I	L	**29**	H	L
6	I	L	**30**	H	L
7	I	H	**31**	H	H
8	I	H	**32**	H	H
9	I	H	**33**	H	H
10	I	E	**34**	H	E
11	I	E	**35**	H	E
12	I	E	**36**	H	E
13	L	I	**37**	E	E
14	L	I	**38**	E	E
15	L	I	**39**	E	E
16	L	L	**40**	E	L
17	L	L	**41**	E	L
18	L	L	**42**	E	L
19	L	H	**43**	E	I
20	L	H	**44**	E	I
21	L	H	**45**	E	I
22	L	E	**46**	E	H
23	L	E	**47**	E	H
24	L	E	**48**	E	H

3.2. Experimental setup

Experiments for this project were conducted using a 5-litre tall form glass beaker of even diameter as a leaching vessel. No baffles were positioned in the beaker and a 50 mm 4 blade agitator was used for mixing. This agitator's blades were positioned at a 30-degree angle to the shaft. The agitator was positioned approximately 15 mm from the bottom of the beaker.

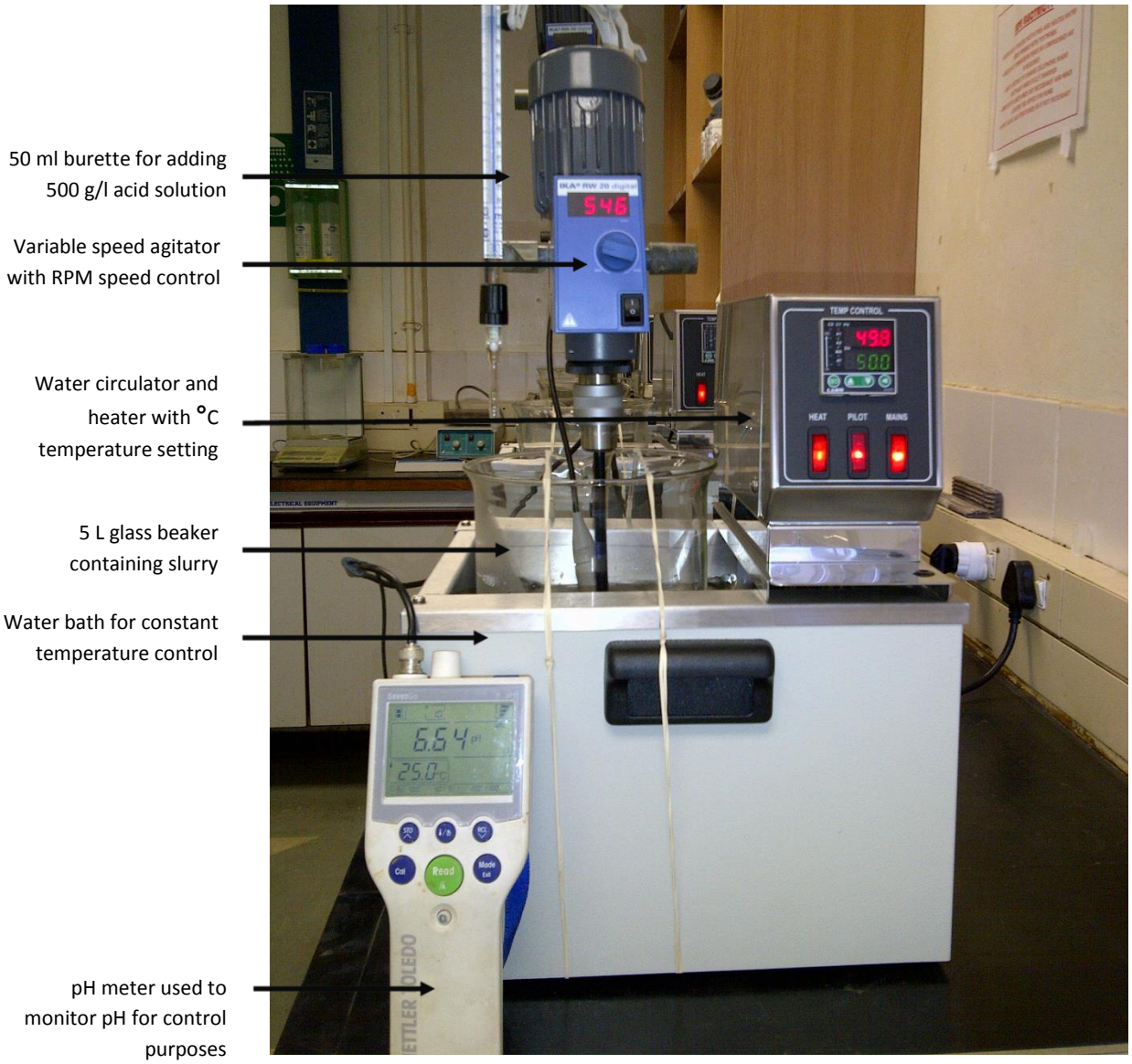

Figure 8. Photograph displaying experimental set up used for the project.

A variable speed agitator was used to rotate the blade at a fixed revolutions-per-minute rate, as set by the user using the speed adjustment knob. The beaker was placed in a water bath fitted with a water heater and circulator, which could be set to a range of temperatures.

The acid solution used to maintain the pH of the solution was placed in a burette, which was fitted over the edge of the beaker, using a burette stand, as shown in Figure 8. A portable pH meter was positioned so that its probe was at the furthest point away from the acid addition in the beaker, while being properly submerged in the slurry.

3.3. Resource requirements

Experimental equipment required to perform the experiments for this project included a 5 litre glass beaker, a 14 litre water bath with water circulator and heater, with temperature control varying between 30 and 100 ˚C, and a pH probe and meter. Due to the different temperatures investigated, the pH meter used had to have the ability to compensate for the effect of temperature on pH. In addition, an agitator with RPM speed controller and an agitator blade were required to perform slurry mixing throughput the course of the experiment. In this case, based on the resources available, a 4 blade agitator, 50 mm in diameter with 30 degree blades was chosen for the task.

For acid dosing, a 50 ml burette with Teflon tap and angled spout were used. Raffinate was added to the slurry using a 1000 ml cylinder, and all samples were taken using a 100 ml beaker attached to a rod for dip-sampling purposes. These small samples were filtered using a syringe and 0.45 micron micro filters. The final slurry was filtered using a vacuum pot, and compressor setup.

Synthetic solution makeup required the following reagents:

- Zinc sulphate heptahydrate
- 98% Sulphuric acid (analytical grade)
- Demineralized water

To ensure that sufficient quantities of these reagents were available to perform all the tests, 25 kg of zinc sulphate was obtained, along with 12 kg of sulphuric acid. Demineralized water was freely available on site, but because of varying water quality, control samples had to be submitted for each new demineralized water batch collected. All control samples showed that all dissolved salts were below the detection limits on the laboratory's ICP. Solid samples of the different zinc secondaries were obtained from each supplier selected independently. These samples required drying, in the on-site laboratory's oven, and pulverization, which was performed in the on-site laboratory's pulveriser.

Skorpion being equipped with a full-scale on site laboratory meant that all analyses could be performed on site. Liquid samples required ICP elemental analyses and acid titration to determine the amount of free acid present in the samples. For the analyses on the solid samples, a fume cupboard and acids were required, so that an acid digestion could be performed. The resulting solutions were then also analysed on the ICP.

Table 13. Resources required to execute the experiments detailed in the experimental methodology section.

Equipment	Reagents	Analyses
5 L glass beaker	Zinc sulphate heptahydrate	Acids for acid digestion
14 L water bath with heater	98% sulphuric acid	• Perchloric acid
pH probe and meter	Demineralized water	• Hydrochloric acid
50 ml burette	Solids samples	• Nitric acid
1000 ml glass cylinder		ICP analysis
100 ml glass beaker		Acid titrator with NaOH
Agitator and blade		
Syringes and microfilters		
Drying oven		
Pulverizer		
Vacuum pot and compressor		

3.4. Experimental procedure

Skorpion Zinc uses a standardized procedure for all leaching experiments. To ensure that the results obtained from the leaching experiments for this project were comparable with the plant conditions and other leaching tests performed for this company in the past, this procedure was used for all test work performed.

Before starting the experimental work, all the solids had to be prepared for use. This preparation involved sifting out the particle size fraction greater than 180 µm in size, and pulverizing this size fraction until all solids had a P80 of 180 um. In addition, due to the varying moisture contents of the different materials, all solids had to be dried in a laboratory oven at 50 ˚C for 2 days or until no more change in mass was detected. This was done before the PSD was addressed, as moisture in the material would cause clumping of the solids during pulverisation.

The experiments performed required the addition or use of different solutions, including synthetic raffinate and 500 g/l acid solutions. For ease of operation, these solutions were prepared before commencement of the experiments. The procedures for preparing each of these solutions are detailed in Appendix C: Experimental procedure, along with the detailed experimental procedure.

Once both the synthetic samples and the solid had been prepared, 136 g of the solid sample was weighed out. The water bath was set to the desired temperature and allowed to warm up. In the meantime, 500 ml of demineralized water was measured out into a 5 litre glass beaker. The beaker, containing the demineralized water, was placed inside the water bath and allowed to heat to the required temperature.

The pH probe was calibrated, and once the demineralized water in the beaker had reached the desired temperature, the agitator was started at a low speed (approximately 200 rpm). Slowly, the solids were added to the demineralized water. After waiting for roughly 5 minutes for the temperature to return to set point, the pH of the starting slurry was measured. A timer was then started and raffinate added in small batches (20-50 ml at a time) for the next 15 minutes, until the pH was relatively stable around the desired set point.

Hereafter, the 500 g/l synthetic acid solution was added to the beaker to maintain the pH within a 0.05 range around the desired pH set point. The slurry was allowed to react for the next 120 minutes, while adding the 500 g/l acid solution. Samples were taken at intervals of every 10 minutes for the first 60 minutes of the experiment. Thereafter, sampling intervals were changed to every 20 minutes, as it was reasoned that the reaction would have slowed down at this point. Samples were filtered through a syringe filter and the solutions submitted for analyses.

After the full 120 minutes reaction time, the final slurry was filtered in a vacuum filter pot. Filtrate was collected, weighed and the volume measured, then submitted for analysis. The remaining solids were washed with a pre-prepared pH 2 solution to remove all remaining soluble zinc. Residue solids were then weighed and dried to establish moisture content before submitting the solids for analysis.

The following analyses were performed on the samples collected:

- **Moisture analysis** – performed on solid feed and residue samples

  Samples were placed in an oven at 70 ˚C for 24 hours. The samples were then removed from the oven, weighed and placed back in the oven. After an additional two hours, the samples were once again removed and weighed.

  This weight was then compared to the weight recorded after 24 hours. If no weight discrepancy was noted, the sample was deemed dry. If a different mass was observed, the sample was placed I the oven for an additional 2 hours, and the process repeated until no mass change was observed. Moisture was determined using the following formula:

$$Moisture\ (\%) = \frac{Wet\ mass - Dry\ mass}{Wet\ mass} \times 100$$

- **Particle size distribution** – performed on solid feed and residue samples

  These analyses were performed using a combination of wet screening and the Malvern particle size analyser available in Skorpion Zinc's on-site laboratory.

- **Free acid determination** – performed on all solution samples

  Free acid analyses were performed using the Metrohm potentiometric auto-titrator in Skorpion's on-site laboratory.

- **Elemental analyses** – performed on all solution samples

  All solid and liquid samples should were analysed for the elements shown in Table 14.

Table 14. List of elements for analysis of solid and liquid samples from leach test.

Al	Ca	Cd	Co	Cu	Fe	K	Mg	Mn	Na	Ni	Pb	Si	Zn

Elemental concentrations were determined using inductively coupled plasma optical emission spectroscopy (ICP-OES) in Skorpion's laboratory.

4. Experimental results and discussions

4.1. Agitation tests

The effect of agitation rate on zinc dissolution was briefly examined. This was done with the main objective of determining whether there was an optimum agitation rate, or a rate beyond which zinc dissolution was no longer impacted by increasing mixing speed. This optimum or minimum required agitation rate could then be used in all further experiments to eliminate the effect of agitation rate on the system.

The results of varying agitation rate on zinc dissolution at different residence times throughout the course of the experiment are shown in Figure 9.

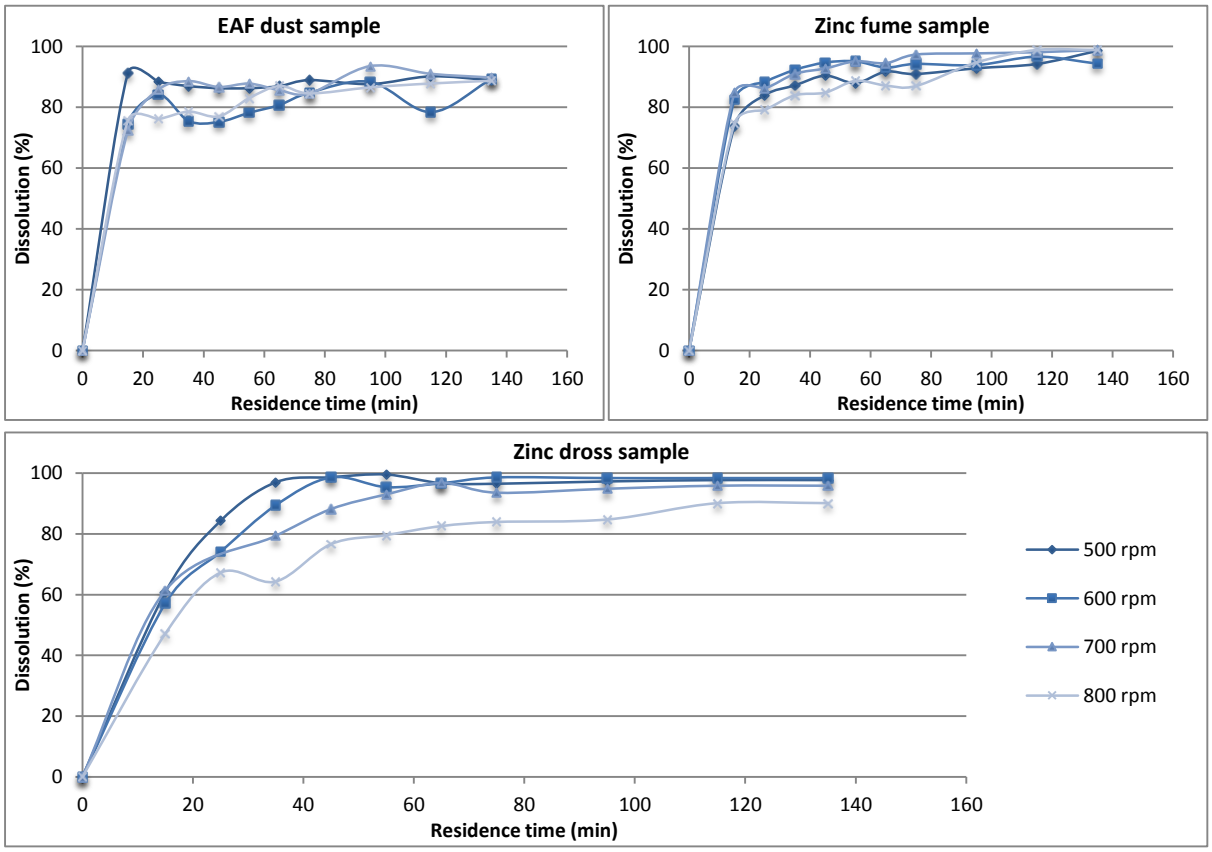

Figure 9. Graph values showing a comparison of the effect of increasing agitation rate on zinc dissolution for different samples.

Examination of this figure shows that the zinc dross sample's zinc dissolution does not seem to be significantly impacted by the agitation rate at any residence time. The decrease in zinc dissolution at 800-rpm for this sample can be explained by the fact that the high agitation rate created turbulence in the leaching vessel, which caused some of the slurry to splash up onto the sides of the container, where the solids remained. Solids being stuck to the sides of the container resulted in a lower overall recovery, as these solids had less contact time with the solution and did not leach properly. A similar effect was also observed with the other two samples at 800-rpm agitation speed.

The zinc oxide sample obtained from smelter fumes does not seem to experience significantly higher zinc dissolution as agitation rate is increased from 500- to 600-rpm and to 700-rpm. The overall dissolution achieved after 135 minutes varied between 94 and 98% for the different agitation rates. This seems to suggest that the agitation rate may not have a notable effect on the overall zinc recovery from this particular solid sample. It is possible that the residence time is long enough that the sample can leach fully before the 135 minutes is complete.

Unlike the other two samples, the EAF dust does not seem to consistently suffer lower recoveries at 800 rpm, despite the fact that some splashing of the sample was observed at this speed. In addition, this sample generally seems to experience higher recoveries at 500 rpm for residence times lower than 135 minutes. However, this sample's overall zinc recovery does not seem to be severely impacted by agitation rate, as the zinc recovery at 135 minutes is similar (less than 1% difference) for all agitation rates. It is unclear why the 500-rpm speed seems to provide higher initial recoveries at the shorter residence times.

Due to the splashing observed at 800 rpm, it was decided not to run higher than 700-rpm agitation speeds. However, due to the general increase in leaching rate for zinc fume and EAFD between 500 and 700 rpm, it was decided that the maximum possible agitation rate should be used. Thus, all further test work was performed at 700-rpm agitation rates. The apparent independence of the zinc dross sample's zinc dissolution from agitation rate seems to suggest that this particular dissolution reaction is not diffusion rate controlled. On the other hand, the zinc fume oxide seems to be initially diffusion controlled (recovery increases with increasing agitation rate in all but the very last residence time period selected).

These agitation tests were not designed to mimic the agitation effects in the Skorpion refinery, as there are many variables which impact on the effect that agitation rate has on the leaching of solids. Since this project was not aimed at creating an exact replica of the Skorpion refinery, but rather at attempting to understand how to leach the alternative oxides in the refinery, agitation tests were designed to see whether the effect of agitation on the leaching could be limited. This would allow for a better representation of the effects of the other factors on the leaching of the solids. It should be noted that these tests were limited by the physical observations and by the equipment used for the experiments as well as the results of the experiments. As such, the effect of agitation on the different tests could not be completely removed.

4.2. Particle size tests

The particle size distribution for the normal, coarse and fine particle sizes of the different zinc secondaries solid feed samples can be seen in Table 15.

Table 15. Summarized particle size distributions for each of the different particle size groupings for the different feed solid samples.

	P10 (um)	P50 (um)	P80 (um)	P90 (um)
Zinc dross				
Coarse	11	209	586	851
Normal	4	72	172	242
Fine	5	151	391	550
EAFD				
Coarse	1	24	379	671
Normal	2	41	264	465
Fine	1	3	38	87
Zinc fume				
Coarse	9	603	1074	1336
Normal	1	22	193	256
Fine	1	8	101	232

It can be noted from the table above that, although the entire sample has been pulverized to obtain the fine zinc dross sample, the fine sample has a larger size than the normal distribution (where only the coarse size fraction is pulverized). This may potentially be attributed to the nature of the zinc dross. Milling the impure dross from the furnaces in a ball mill is the process typically used to refine zinc dross. Metallic particles in the dross are flattened, rather than ground, increasing the perceived particle size (de Walens, J., 2002).

The finer dust component of the zinc dross also contains some very small metallic zinc particles, and some oxidized zinc. These fine zinc particles may be flattened during the pulverization process (much like the formation of prills for larger particles), causing the particles to increase in size.

Very little difference between the zinc fume's normal and fine size groupings could be seen. However, the coarse size fraction was notably larger than the normal and fine fractions. This may be in part due to the very high moisture content of this material when it was received. The high moisture caused the particles to agglomerate, forming larger particles. Although the material was dried before being leached, the coarse sized fraction was not pulverized or milled after drying. Thus, the agglomerated particles cause the PSD to be somewhat overstated. However, the drying process did seem to lend some structural stability to these particles, which did not break apart a great deal during leaching.

Table shows the particle size distribution of the various solid residues following leaching with synthetic raffinate solution. As expected, there is a general reduction in particle size across the board. However, in some cases, the 10% passing and 50% passing sizes have increased. This may be a result of the reduction in diameter of the particles in larger size fractions. As leaching takes place, these particles decrease in size, causing them move into a different size fraction group.

Table 16. The particle size distributions of the residue obtained from the experiments performed on each size grouping for each of the different zinc secondaries samples.

	P10 (um)	P50 (um)	P80 (um)	P90 (um)
Zinc dross				
Coarse	17	191	446	642
Normal	1	3	7	31
Fine	2	39	190	320
EAFD				
Coarse	2	44	239	408
Normal	1	7	101	249
Fine	1	4	28	62
Zinc fume				
Coarse	1	105	393	618
Normal	1	3	13	60
Fine	1	3	8	37

One noteworthy observation regarding the zinc dross sample is that the normal size fraction experienced the largest reduction in particle size. During the pulverization process, it was noted that the zinc dross formed what appeared to be larger flakes of metallic zinc after being pulverized. This will be discussed in the following section.

4.2.1. Zinc

The dissolution of zinc in each of the different zinc samples, using different particle size distributions is shown in Figure 10.

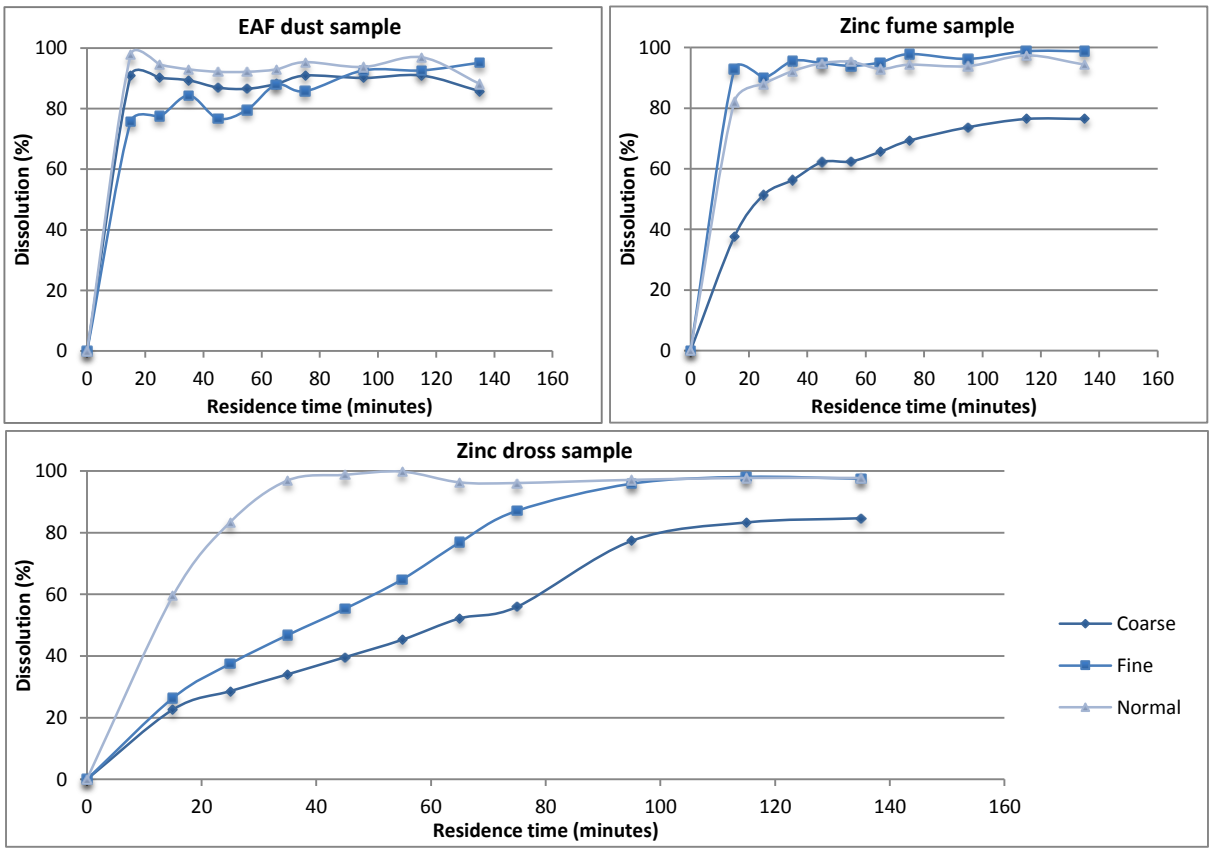

Figure 10. A comparison of the effect of different particle sizes on zinc dissolution for different zinc secondary sources.

The zinc fume sample experienced higher zinc dissolution for the finer particle size fraction than for the coarser size fractions. In a similar way, the normal size fraction had higher zinc dissolution than the coarse size fraction.

It is not entirely clear why the overall dissolution for the coarse size fraction is lower for the zinc fume and dross samples. Since the system achieves equilibrium in the residence time used, it was expected that overall recovery would be the same. One possible suggestion is the fact that the zinc in contaminated ZnO from the fume dust, as well as zinc from the zinc dross sample, may be trapped in larger particles with impurity substances. When crushed, the zinc may then become exposed to the solution, allowing for leaching, while it is not exposed to the solution, if left in the coarse form. Fine particles have a greater overall surface area with which the lixiviant can make contact and therefore leaching kinetics would be expected to be faster.

On the other hand, the zinc dross and EAF dust samples both exhibit different behaviour to what was expected from the literature (Moradi and Monhemius, 2011). Instead of obtaining the highest and fastest zinc dissolution form the fine size fraction, the fine zinc dross sample initially experiences much slower kinetics overall than the normal size fraction. This can be attributed to the fact that the fine class actually contains larger particles than the normal class, as seen in Table 16. Thus, this in line with what was expected from literature (Moradi and Monhemius, 2011). The overall dissolution remains relatively close to the normal size fraction dissolution (97.8% final dissolution for the normal size fraction, versus 97.5% dissolution for the fine size fraction), which suggests that all size fractions are small enough for equilibrium to be achieved within the 120 minutes residence time.

The initial slow kinetics could potentially be attributed to the behaviour of the zinc dross sample during milling and pulverization. It is evident from Table that milling the solids to create the fine size fraction actually resulted in an overall increase in particle size for each size fraction. As stated in section 4.2, this may be due to the fact that zinc dross contains some metallic components (roughly 6-10% of the total mass). These metallic components will, during the pulverization or milling process, be joined together to form larger metallic particles. These larger particles will have a reduced surface area, relative to the original sample and may therefore have slower dissolution rates.

If the majority of the metallic components were originally in the finer size fractions of the zinc dross, milling only the coarser particles to produce the “normal” size fraction would not have resulted in so much melding together of the metallic components. This may explain why, despite the milling that is done to form the normal size fraction, this group has faster reaction kinetics than the coarse size group. No milling or pulverization is done on the coarse size group. From Table 16, it is clear that the coarse zinc dross group does have the largest particle sizes (P80 of 586 µm) of the three groupings. This large particle size will decrease the specific surface area of the particles in contact with the lixiviant, reducing the leaching reaction kinetics.

Based on literature (Su and Shen, 2009), it could be deduced that the coarse EAFD sample consisted of predominantly large spherical, difficult-to-leach zinc ferrite particles, to which the smaller, irregular zincite particles were fused. To form the “normal” EAFD sample, the fine particles were first removed. Since the smaller particles were seen to be predominantly zincite in literature (Suetens, *et al.*, 2015), it is assumed that the remaining coarse particles that were ground were a combination of the

franklinite and attached ZnO particles. Pulverizing this size fraction should have reduced the size of both the ferrites and the zincite particles. Thus, the “normal” sample should have had higher recoveries than the “coarse” sample, as was seen in the experimental results. This is once again due to the overall smaller particle size of the normal size fraction and the increased surface area associated with the smaller PSD.

However, contrary to literature (Moradi and Monhemius, 2011), the fine size fraction presents slower kinetics and lower overall recovery. Particle size distribution analyses presented in Table 16 show that this size fraction does indeed have a smaller size distribution than the other two size fractions, and should therefore have a larger surface area, increasing kinetics and dissolution.

Following the observations made by Suetens, *et al.* (2015), decreasing the particle size of EAF dust should break apart the clusters of smaller zinc-containing particles that dominate the larger size fraction of the EAFD. This would then increase the overall surface area of the zinc containing particles and lead to higher overall zinc recovery. This may explain why the normal size fraction experiences higher recoveries than the coarse size fraction – since only the oversized material is pulverized to reduce the size. In the case of the fine material, where the entire sample is pulverized, it is possible that the particles that do not contain zinc – in both the mid-range size fraction (40-250 microns in the Suetens, *et al.* (2015) study) and in the large size fraction were broken apart.

This may have provided a larger surface area for leaching of non-zinc containing components, leading to more competing reactions in the system. These competing reactions may have caused the sulphuric acid to become the limiting factor in the system and reduced the overall zinc recovery, while increasing the recovery of some of the other components contained in the EAFD sample.

The observations made by Kukurugya, *et al.* (2015) regarding the rate limiting step and the mechanism of leaching of EAFD may provide some explanations for the difference in leaching rates for different particle sizes of EAFD. Zincite leaching was found to be the first step in the leaching of EAFD, and was a diffusion-controlled step. Thus, reducing the particle size of the zincite should help increase the kinetics of the zinc leaching. However, franklinite leaching, the second step in EAFD leaching was chemical reaction controlled. Thus, decreasing the particle size of the franklinite particles to expose more surface area to the solution would not affect the leaching kinetics of this particular phase.

The “fine” EAFD sample studied in this set of experiments was generated by milling a split portion of the total raw EAFD received from the supplier. PSD analyses show that this process was successful in reducing the overall particle size of the material. It is therefore speculated that the fine sample was composed of a number of fine ZnO particles, whose size had been further reduced from the “normal” sample. These particles would have reacted faster than for the “normal” and “coarse” EAFD samples. Slag particles would also have been broken apart, potentially allowing other impurity elements contained in the slag to leach from the particles faster.

Finally, the franklinite particles in the “fine” EAFD samples would also have been broken apart, and would therefore have a larger surface area exposed to the solution. However, since the rate limiting step in this case is not the diffusion, but rather the reaction between the franklinite and the sulphuric acid, the act of reducing these particles’ sizes would not have resulted in an increased rate of reaction.

In fact, reducing the particle size of these particles may have introduced competing reactions for the ZnO particles, which would then limit the rate of reaction of the acid with these particles, despite their smaller size.

Comparing the zinc dissolution between the different types of zinc sources, one can see that the zinc dross sample has the lowest kinetics of the three different types of zinc sources for each size fraction. In contrast, the EAF dust samples have the highest kinetics for each size fraction. The slow kinetics of the zinc dross sample may be explained by the larger particle size of the zinc dross samples for each size fraction, as can be seen in Table 16. However, one exception to this observation exists: the coarse size fraction of the zinc fume sample is considerably larger (the P80 is 60% larger than the P80 for zinc dross) than the coarse zinc dross sample, yet the kinetics are slightly faster than those of the coarse zinc dross.

This can possibly be due to the fact that the very large particle size of the coarse zinc fume sample is predominantly a result of the very high moisture content of the original zinc fume sample (~7% moisture). Higher moisture caused the particles of the zinc fume sample to clump together as larger particles, while drying these particles then reinforced the agglomerates.

Since these coarse particles were not really singular large particles, when added to water, they started to break apart, exposing larger surface area to the solution and allowing faster reaction. However, complete separation of the agglomerated particles probably did not occur, as the residue size PSD shows that the particles were still quite large upon completion of the test (P80 was 393µm). This may explain the faster kinetics than the zinc dross sample, despite larger particle size, while still explaining why the coarse sample had lower kinetics than the other zinc fume samples.

The faster kinetics of the EAFD may be explained by the fact that it has the smallest particles for each size grouping, except the normal group, where the zinc fume is smaller (P80 of 465µm for EAFD, versus 256 µm for zinc fume). The slightly larger normal particle size distribution of EAFD may also explain why the normal size samples for EAFD and zinc fume have similar kinetics.

Overall zinc dissolution was slightly higher for the zinc dross sample of each size fraction, while the EAF dust had the lowest overall zinc dissolution for each size fraction. The lower dissolution of the EAFD zinc may be explained by the composition of the EAF dust. Zinc in EAFD dust is present as metallic zinc, zinc oxides and some ferric zinc. Typically, ferric zinc is difficult to recover and is normally leached at high temperatures or low pH values (or high pressures). Thus, it is possible that the conditions used for these tests (50 ˚C, pH of 1.8-1.85 and atmospheric pressure) were insufficient to recover the majority of the zinc contained in ferric zinc forms.

Zinc dross, on the other hand, consists mostly of zinc in metallic forms, along with zinc oxides (mainly in the zincite form, or in complexes with other metals). While zincite leaches relatively quickly, elemental zinc takes longer to leach. Reaction rates of the various complexes are difficult to define, as the reaction rates are heavily dependent on the complexes' structure, but it is likely that the complexes will leach more slowly than the zincite. It is therefore understandable that the zinc dross/ash sample has the slowest kinetics of the three samples, for all particle sizes.

Given that the zinc contained in the natural state zinc oxide from fuming is contained chiefly in a zincite phase, it is expected that it would experience the fastest leaching kinetics. However, it was difficult from these experiments to ascertain whether this sample or the EAFD had the faster kinetics for the fine and normal samples. Due to the very large size of the zinc fume particles in comparison to the EAFD particles, the coarse zinc fume sample leached much slower than the EAFD sample.

The higher overall recoveries obtained for the fine and normal zinc fume samples can be related to the composition of the zinc fume. While this sample contains mainly ZnO, which is easily leached, the dross/ash and EAFD samples contained metallic zinc and zincite respectively – both of which are more difficult and time-consuming to leach at the given operational conditions.

4.2.2. Aluminium and iron

The behaviour of aluminium in the different secondaries samples using different size fractions can be seen in Figure 11.

Zinc dross formed in a hot dip galvanizing bath consists of large quantities of aluminium and zinc (40-70% zinc and 5-7% aluminium). This is due to the fact that the galvanizing bath consists of molten zinc and a small amount of molten aluminium, which assists with the coating process. Since both of these elements exist in a molten metal state in the galvanizing bath, the dross contains both metallic zinc and metallic aluminium.

Due to the similarity of the states of these two metals, it can be deduced that the aluminium and zinc will behave in a similar manner in the dross sample. This is indeed the case, as the fine sample has slightly reduced reaction kinetics, but similar overall aluminium dissolution (69.9% dissolution in the fine sample, in comparison to 67.5% dissolution in the slightly coarser normal fraction). As with the zinc, this can potentially be explained by the increase in particle size in the fine fraction, due to agglomeration of the metallic particles in the fine size fraction of the zinc dross.

Once again, the coarse size fraction has vastly reduced kinetics and overall dissolution (52.0% dissolution). This may be explained by the reduced surface area for reaction, due to the larger particle size.

The zinc fume sample once again behaves as expected from literature (Moradi and Monhemius, 2011). The coarse size fraction has lower overall dissolution of aluminium (40.4%) and slower kinetics than the other two samples. On the other hand, the fine sample has the best overall dissolution (56.0%) and reaction kinetics that are very similar to the normal size sample, although slightly faster, especially near the end of the experiment.

The aluminium in EAF dust exhibits slightly different behaviour to that of the zinc. Here, the coarse size fraction has the fastest reaction kinetics and highest overall dissolution (50.2%), while the fine sample has the lowest dissolution (30.7%) and slowest kinetics. Comparing the dissolution of aluminium in the different feed solids to one another, it is evident that the zinc dross again has the slowest kinetics for each size group. The reduced reaction kinetics of the zinc dross may again be attributed to the larger particle size of this particular solid source.

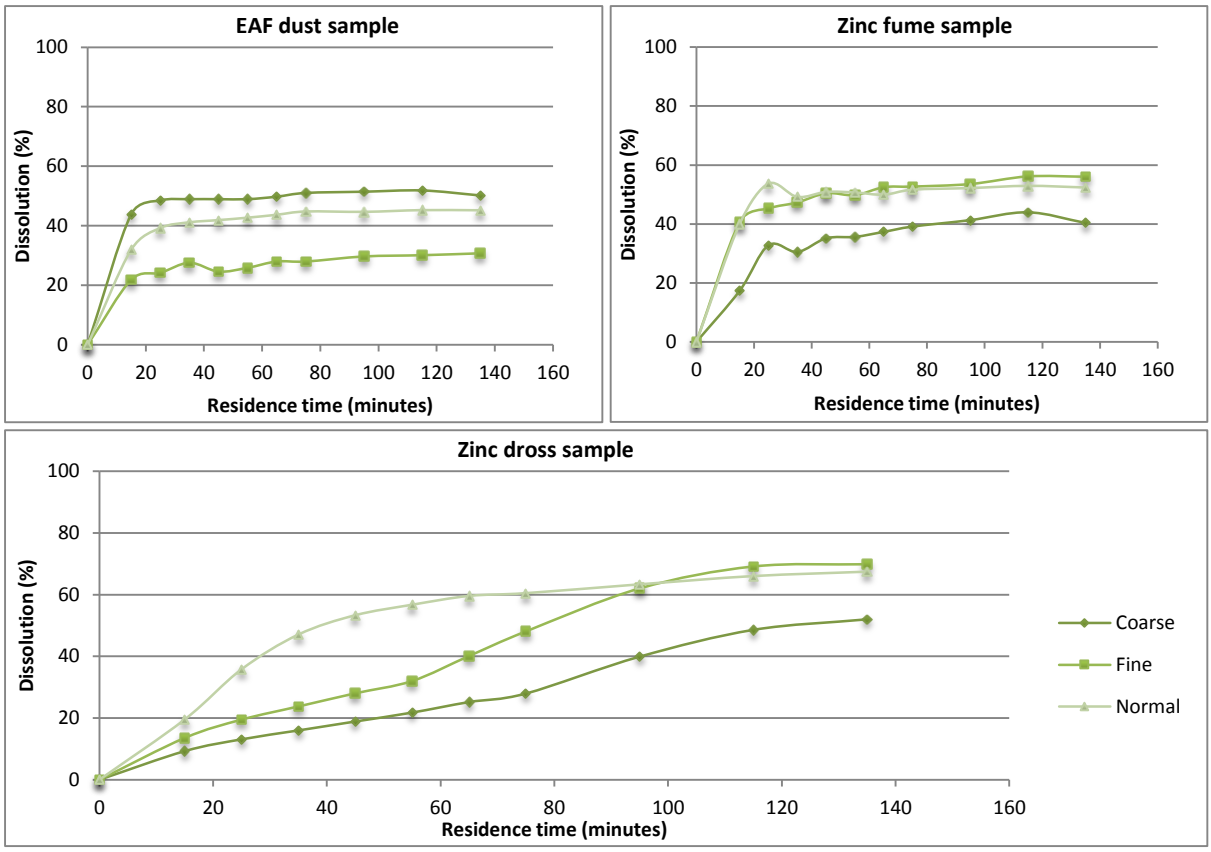

Figure 11. A comparison of the effect of different particle sizes on the dissolution of aluminium in different zinc secondaries.

Using the data in Figure 12, which shows iron dissolution for the different source samples, using different particle size groups, it is clear that the EAF dust sample has the lowest overall iron dissolution for each size sample. If the iron is present predominantly as ferric zinc, it may be difficult to leach under the conditions used for these experiments, causing a lower overall dissolution. In addition, the coarse size sample has the highest dissolution and fastest kinetics, while the fine sample has the worst dissolution and slowest kinetics in the EAFD case.

The zinc dross sample once again experiences the lowest dissolution and slowest kinetics for the coarse sample, with the fine sample having slower kinetics than the normal sample. However, in this case the overall dissolution for the fine sample is considerably lower (64.0% versus 85.2%) than the overall dissolution for the normal sample.

Iron dissolution for the zinc fume samples behaves as expected – smaller particle size results in faster kinetics and better overall dissolution. This is again due to the increased surface area available for reaction.

Overall iron dissolution is highest in the case of the zinc dross sample (normal size distribution). The reason for this high iron dissolution from the zinc dross relative to the dissolution from the zinc fume and EAFD samples may lie in the way in which iron is included in the sample. Research suggested that the iron in the zinc dross and fly ash samples formed complexes with the zinc components of the oxides (Bahram, *et al.*, 2013).

This seemed to be mainly because of the fact that the iron dissolved into the molten zinc during the galvanizing process. EAFD contains iron as either separate oxides, such as haematite or magnetite, or as part of the zinc ferrite phase, which is very stable and difficult to leach due to the stable nature of the ferrite.

Zinc fume contains iron in separate oxide form, which leaches relatively easily. However, the large particle size of this sample relative to the other two may partially account for the relatively low iron dissolution. In addition, this sample contains considerably lower iron concentrations than the other 2 samples, because it does not come from a ferrous-metal based source. This may also contribute to the lower overall iron dissolution.

Once again, the zinc dross sample has a higher dissolution rate at the normal size distribution than at the fine, with the coarse distribution being the slowest, and leaching the least iron. If the theory regarding metallic components holds true for zinc and aluminium, it may be applicable to iron too, because the iron will be combined with the zinc in most cases, due to the dissolution of iron that takes place in the melting bath.

The iron dissolution from the EAFD sample is highest for the coarsest sample and lowest for the fine sample. However, the overall dissolution only changes by roughly 3% from the lowest to highest dissolution. This seems to suggest that the dissolution of iron in the case of the EAFD is not controlled by the diffusion rate, but rather by the chemical reaction rate.

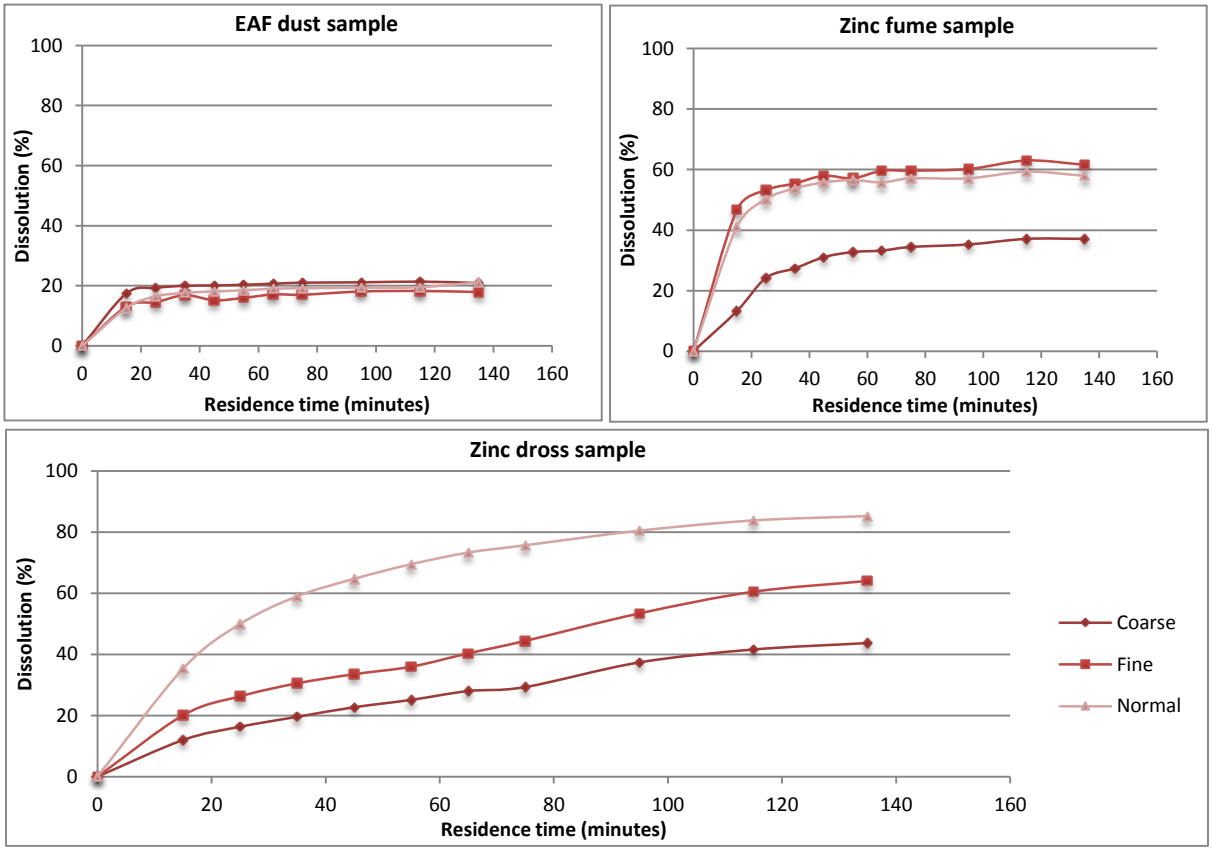

Figure 12. A comparison of the effect of different particle sizes on iron dissolution across different types of zinc secondaries samples.

4.2.3. Calcium

Figure 13 represents the dissolution of calcium in each size group sample, for the different source samples.

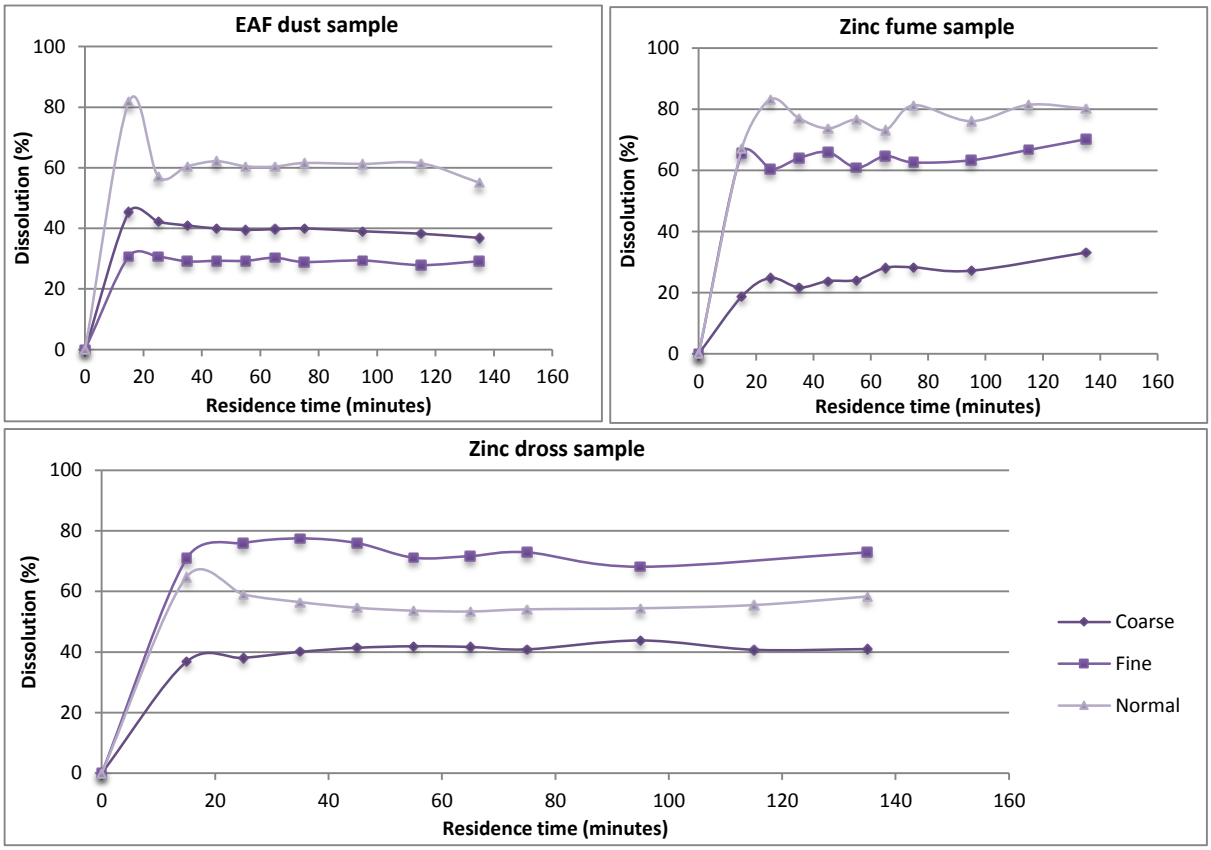

Figure 13. A comparison of the particle size effect on dissolution of calcium in different zinc secondaries sources.

Here, the zinc dross behaves as one would expect – the coarsest size group has the lowest overall dissolution and fastest kinetics, while the finest group has the best overall dissolution and fastest kinetics. This may be due to the fact that calcium is not present in the zinc dross in its metallic state (Shitov, *et al.*, 2005). Thus, when the coarser particles are milled, any calcium containing components are broken into smaller particles, which will have a larger overall leaching surface area.

On the other hand, the zinc fume sample exhibits better calcium dissolution in the normal size group than in the fine size group. The coarse size group still has the lowest overall calcium dissolution and slowest kinetics, as would be expected. Calcium dissolution in the EAFD sample is best for the normal size group, while the fine size group has the least calcium dissolution. This does not correlate with what would be expected based on results reported by Moradi and Monhemius (2011). In the case of EAFD, the reason for this may have to do with the fact that the calcium in solution (600 ppm) exceeds the calcium saturation limit (500 ppm). Thus, some of the calcium may start to precipitate out of solution, skewing the results and creating a false impression of what is happening in the system.

Zinc fume and zinc dross calcium levels are below 100 ppm and are therefore are not expected to precipitate.

4.3. Solids content

4.3.1. Zinc

Figure 14 shows the dissolution of zinc from the different source samples, using 20, 30 and 40% solids in the feed slurry.

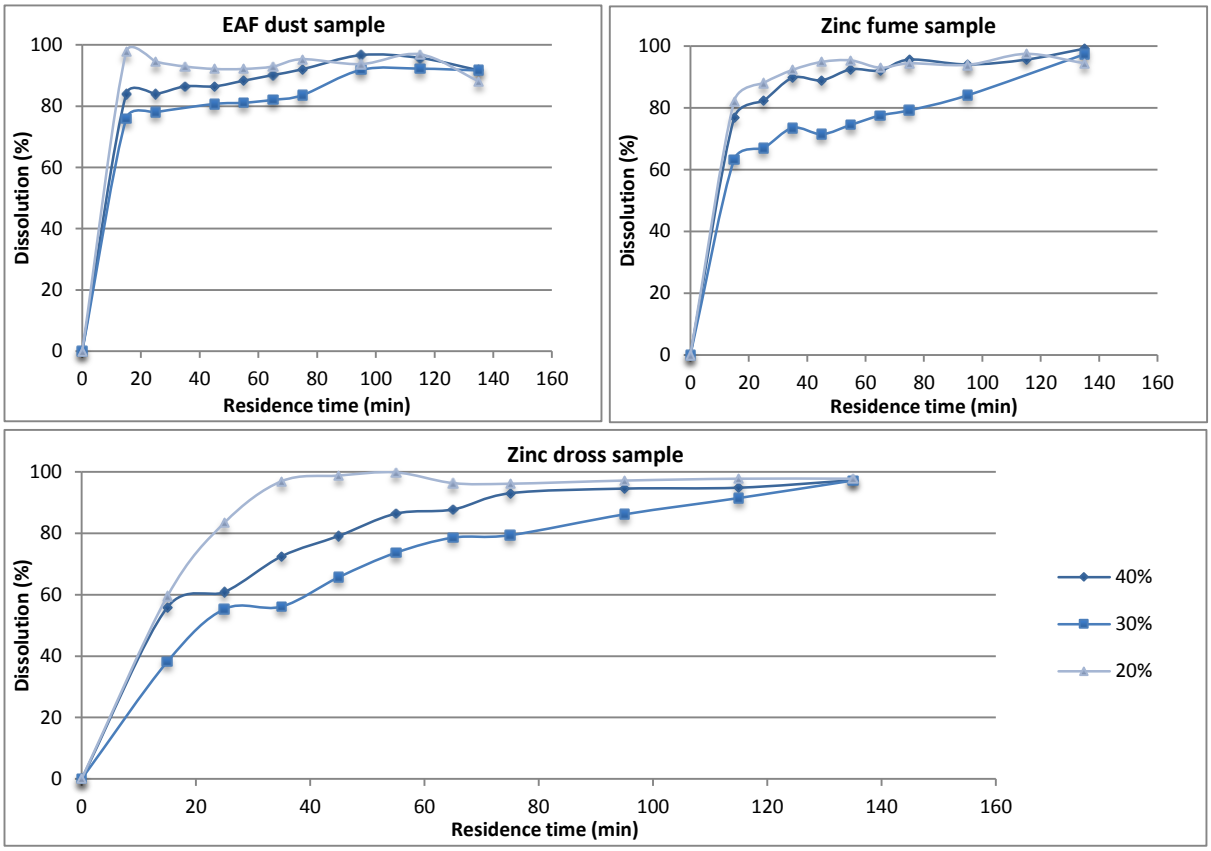

Figure 14. The effect of different amounts of solids on the dissolution of zinc in different zinc secondaries.

According to literature (Havlik, *et al.*, 2005), dissolution is inversely proportional to the solid-liquid ratio. Thus, it was expected that the 40% solids would provide the slowest kinetics, with 20% being the fastest dissolution.

All samples appeared to achieve similar overall zinc dissolution, indicating that equilibrium had been achieved in the system. In each case, the 20% sample experienced the fastest dissolution kinetics. The excess of lixiviant present at lower solid-liquid ratios can explain this. In addition, lower solid-to-liquid ratios will allow the solid particles to be completely surrounded by liquid, presenting a larger surface area for reaction.

However, in each of the cases presented in Figure 14, the 30% solids content test experiences lower and slower dissolution than the 40% solids tests. This can be supported by the theory that was put forward by Shawabkeh (2010), which suggested that higher solid-to-liquid ratios presented a larger overall solid surface area to the liquid, allowing better leaching kinetics. This theory is however flawed in that increasing the solids charge increases the amount of zinc in the circuit, as well as the total surface are. Thus, by reporting % dissolution, the mass leached has been normalized relative to the mass fed.

To maintain a constant pH in the system, acidic solution was constantly added to the system. This resulted in dilution of the solids in the circuit. Thus, the final solids content was not the same as at the start of the experiment. The actual final solids contents for the different experiments are shown in Table 17.

Table 17. Actual solids content in system after leaching has been completed.

	Initial solids content (%)	Final solids content (%)	
	Zinc dross	EAFD	Zinc fume
20	7	6	5
30	6	9	7
40	8	7	5

Using this final solids content, it is clear that the 30% solids content sample for the EAFD actually has the highest solid to liquid ratio. This explains why the kinetics of dissolution are slower for this sample than for the 40% sample. A similar situation applies for the zinc fume sample.

4.3.2. Aluminium and iron

From Figure 15 it is possible to see the effect of slurry solids content on the dissolution of aluminium from the different source solid samples.

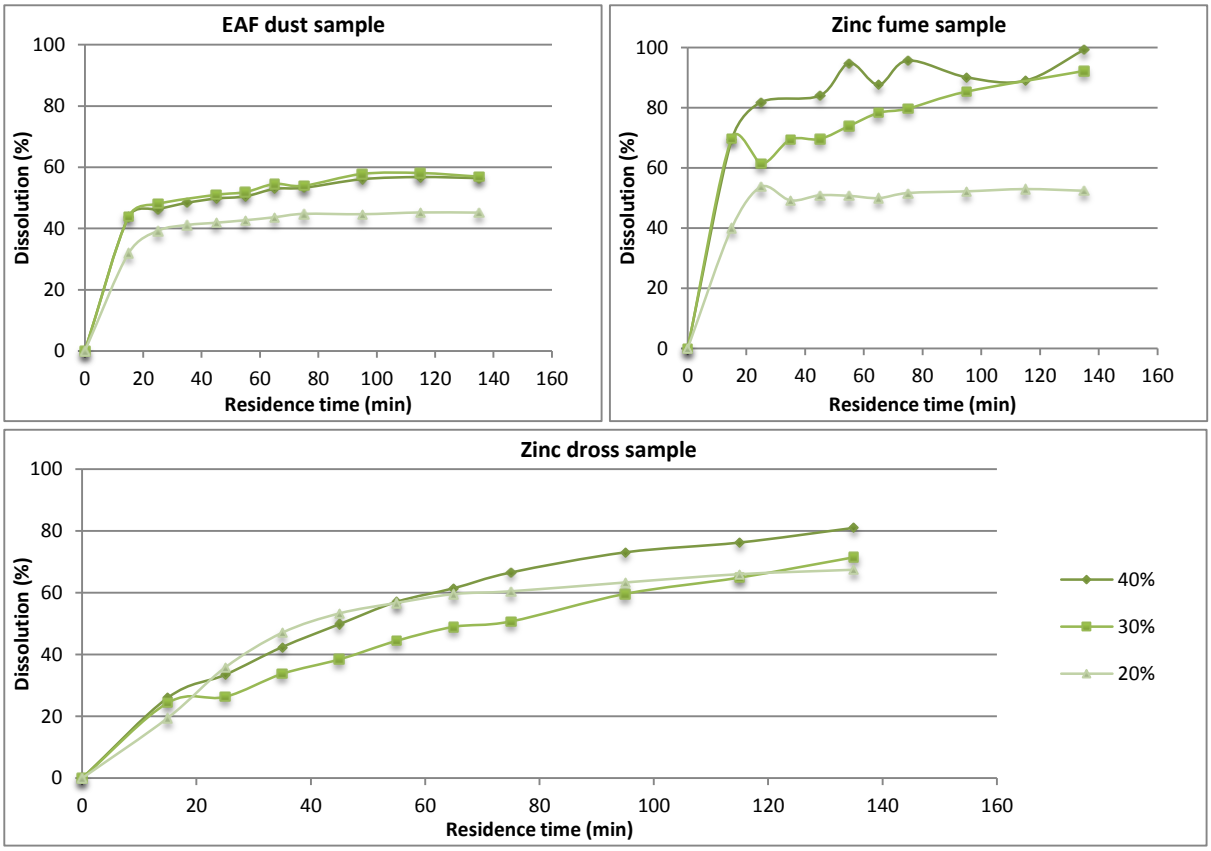

Figure 15. The impact of slurry solids content on aluminium dissolution in different sources of zinc secondaries.

It is evident from this figure that both the EAF dust sample and the zinc fume sample experience increasing aluminium dissolution and faster aluminium dissolution kinetics with increasing solids

content in the starting slurry. This can be explained by the final solids contents, after leaching has been completed.

However, the zinc dross does not follow the same trend. Instead, the overall dissolution is highest for the 40% solids, and lowest for 20% solids, but the kinetics do not follow the same trend. Initially, it appears that the 20% solids sample has the fastest kinetics, but at around 60%, the speed of dissolution starts to decrease, and lowering the overall aluminium dissolution. This may be as a result of the solution addition to the system, as the pH changes.

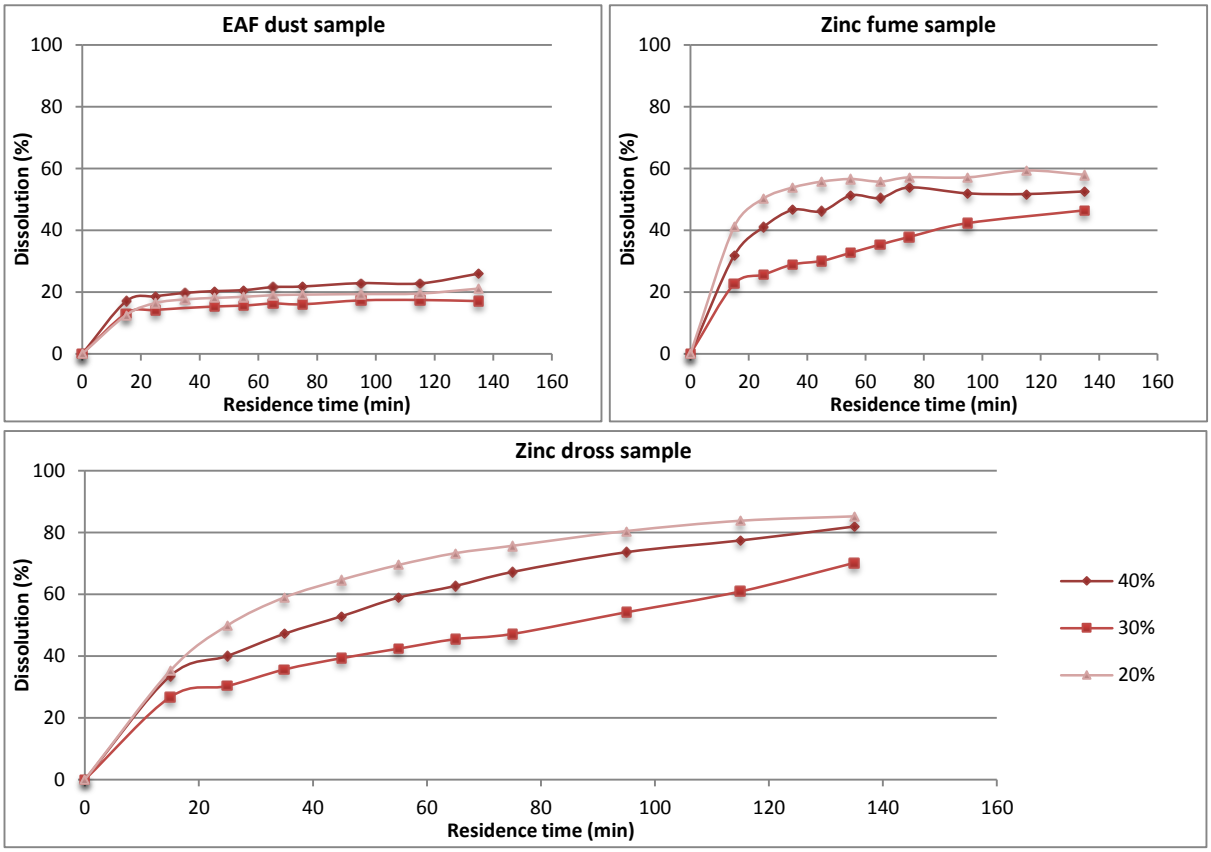

Figure 16. A comparison of the effects of different solids concentrations on the dissolution of iron from zinc secondary sources.

EAF dust seems to experience an intial decrease in iron dissolution with increasing solid-to-liquid ratio (increasing between 20 and 30% solids). This aligns well with theory (Havlik, *et al.*, 2004 and Havlik, *et al.*, 2006 and Herrero, *et al.*, 2010), which suggests that higher solid-to-liquid ratios result in reduced recoveries, because the solution does not necessarily completely surround each of the particles, as it would for lower ratios. However, considering the large standard deviation of 3.6% observed for EAFD in the repeatability tests (see Appendix D), it is possible that the variation in iron dissolution observed for this sample may be attributed to experimental error, since the variation in dissolution for different pulp densities is small (less than 4% variation in dissolution between two trends).

Both the zinc dross and zinc fume iron dissolution behave as per literature (Havlik, *et al.*, 2004; Havlik, *et al.*, 2006 and Herrero, *et al.*, 2010), in that the lowest solid-to-liquid ratio results in the highest iron dissolution. However, the highest ratio does not result in the lowest recovery. Instead, the 30% solids

experiment resulted in the lowest iron dissolution in both cases. Once again, this can be explained by the the fact that the 30% solids content sample actually has the lowest final solids content.

4.3.3. Calcium

Calcium dissolution under different solid-to-liquid concentration conditions for each of the zinc secondary samples can be seen in Figure 17. These graph values show that, as per the theory, calcium dissolution is highest at the lowest percentage solids (20%) for each sample. In this case, the lower final solids content for 30% once again becomes evident. The 30% sample has the fastest leaching kinetics for zinc fume and EAFD.

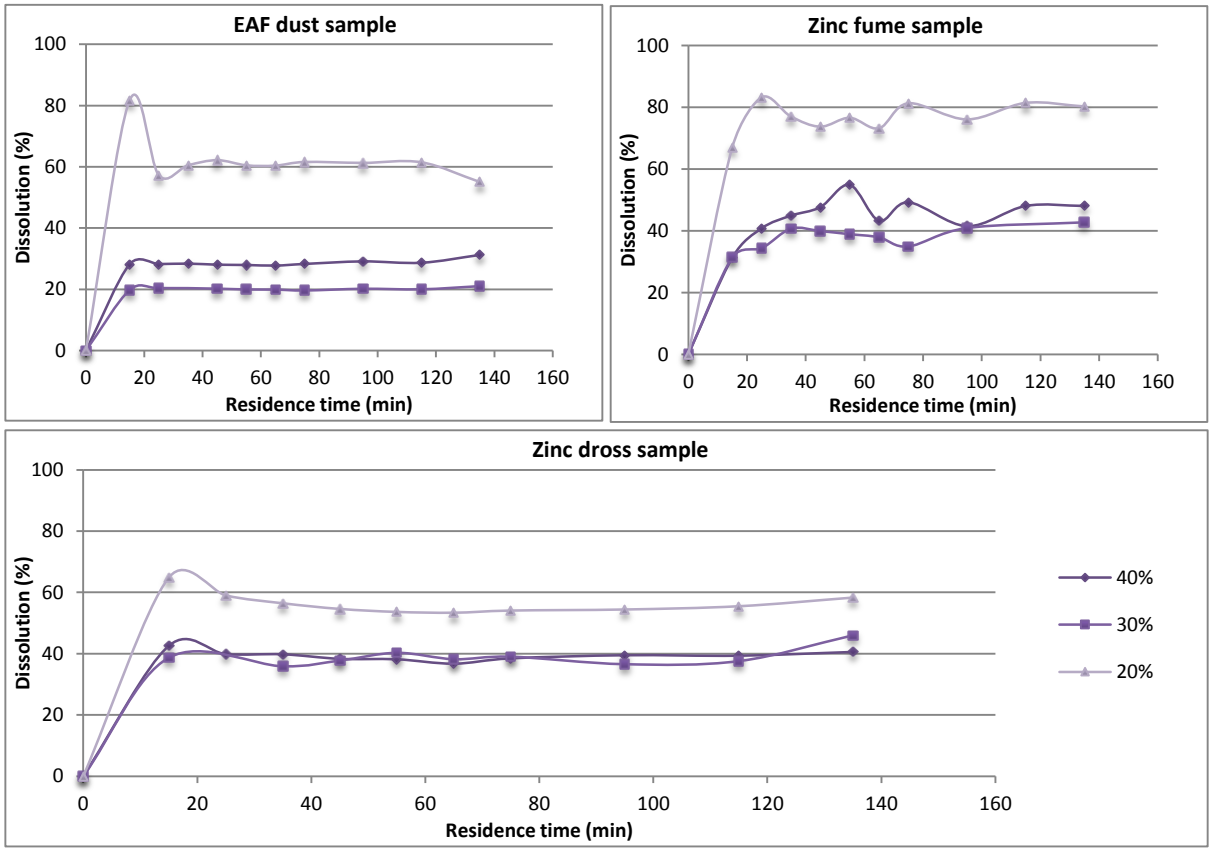

Figure 17. A graphical representation of the effects of solids content on the dissolution of calcium from alternative sources of zinc oxides.

These calcium results correlated well with the results observed for the other elements in these experiments. Thus it is likely that this observation is related to the physical method used for the tests.

4.4. Optimization tests

4.4.1. Zinc

Zinc dross

Figure 18 shows a comparison of zinc dissolution from zinc dross at different pH values and temperatures.

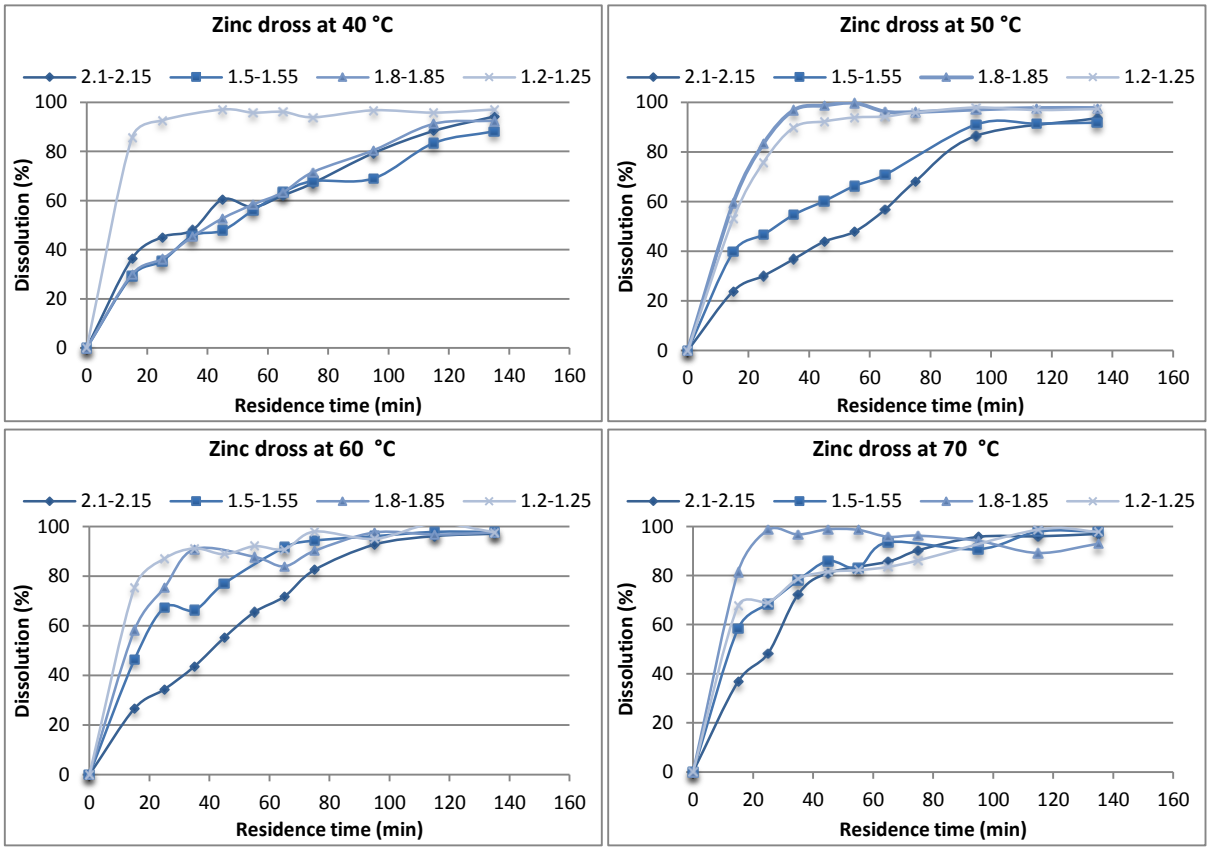

Figure 18. Variations in temperature and pH and the effect of these variations on zinc dissolution from zinc dross.

As expected from the literature (Rabah and El-Sayeh, 1995), a pH of 1.2-1.25 has the best reaction kinetics and overall recovery at temperatures of 40 and 60 ˚C. However, for the 50 and 70 ˚C tests, the 1.8-1.85 pH provides faster kinetics and similar overall recovery. This does not correlate well with what was suggested by the literature (Moradi and Monhemius, 2011), which suggested that lower pH values would provide better overall recovery and faster leaching kinetics. It is most likely that this may then be due to experimental or analytical error.

Running at lower pH values with the zinc dross sample was difficult to control. A large amount of foaming was observed when the raffinate and acid solutions were added to the zinc dross sample. This foaming was more severe at higher temperatures and the lower pH set points. This foaming was most likely caused by the release of hydrogen when the metallic zinc contained in the dross started to react with the sulphuric acid leachant. Due to this foaming, it is possible that the sample obtained was not representative or properly mixed.

A comparison of the overall zinc recovery at different residence times (15 and 135 minutes) for various pH values and temperatures shows that decreasing the pH has the expected effect of increasing the

kinetics, as evidenced by the higher recoveries after 15 minutes reaction time at lower pH values. The decreasing pH does not; however seem to make a significant difference to the overall recovery, with the decrease in pH only causing a total of 1% difference in overall recovery, from a pH of 2.1 to a pH of 1.2.

EAF dust

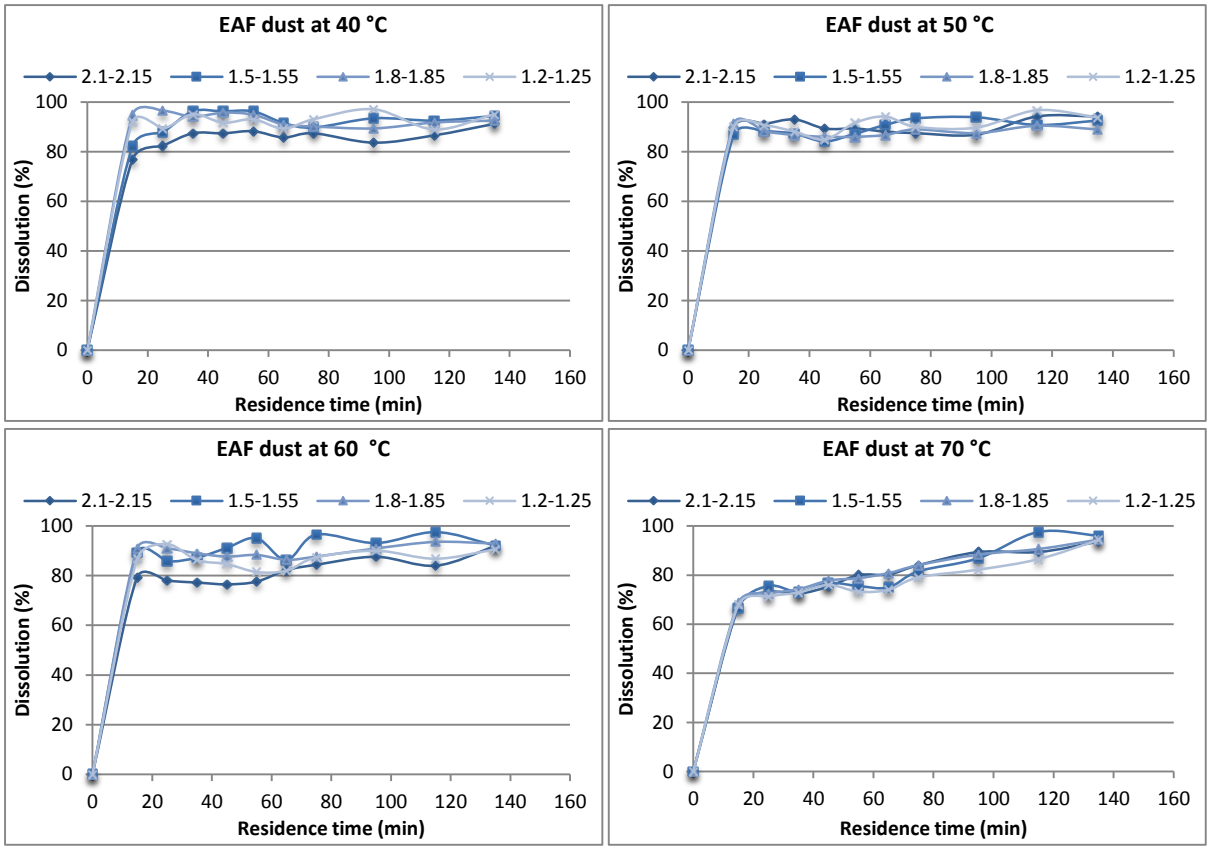

Figure 19. The effect of varying pH and temperature on recovery of zinc from EAF dust.

Zinc recovery from EAF dust under different temperature and pH conditions can be seen in Figure 19. Overall, this sample does not appear to be heavily affected by changing pH values at different temperatures. While the kinetics are somewhat affected, the small changes in concentrations of the samples generated and the 95% confidence on the Skorpion laboratory analyses makes it difficult to identify whether these kinetic "differences" are truly a result of the reactions in the system, or whether they can rather be related to the laboratory's limit of accuracy.

In all of these cases, there is less than a 3% difference in the final zinc recovery after 135 minutes of leaching. This difference is so small that it may once again be related to the laboratory's confidence level.

The lack of dependence on pH in the leaching system may suggest that this EAFD sample contains very little zinc ferrite, so that most of the zinc contained in the sample is easily leachable at pH values as high as 2.1.

The temperature also does not seem to have a very large impact on the kinetics or overall zinc recovery from this sample, with the overall recovery varying within a range of roughly 5% overall. Kinetics of the 70 ˚C samples seems to be slower than the kinetics at the other temperatures. This is contrary to what was expected from literature (Jha, *et al.*, 2001).

This can potentially be explained by the experimental method used. Cold synthetic raffinate was added to the circuit during the first few minutes of leaching. This caused a temperature drop to take place. Although this temperature drop was evident for all temperatures, the largest delta in temperature drop was experienced for the 70 ˚C experiments. Another potential explanation is the fact that the reactions in the system are exothermic (as determined by the enthalpy of the reaction, which was found to be negative for both zinc oxide and zinc ferrite reacting with sulphuric acid). This, increasing the temperature to this level could be causing a reduction in kinetics, rather than an increase.

Zinc fume

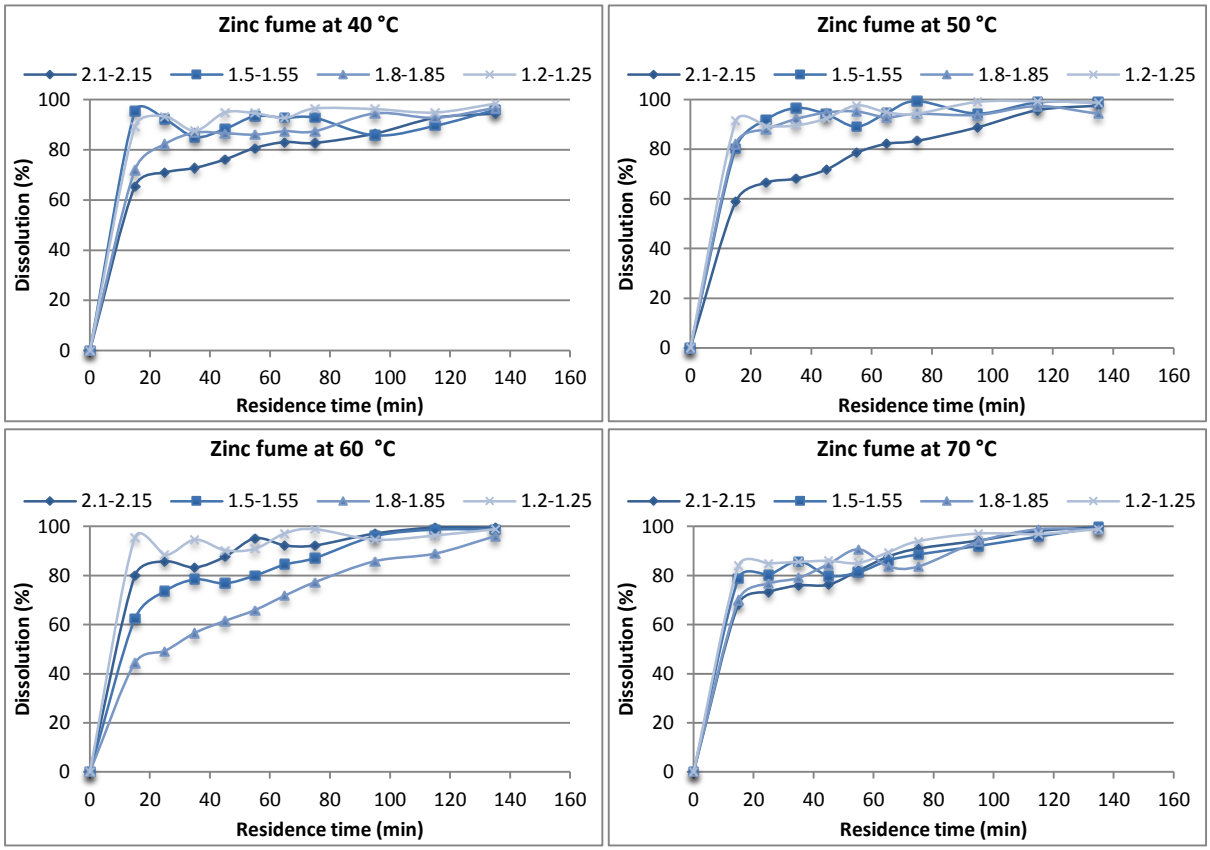

Figure 20. Illustration of the effect of pH and temperature variations on zinc dissolution from zinc oxide formed from fume dust.

Figure 20 shows the results of the leaching of the zinc fume oxide at different pH and temperature set points. Here, the final recovery does not seem to be heavily impacted by the change in temperature or pH, and in general there is less than 2% difference between the final recoveries obtained for each set of conditions. This change is so small that it may be related to the lab's analytical confidence level.

On the other hand, kinetics of leaching do seem to be affected by the different experimental conditions. From literature it was expected that, increasing temperature and decreasing pH would cause an increase the rate at which this leaching took place (Moradi and Monhemius, 2011).

At 40 ˚C, the pH theory seems to hold true to a point. Kinetics seem to increase with decreasing pH. However, there is no clear difference in the kinetics of the 1.5-1.55 pH sample and the sample run at 1.2-1.5 pH.

The experiments run at 50 ˚C seem to have similar kinetics and overall leaching for the 1.2, 1.5 and 1.8 pH set points. At 70 ˚C, all the recovery trends are very similar to one another, regardless of the pH set point. Thus, it doesn't seem as though the pH has any significant effect on the leaching kinetics or overall recovery at 70 ˚C. However, the 60 ˚C tests do not correlate well with the other three sets of data. All rates differ significantly from one another, with the difference in dissolution as high as 40% at certain time intervals. Since this is the only group of data that indicates that pH has any significant effect on the leaching beyond a certain temperature, it seems likely that some of the variation in dissolution observed could be attributed to experimental error.

Based on the general observations from these graph values, it seems that the pH will not have a notable impact on the leaching efficiency of the zinc fume oxide, provided the leaching temperature is equal to or higher than 50 ˚C. In addition, the pH will have to be kept at 1.8-1.85. Considering the additional acid costs that will be incurred to decrease the pH further, it seems most reasonable to operate at a pH of 1.8-1.85.

The data presented does not allow for conclusive evaluation of the effect of temperature on the leaching kinetics or leach efficiencies. This is due to the fact that none of the experiments of a certain pH have a clear trend of consistently changing in relation to the changes in the system temperature.

Slower initial kinetics at 70 ˚C may be explained by the fact that cold raffinate was added to the solution. At this temperature, it seems as though the reaction is proceeding in 2 defined steps, with the first step being completed in the first 15 minutes of leaching. This may be the dissolution of the zincite species, which takes place faster at the higher temperature. The slower reaction that seems to occur between 15 and 135 minutes could be the leaching of other species, such as franklinite, and complexes of zinc with other metals, which are more difficult to leach

Leaching systems have been shown to generally be diffusion controlled systems, particularly in the case of zinc oxides. Thus, temperature would have a less significant impact on leaching kinetics than on a chemical reaction controlled system. This may be why it is difficult to obtain a clear recovery versus temperature relationship.

A comparison of the recovery trends for the different samples reveals that the zinc fume has the highest overall zinc recovery under all conditions, achieving between 94 and 98% recovery. Zinc dross follows – between 92 and 97% (with the exception of one trend which lies at 88% - most likely the result of either analytical or experimental error, since the trend does not provide a consistent curve as it should), while EAFD recovery varies between 90 and 95%.

4.4.2. Aluminium and iron

Zinc dross

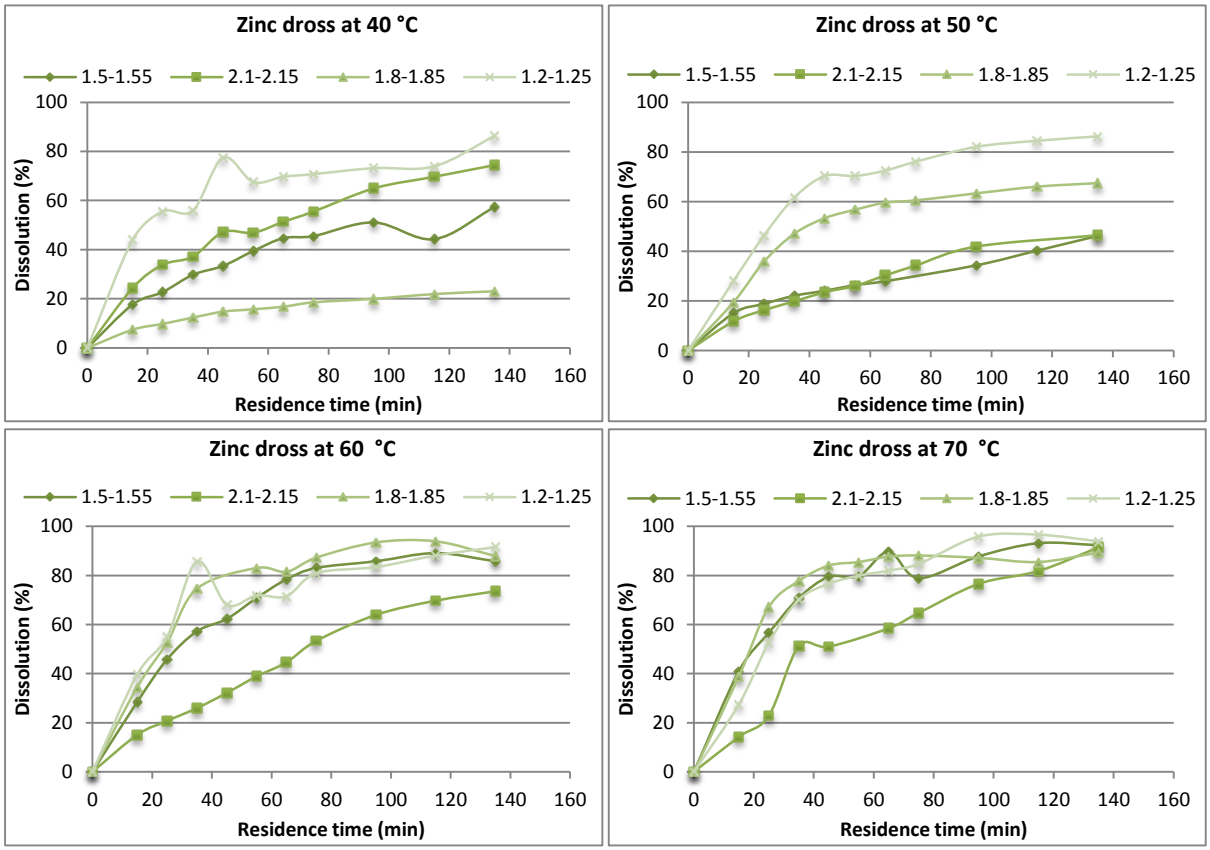

Figure 21. Aluminium dissolution from zinc dross at different temperature and pH conditions.

Aluminium dissolution from zinc dross seemed to be affected by the temperature and pH. This was expected from the literature reviewed (Jha, *et al.*, 2001; Moradi and Monhemius, 2011) – with an increase in temperature and decrease in pH, aluminium dissolution was expected to increase. However, these trends are too variable to allow for any conclusive deduction regarding the effect of pH and temperature on the aluminium dissolution. Nonetheless, one important thing that can be noted from these results is the fact that the aluminium dissolution at temperatures above 50 ˚C is roughly 80% of the total aluminium, regardless of the pH. At the Skorpion operating conditions of 50 ˚C and 1.8 pH, aluminium dissolution from the zinc dross was roughly 65%. This means that a large amount of aluminium will be leached from this sample and may cause process upsets.

Overall iron dissolution seemed to be highest at the lowest pH set point of 1.2, as expected from the literature studied (Moradi and Monhemius, 2011). In addition, the lowest overall iron dissolution generally took place at a pH of 2.1, for each temperature tested. The slightly higher dissolution at 70 ˚C for the 2.1 pH is most likely a result of the confidence level on the lab analyses. However, this does not hold true for the 40 ˚C tests, where the 2.1 pH resulted in the second highest iron dissolution.

Once again, it is difficult to draw conclusions about the effect of temperature and pH on the iron leaching from these trends. However, it is clear that at temperatures of 50 ˚C or above, at least 60 % iron is dissolved. At 70 ˚C, the dissolution Is higher than 80 % for all pH tested. At Skorpion's operating parameters, roughly 85% of the iron is leached. Once again, it is important to note that, due to high

iron concentration in the circuit, such high dissolution may result in the circuit being overloaded. Further investigation will be required to establish whether the Skorpion circuit will be capable of handling these iron and aluminium levels.

EAF dust

Figure 22. Dissolution of iron from zinc dross at different pH and temperature set points.

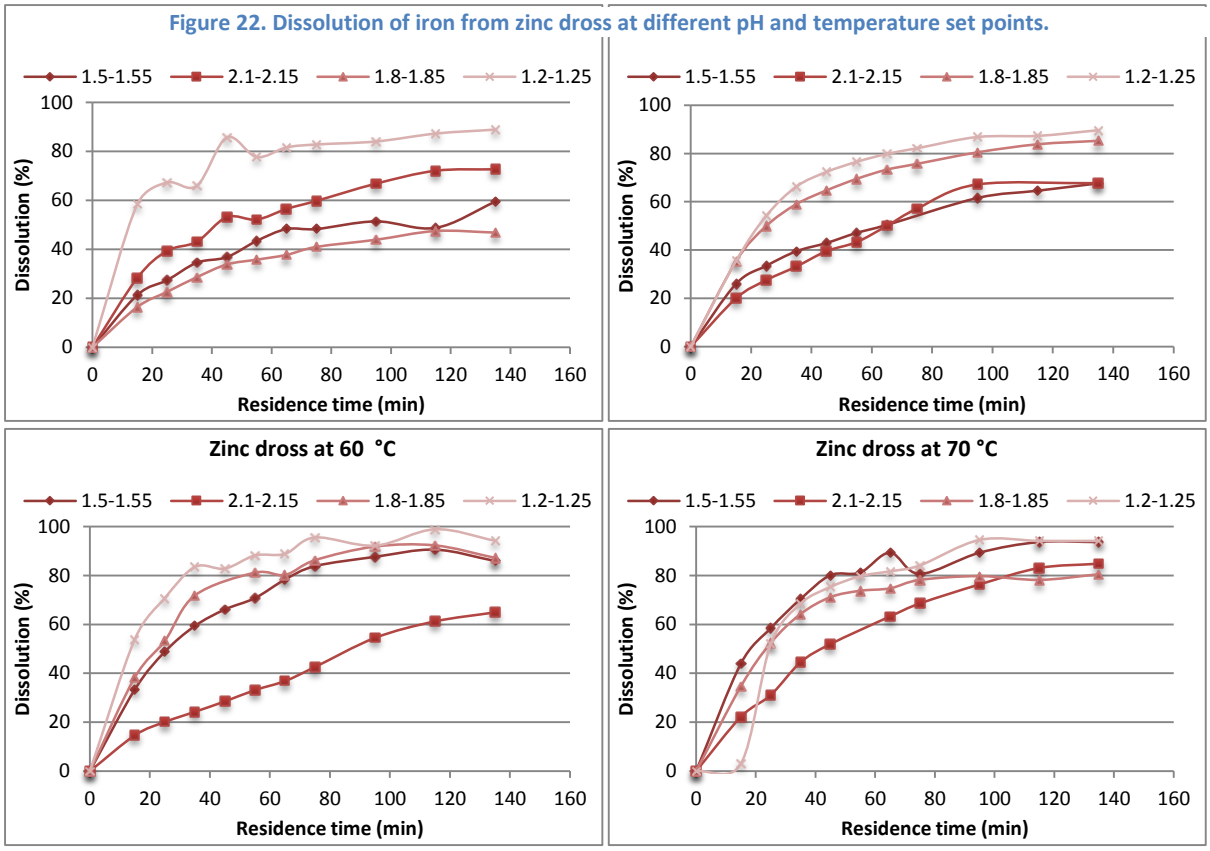

At all temperatures aluminium dissolution (Figure 24) from EAF dust does not seem to be severely impacted by the change in pH between 1.5, 1.8 and 2.1, with less than 5% difference in aluminium dissolution between these three pH values. However, the dissolution is much higher (20-30% higher) when the pH is dropped to 1.2. It therefore seems that pH only affects aluminium dissolution from EAFD from a certain point (1.2 in this case). At 70 ˚C, the 1.2 pH does not seem to affect the aluminium dissolution.

There also does not seem to be much of a difference in aluminium dissolution at different temperatures, with the dissolution generally staying at around 40% to 50% for the pH values 1.5 and higher, while the 1.2 pH experiments remain at around 65-75%. However, the dissolution seems to be higher at 70 ˚C than at the other, lower temperatures for all the pH set points, except 1.2, which remains between 70 and 75%. It therefore seems that dissolution of aluminium is diffusion controlled, and that the diffusion rate only increases beyond 70 ˚C.

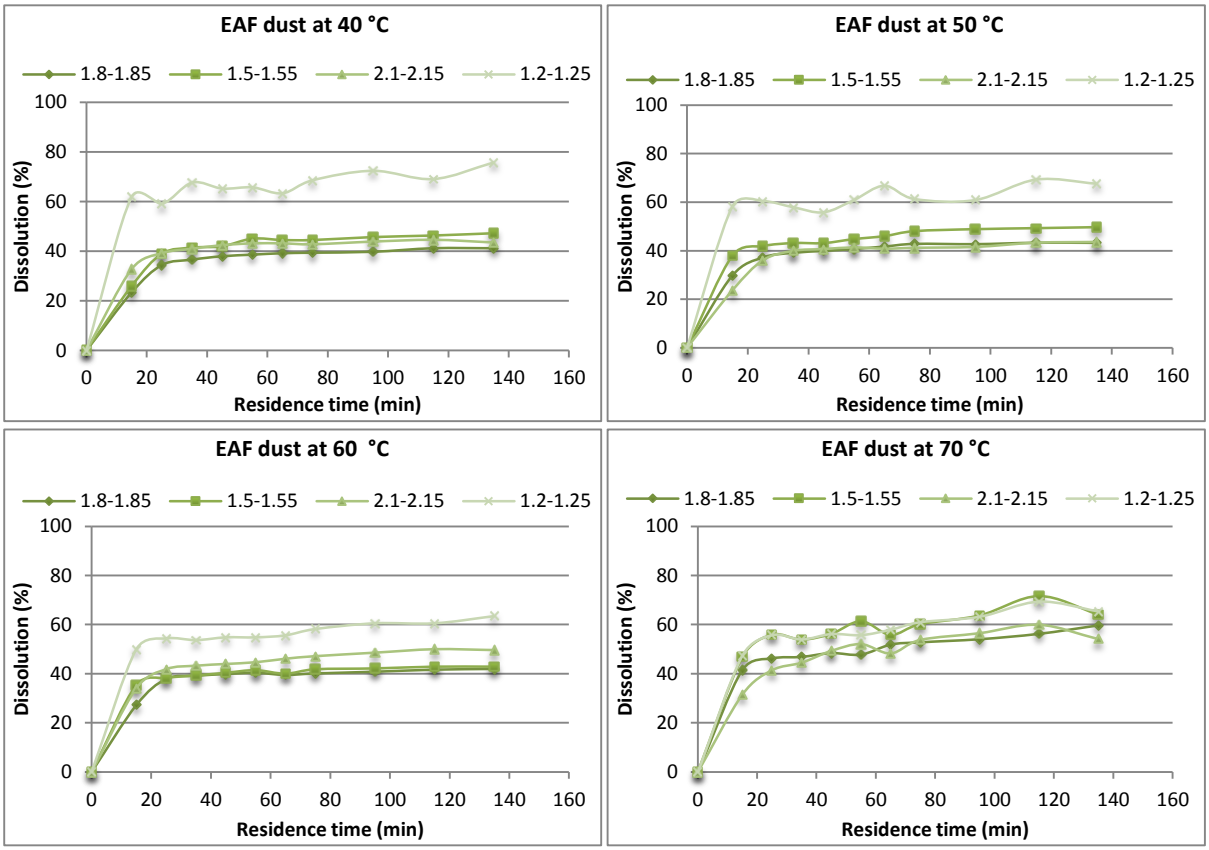

Figure 24. Dissolution of aluminium from EAF dust under different temperature and pH set points.

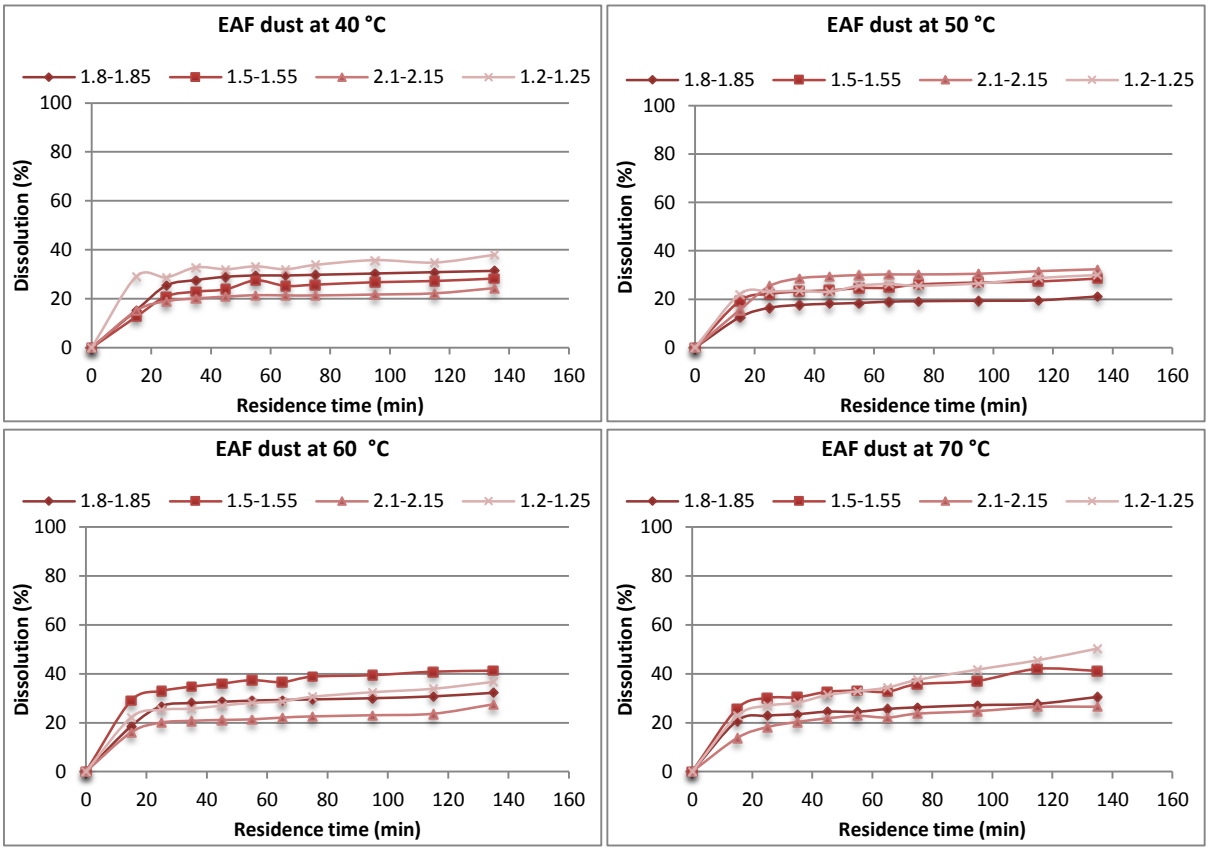

Figure 23. The effect of temperature and pH on the dissolution of iron from EAF dust.

Iron dissolution (Figure 23) does not present a clear trend with changing temperature and pH, as there is no consistency between the results. It can however be noted that the iron dissolution remains between 20 and 40% at all temepratrues, except 70 ˚C, where the dissolution is 50% at the lowest pH. From literature (Duyvesteyn and Jha, 1986; Cruells, *et al.*, 1992), it was expected that higher temperatures and lower pH values would result in more iron dissolution from EAFD. This was due to the zinc ferrites, which are very stable and therefore required high temperature and low pH to leach. The fact that this does not seem to be the case seems to suggest that the EAFD sample tested does not in fact contain a lot of franklinite. This is supported by the observations made with regards to zinc leaching from this sample.

The fact that iron dissolution does not seem to be affected by pH and temperature means that zinc leaching from this solid can be optimized without the concern that iron dissolution will be increased.

Zinc fume

The dissolution of aluminium (Figure 26) and iron (Figure 25) from the zinc fume oxide sample do not bear clear and evident relationships with the temperature and pH at which the leaching experiments were performed. Unlike the increase in dissolution with increasing temperature and decreasing pH that was expected from literature (Duyvesteyn and Jha, 1986; Cruells, *et al.*, 1992), there does not seem to be any relationship between the factors whatsoever.

It can however be noted that the aluminium dissolution at Skorpion's process set points is approximately 52%. For the other set points aluminium dissolution is generally higher (80-85%). Since the aluminium content in the sample is low in comparison to the other two samples, and the resultant aluminium concentration in the PLS (see Table 18 in Section 76) is below acceptable limits for the circuit, the aluminium dissolution should not be a cause for concern.

It is also difficult to identify a relationship between the iron dissolution and temperature or pH from the trends generated from the experimental data. It can be noted that at 70 ˚C changing the pH has less effect on the iron dissolution than at other temperatures, resulting in less than 6% overall change in iron dissolution versus 20-40% change at some of the other temperatures. At 50 ˚C, only the pH 2.1 experiment shows significantly different dissolution as compared to the other 3 pH tests. This recovery is 10% lower than the others, while the other 3 pH values' recoveries vary by 5%. Iron leaching at 60 and 40 ˚C do not exhibit similar trends.

However, iron recovery at tests performed at 50°C and above is generally higher than 60%. Once again, the iron content in this sample is lower than in the other two samples, so the resultant PLS iron concentration, at 210 ppm, is lower than the limit that the plant can handle (240 ppm). This, iron dissolution should not cause any problems in leaching this particular sample.

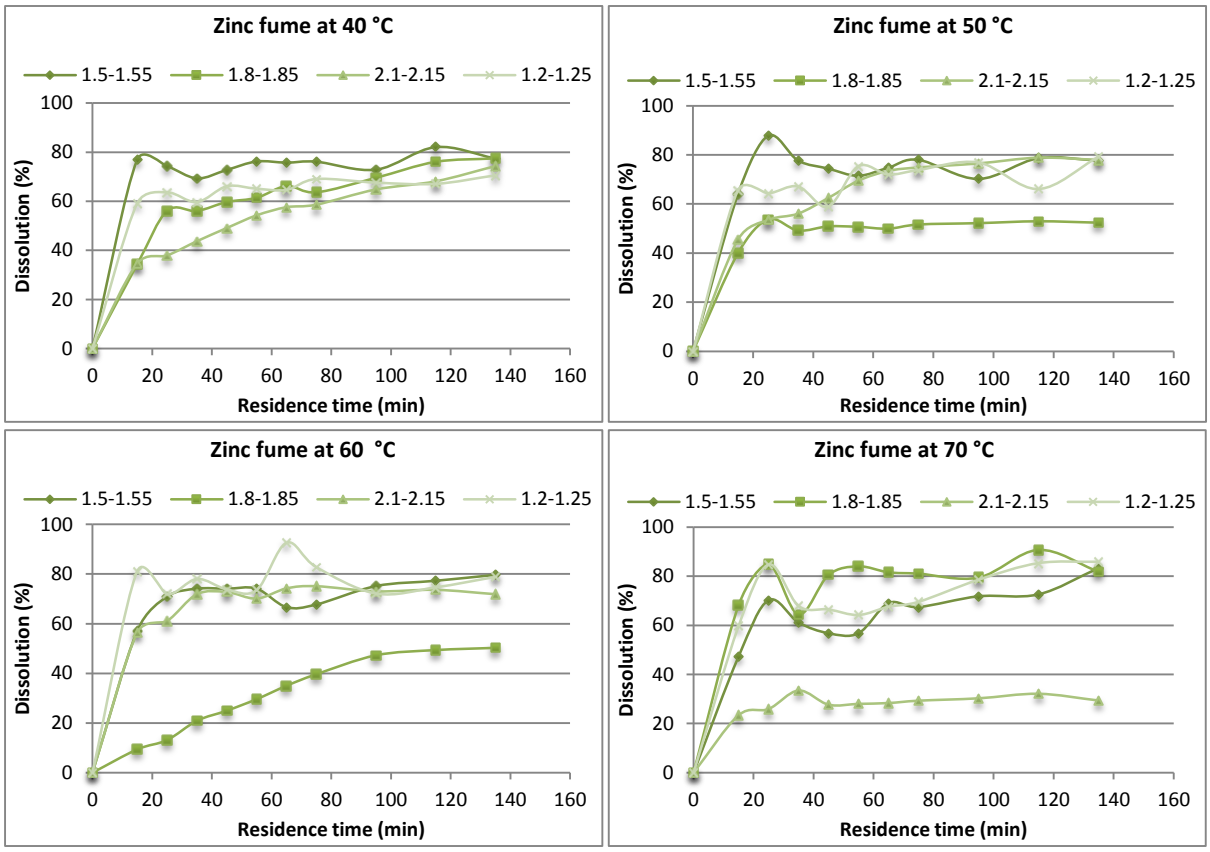

Figure 26. Aluminium dissolution from zinc fume oxides at different pH and temperature conditions.

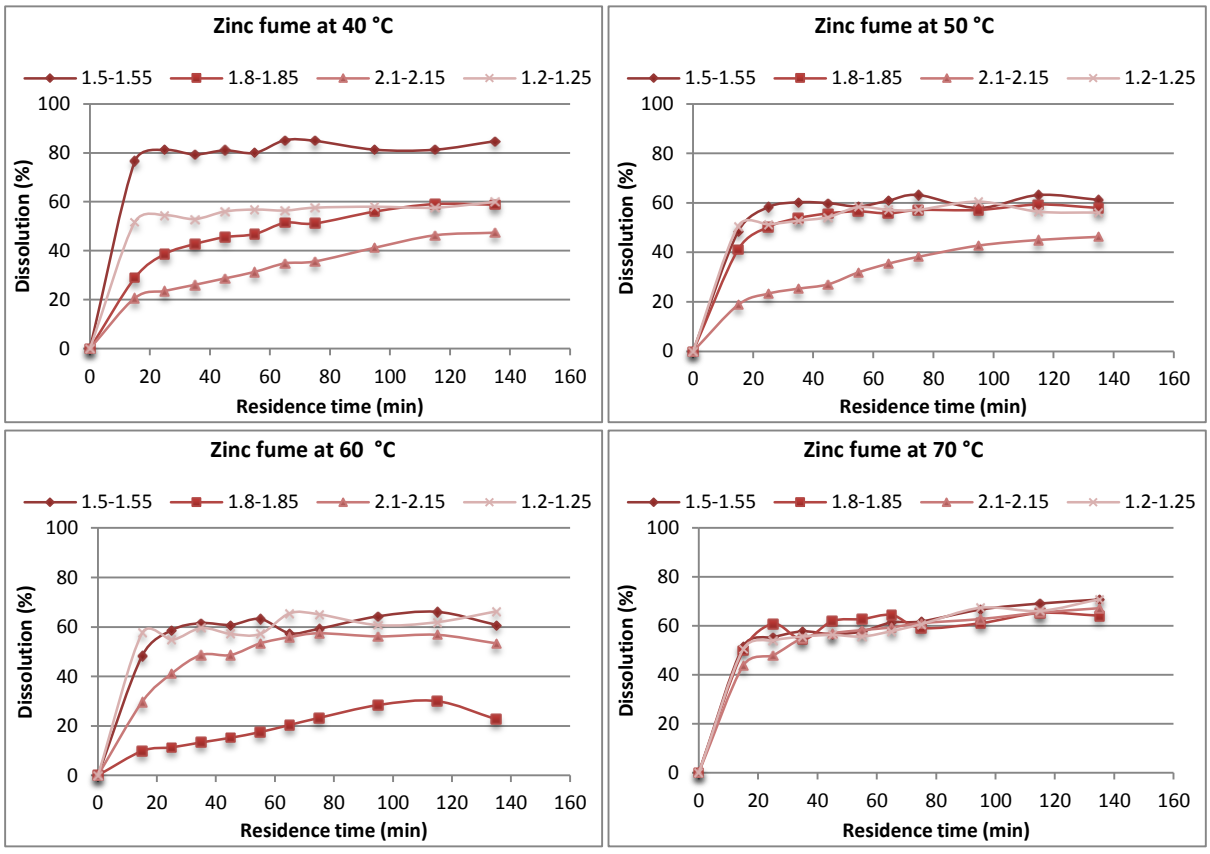

Figure 25. Iron dissolution from zinc fume oxides and the effect of pH and temperature variations on dissolution.

4.4.3. Calcium

Figure 27, Figure 28 and Figure 29 show the dissolution of calcium. Calcium dissolution varies widely across the different plots for each of the different zinc oxide sources. Most literature did not address the calcium dissolution, so there is no real data in literature to compare the calcium dissolution to. However, several literature sources stated that the leaching of CaO was a reaction that took place at all temperatures and pH values and that it took place fast (Havlik, *et al.*, 2004).

There does not seem to be a clear trend in the effect of temperature and pH on the calcium dissolution. Since calcium exceeded the saturation limit in the resultant PLS for the EAFD sample (sample contained calcium at levels of 600 ppm in solution, while the saturation limit is typically around 500 ppm), it is possible that the calcium had started to precipitate from solution in this case, creating the inconclusive dissolution trends seen in Figure 28. Both the zinc dross and zinc fume samples in Figure 27 and Figure 29 also exhibited signs of calcium precipitation. This is evident from the high dissolution after 15 minutes of leaching, followed by the decrease in dissolution.

Precipitation chemistry is in itself a complex field. Since calcium is not the element of interest, no further analysis of the precise dissolution mechanism is covered. However, what is clear from these trends is the fact that the calcium dissolution varies between 25 and 85% in the zinc dross, while calcium dissolved from the EAFD varies between 40 and 85%. The zinc fume sample's calcium dissolution varies between 40 and 98% dissolution. Of these sources, the EAFD contains the most calcium, at up to 2%. At 80% dissolution, this is considerable, but since the other two samples contain only 0.2% calcium, acid costs should not be significantly affected by the high calcium dissolution.

Zinc dross

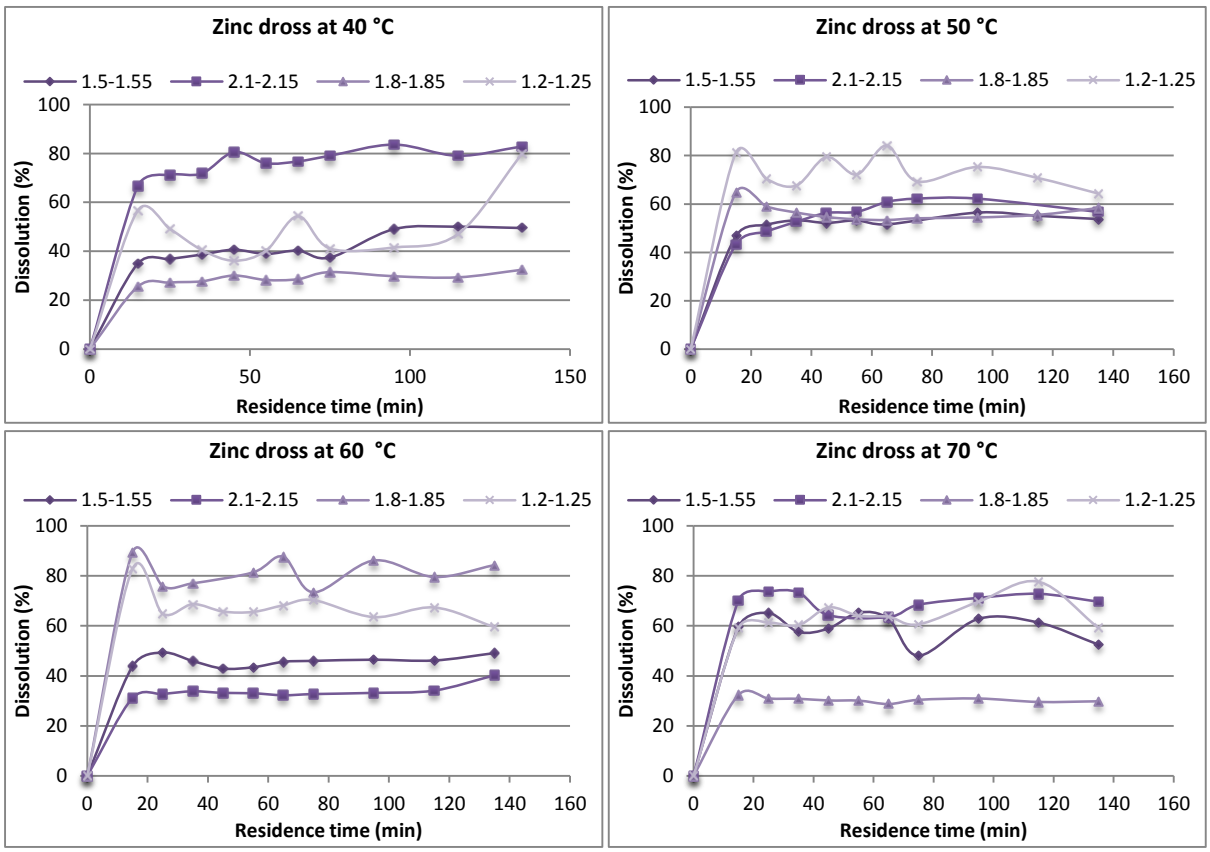

Figure 27. The dissolution of calcium from zinc dross at different pH and temperature set points.

EAF dust

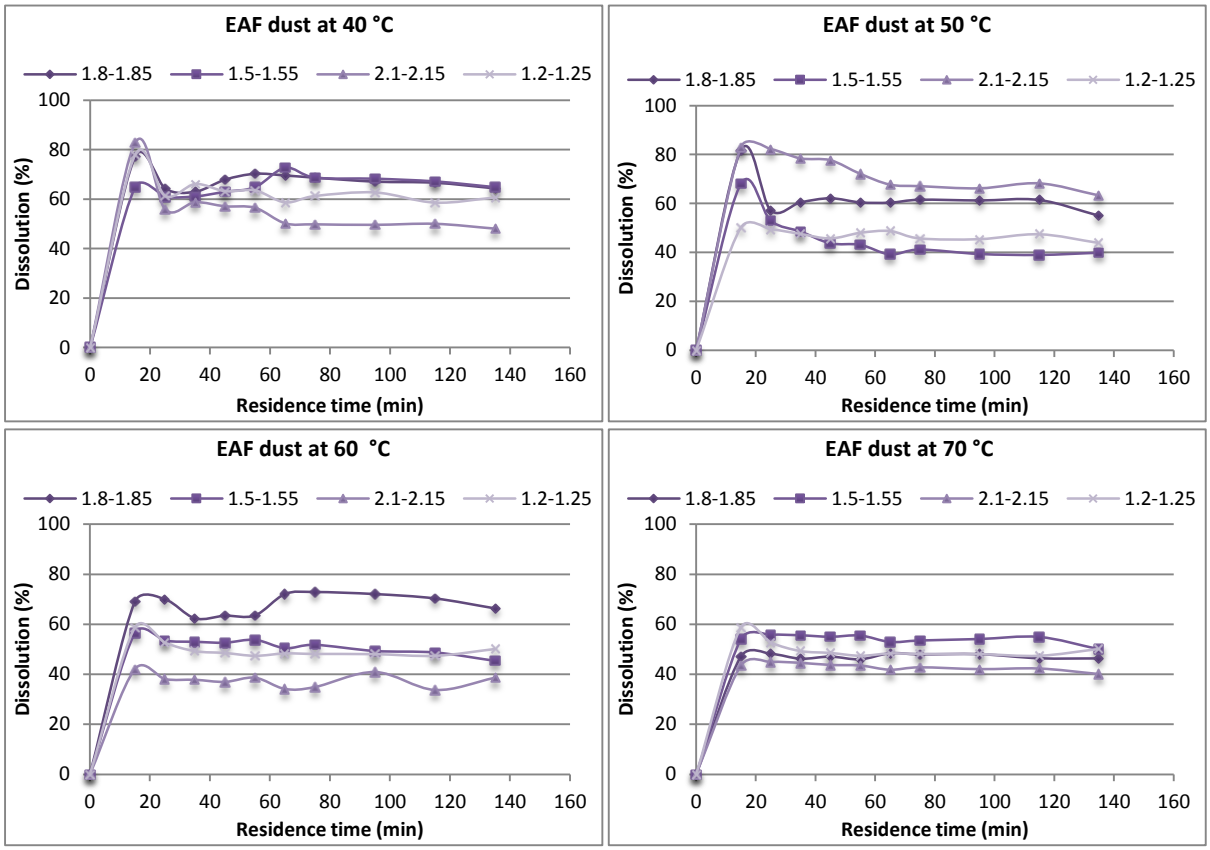

Figure 28. The effect of temperature and pH variations on the dissolution of calcium in EAFD.

Zinc fume

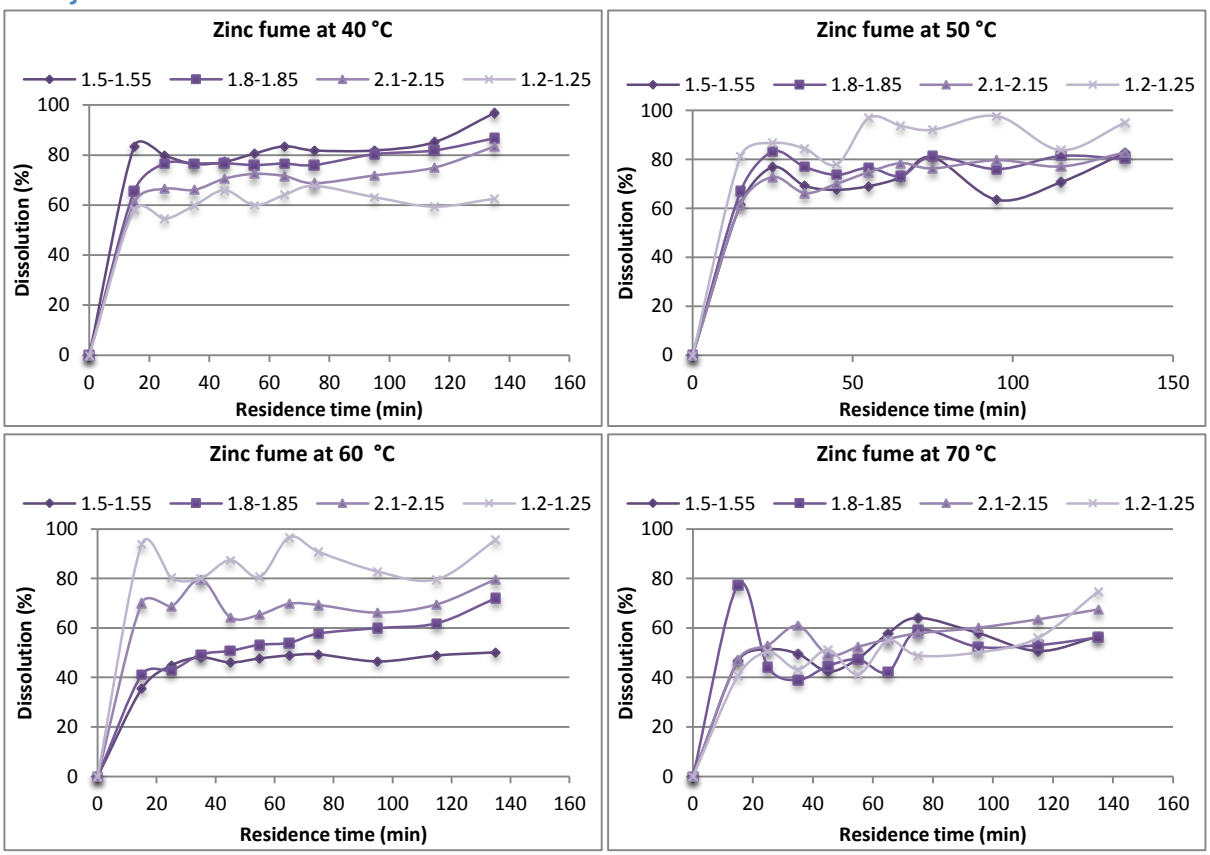

Figure 29. Zinc fume oxides calcium dissolution at different process conditions.

4.5. Acid consumption

Due to the significant contribution of acid to the operating costs of the Skorpion leaching plant, it was important to establish the acid consumption of the various potential zinc secondary sources. This was done only for the base case setup, in which Skorpion's normal operating parameters were used (i.e. 50 ˚C, 20% feed solids slurry and a pH of 1.8-1.85).

Figure 30 shows the total acid consumption which takes place in the leaching circuit alone (excluding acid consumption that takes place during filtration on the residue belt filters during the acid wash stage).

It is clear from this graph that the EAFD has the lowest leaching acid consumption at a total of 700 kg/t of feed, while the zinc dross has the highest (1380 kg/t of feed material). The zinc fume acid consumption is relatively low (1100 kg/t feed) in comparison to the zinc dross, potentially because of the fact that it has the fewest impurities. However, it is higher than the EAFD consumption, probably because it contains a higher zinc concentration.

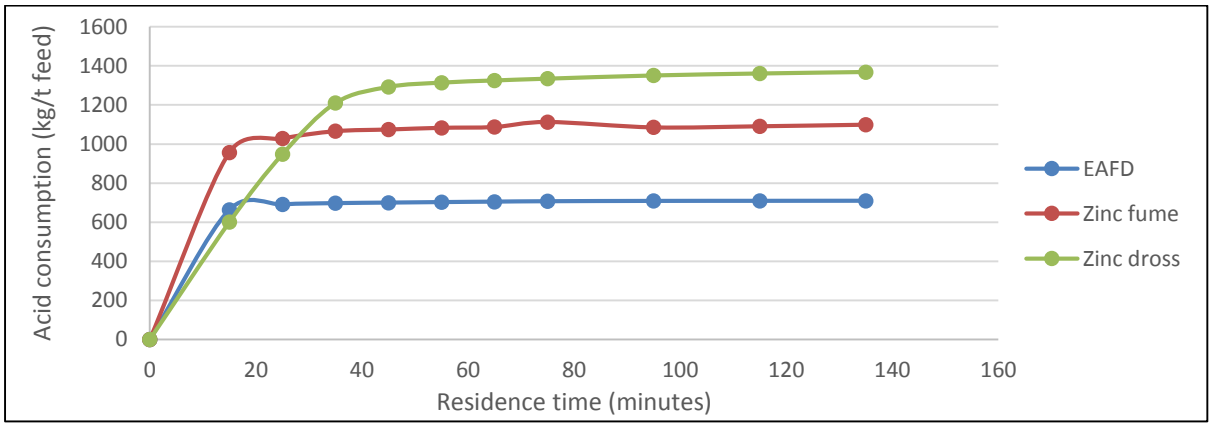

Figure 30. Comparison of the total acid consumption of the secondary oxides at standard Skorpion operating conditions.

Examining the gangue acid consumption for the different secondary oxides (shown in Figure 31) may help to explain where the difference in the different leaching acid consumption figures lies. It is evident from this figure that the zinc dross has the highest gangue acid consumption, at a total of roughly 540 kg/t of feed material. This explains why the total leaching acid for this particular source is so high. The zinc fume is, as expected, the source with the lowest gangue acid consumption (47 kg/t of feed once leaching has been completed). This can be attributed to the relative purity of source in comparison with the other two oxide sources.

Although the EAFD contains the least zinc, and therefore the most impurities, it has a lower gangue acid consumption than the zinc dross at a total of 330 kg/t of feed. This may be due to the manner in which EAFD's are produced. Some of the gangue elements may be caught up in stable ferric matrices, making them more difficult to leach than the predominantly oxide-based impurities contained in the dross/ash mixture.

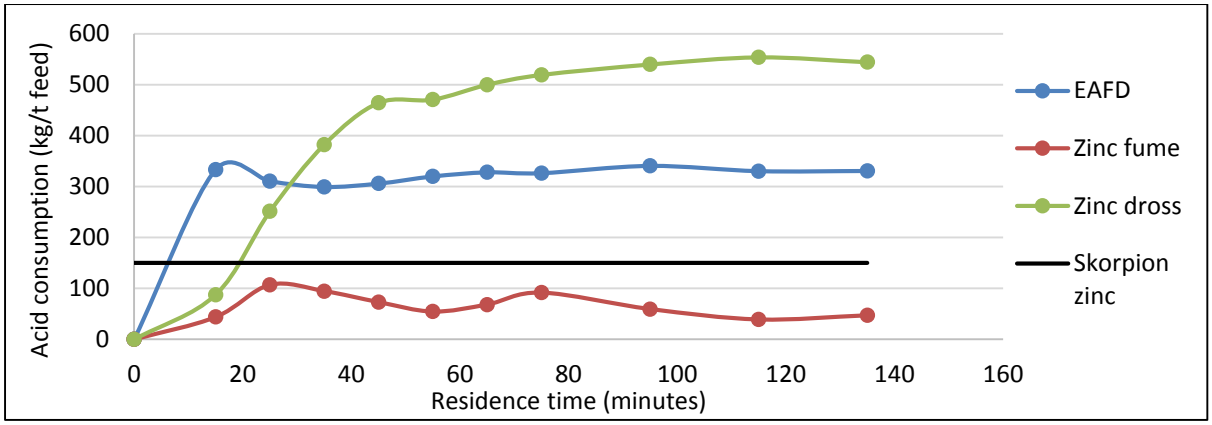

Figure 31. Comparison of the gangue acid consumption of the secondary oxides at standard Skorpion operating conditions.

Skorpion targets a gangue acid consumption of 150 kg/t for the ore to ensure that operating costs remain within the economically viable region for the Skorpion ore. Based on this target, only the zinc fume sample lies within the budgeted gangue acid consumption. However, since the zinc content in these samples is significantly higher than the Skorpion ore, it may be possible to economically refine the samples regardless of the high acid consumption.

To determine this, it was first necessary to determine the total acid consumption for each source, including the acid consumed during re-acidification of the thickener underflow, and during acid washing of the residue on the RBF's.

The targeted total overall acid consumption for Skorpion's ore body is 1.5 t/t of zinc. From Figure 32, it is clear the acid consumption for all three oxide sources is lower than this target. The zinc dross has an overall consumption of 1.0 t/t of zinc, EAFD's acid consumption is 1.3 t/t Zn and the zinc fume acid consumption is the lowest of the three at 0.1 t/t Zn. This is expected, as the gangue acid consumption is significantly lower (290 kg/t lower than the EAFD) for this sample, while the zinc content is approximately 78% (versus the 30% for EAFD and 60% for zinc dross). The zinc dross overall acid consumption per ton zinc is lower than the EAFD acid consumption, despite a higher GAC, because it contains approximately double the amount of zinc.

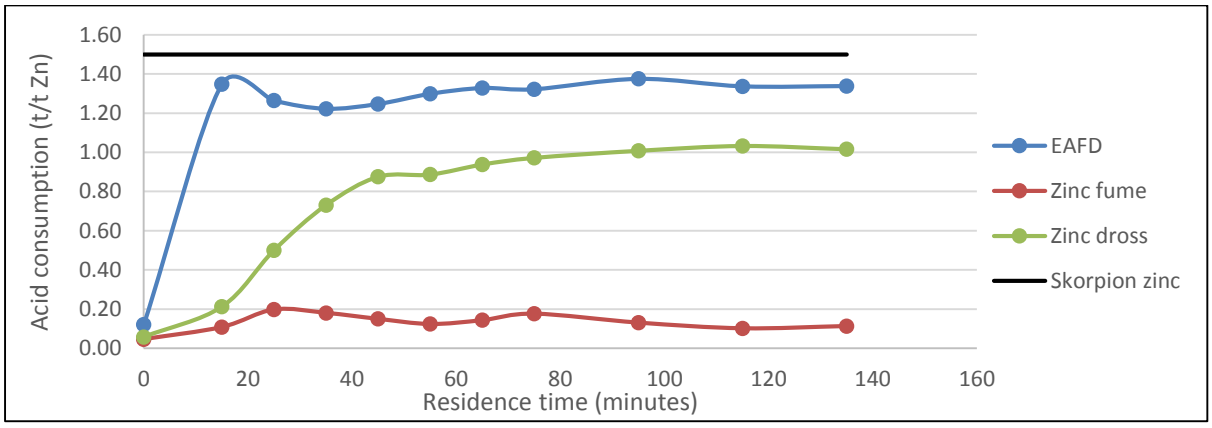

Figure 32. Comparison of the total acid consumption of the secondary oxides at standard Skorpion operating conditions, including losses during filtration.

4.6. Summary of key findings

Although the optimization experiments performed did not correlate well with the expectation based on the literature review, the results did show that it would be possible to obtain leaching efficiencies from the different oxides as follows (for the range of factors tested):

- EAFD leaching efficiencies in excess of 90%, on average, or 88%, based on the worst case scenario
- Zinc dross leaching efficiencies of roughly 93%, on average, or greater than 86%, using the worst case scenario
- Zinc fume oxide leaching efficiencies of above 96%, on average, or 94% for the worst case scenario

Due to the nature of the zinc secondary oxide samples used for the test work conducted, the composition of the samples tested was variable. Since samples used in literature were usually of a fixed composition, the variability of the composition of the samples tested may have contributed to the fact that the tested samples did not behave according to expectations based on the literature reviewed.

At Skorpion's standard operating conditions of 50 ˚C and 1.8-1.85 ˚C it was possible to obtain the following zinc recoveries:

- EAFD – 93.0%
- Zinc dross – 96.9%
- Zinc fume oxide – 98.5%

All of these recoveries were attainable in the 120 minutes residence time available in the Skorpion Zinc leaching circuit. In addition, the impurity dissolutions for these sources under the standard operating conditions were (Table 18):

Table 18. Summary of the dissolution extents of the key elements in each oxide source.

	SZ ore	EAFD	Zinc dross	Zinc fume
Zn	89%	93%	97%	99%
Fe	36%	20%	84%	60%
Al	60%	45%	65%	51%
Ca	90%	63%	58%	83%
Cu	60%	75%	0.90%	94%
Ni	60%	21%	55%	18%
Si	34%	54%	29%	40%
Mn	80%	50%	77%	62%
Mg	80%	70%	73%	83%

Approximate elemental concentrations in the leach residue liquor are shown in Table 19. Also shown in this table is the maximum concentration of each element in PLS that the Skorpion circuit was designed to handle. Skorpion's neutralization circuit was designed to cope with an aluminium concentration of 1450 ppm and iron of 240 ppm in the feed solution to neutralization. Thus, there is a risk that the neutralization circuit will be overloaded by the iron and aluminium in the zinc dross PLS, or by the iron in the EAFD PLS. This makes blending with the Skorpion ore to prevent extreme impurity levels even more critical. It also proves that it is unlikely that it will be possible to leach either of these samples without blending them.

Table 19. Approximate leach residue liquor composition, including maximum Skorpion composition, based on design.

	SZ ore	EAFD	Zinc dross	Zinc fume
Zn (g/l)	35	40	70	65
Fe (mg/l)	240	1500	1800	200
Al (mg/l)	1450	80	3800	30
Ca (mg/l)	500	600	85	65
Cu (mg/l)	500	45	2	65
Ni (mg/l)	400	2	70	5
Si (mg/l)	320	350	260	100
Mn (mg/l)	4000	280	75	20
Mg (mg/l)	4000	450	120	35

Acid consumption figures for each of these samples is shown in Table 20.

Table 20. Key acid consumption values for the different zinc secondaries tested.

Sample	Overall leach TAC (kg/t feed)	GAC (kg/t feed)	Total acid consumption (t/t zinc)
EAFD	709	330	1.34
Zinc dross	1369	544	4.24
Zinc fume	1099	47	0.59

5. Mass balance

To determine the conditions under which maximum potential recoveries could be obtained, the results from the experimental test work were used to construct a theoretical mass balance for different blends of Skorpion ore and each of the oxides. For each oxide, blends of 10, 20, 30, 40 and 50% oxide with the ore were considered. Dissolution of each of the elements was based on the results of the leaching experiments performed at 50°C, a pH of 1.8-1.85, 20% solids and with a normal particle size distribution.

The key limiting factor for the different solids types was the impurity build-up in Skorpion's process. Having a circuit that is very sensitive to most impurities meant that all impurities that are not completely removed at some point in the circuit had to be taken into consideration. To this end, calcium, aluminium, iron, silica, copper, nickel, manganese and magnesium were the main impurities considered. Calcium, silica, iron and aluminium are normally completely removed from the circuit with the tailings, due to the combination of the neutralization section, effluent treatment and the bleed from the SX HCl plant. Minor and trace impurities were not measurable in Skorpion's lab, and could therefore not be taken into account.

Although not discussed in detail in section 4, dissolution of silica, copper, nickel, manganese and magnesium was quantified during the experimental phase. These dissolutions will be addressed in the list of assumptions used for the mass balance. The system around which the mass balance was performed is shown in Figure 34.

Setting up the mass balance required a number of assumptions. These are listed below:

- Skorpion's ore feed grade remained constant at 9%. Oxide and ore compositions used for the mass balance are shown in Table 7 in section 3.1.1.
- Ore, limestone and oxides had a feed moisture content of 5%. This is a variable factor for the oxides, but was chosen for the limestone and ore based on the plant data available at the time
- Limestone addition was estimated based on actual plant data to be roughly 16% by mass of the total dry ore feed to the refinery. It was assumed that the limestone addition to the circuit would always be similar to this ratio, so:

$$limestone\ (t\ /\ h) = [ore\ feed\ (t/h) + alternative\ ZnO\ (t/h)] \times 0.16 \qquad \text{Equation 6}$$

- Moisture content in the tailings was assumed to be 40%, based on the average moisture content of the tailings material produced by Skorpion since start-up of the refinery
- Dissolution of the different elements contained in the Skorpion ore was estimated based on historical plant data. Dissolution of these elements from the oxides was determined from the experimental data. Both sets of dissolution data are displayed in Table 18
- Based on the plant design and actual operating data, copper plant was assumed to be able to handle a throughput of 250 m^3/h at a copper concentration of 500 mg/l, resulting in a total copper removal of 125 kg/h or 90 t/month, when operating at 100% capacity
- Nickel plant's assumptions were similarly based on a combination of design and actual experience, and resulted in 60 m^3/h at 400 mg/l Ni – resulting in 24 kg/h or 17 t/month nickel removal at maximum plant capacity

- Assumptions for the copper and nickel plants are summarized in the table below:

Table 21. Maximum throughput conditions for the copper and nickel plants at Skorpion Zinc, based on the plant data.

	Units	Cu plant	Ni plant
Throughput	m^3/hr	250	60
Tenor	mg/l	500	400
Removal rate	kg/hr	125	24
Removal rate	ton/month	90	17
% of capacity	%	100	100

- An overall runtime of 90% was assumed for the plant
- Sulphuric acid addition was calculated based on the Skorpion design target of 1.55 t/t of zinc produced, together with the acid consumption for the respective oxide under investigation (0.11, 1.02 and 1.34 for zinc fume, EAFD and zinc dross respectively)

$$Acid\ added = Zn_{In\ ore} \times 1.55 + Zn_{In\ oxide} \times Overall\ oxide\ acid\ consumption \quad \text{Equation 7}$$

- ETP bleed was assumed to 10 t/h based on the average bleed achieved by the plant at the time
- Residue mass was calculated based on a balance over the entire system:

$$M_{Residue} = M_{Ore} + M_{Oxides} + M_{LS} + M_{Zn\ dust} + M_{Acid} + M_{Salt} - M_{Cu} - M_{Ni} - M_{Zn} \quad \text{Equation 8}$$

- The residue moisture and ETP bleed compositions were determined from Skorpion historical data:

Table 22. Design impurity removal for the Skorpion tailings.

Element	Moisture in residue (g/l)	ETP bleed (%)
Zn	0.70	0.03
Fe	0.01	0.0005
Al	0.30	0.06
Ca	0.00	0.6
Cu	0.00	0.0005
Ni	0.00	0.01
Si	0.04	0.01
Mn	4.00	0.2
Mg	4.00	0.2
Acid	10.00	2.00

- Assuming that aluminium, iron, silica and calcium were completely removed in the neutralization section, the residue solids composition was based on a balance of these elements over the system.
- To determine the maximum tolerable manganese and magnesium contents in the refinery, the amount of Mn and Mg in the residue was calculated using 0 g/l Mn and Mg in the residue moisture.

The basic strategy for balancing the mass balance for each scenario is outlined below:

- First, the desired feed ratio was input
- Then the amount of oxide that could be fed under a certain set of conditions was determined by iteratively adjusting the amount of oxide feed to the system until one of the impurities started to accumulate in the system. Determination of accumulation for each impurity is described below

- This Mn and Mg composition calculated for the residue solids was maintained for all scenarios, and the moisture Mn/Mg content was calculated using Excel Solver.
- Since the Skorpion design limited the Mn and Mg content in the residue moisture to 4 g/l, if the Mn/Mg content in the solved composition was greater than 4 g/l, accumulation would occur.
- For each scenario, copper and nickel were balanced by varying the % of each plant's respective operating capacity. If more than 100%capacity would be required to remove one of these impurities, accumulation of the specific impurity would occur.
- Skorpion's circuit was, at the time of this project, limited to a feed rate of 230 t/h solids (in the form of ore, oxides or both), so if no limiting impurity was found, throughput would be limiting.
- Once the limiting impurity had been determined, and the maximum feed throughput had been iteratively calculated, the rest of the impurities in the circuit were calculated according to their respective methods (described above).

The base case mass balance for the Skorpion refinery assumed that 0 t/h of zinc oxides could be fed to the circuit and that a total of 230 t/h ore could be fed to the circuit. This resulted in a total of 151 000 t zinc production per annum in the mass balance calculation. Once the base case had been established, each of the alternative oxides was run through the mass balance in different ratios with the Skorpion ore, and the maximum achievable zinc production for each scenario was calculated. These results are summarized in Table 23, along with the limiting factor for each scenario.

Table 23. Summary of the mass balance results for different feed blends of alternative oxides with Skorpion ore.

Oxide source	Ore feed %	Oxides feed %	Max total feed throughput (t/h)	Max Zn production (t/h)	Max Zn production (kt/y)	Limiting impurity
Base case	100	0	230	19	151	THROUGHPUT
EAFD	90	10	230	24	186	THROUGHPUT
EAFD	80	20	230	28	220	THROUGHPUT
EAFD	70	30	192	27	214	COPPER
EAFD	60	40	13	4	29	MAGNESIUM
EAFD	50	50	3	2	18	MANGANESE
Dross	90	10	174	23	183	NICKEL
Dross	80	20	115	21	169	NICKEL
Dross	70	30	86	21	162	NICKEL
Dross	60	40	69	20	158	NICKEL
Dross	50	50	57	20	155	NICKEL
Fume dust	90	10	230	34	270	THROUGHPUT
Fume dust	80	20	230	49	389	THROUGHPUT
Fume dust	70	30	202	57	447	COPPER
Fume dust	60	40	173	60	475	COPPER
Fume dust	50	50	152	63	495	COPPER

From this table it is clear that the zinc fume dust provides the highest overall zinc throughput and production at all blending ratios. This is due to the high zinc content-low impurity level combination in this source. Copper becomes a limiting impurity in ratios exceeding 30% zinc fume oxide.

The zinc dross sample is limited in its production ability by the amount of nickel contained in the sample. This alternative oxide source contains the largest amount of nickel at 0.2% - an order of magnitude higher than the nickel contained in the other two sources, each of which contain at most 0.02%. This is probably due to the type of steel used in the hot-dip galvanizing process.

EAFD, despite containing the largest percentage impurities and lowest zinc percentage, is not limited by its impurity content in ratios of less than 20% with the Skorpion ore. Instead, it is initially limited by the plant throughput, which is capped to a maximum of 230 t/h feed. In ratios exceeding 30%, first copper, then magnesium and finally manganese become limiting elements.

Figure 33 represents the total final metal production for the various alternative zinc oxides blended in different ratios with the Skorpion ore feed. Here it is evident that the zinc fume sample provides the highest zinc production at all blends. Since this sample's production capacity is limited by the plant throughput in the two lowest proportion blends, and because it has a much higher zinc grade than the Skorpion ore, the zinc produced decreases as the alternative oxide portion of the feed decreases.

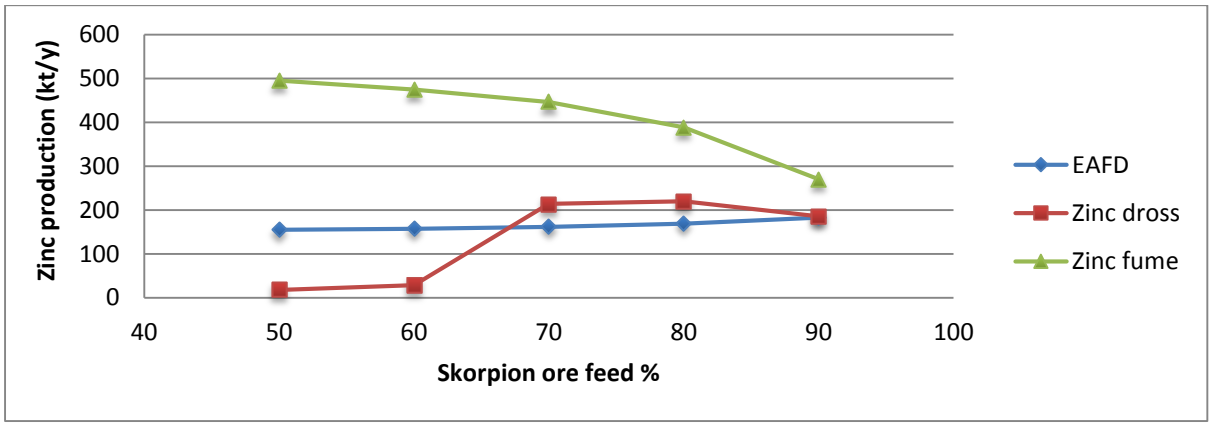

Figure 33. Zinc production based on different ratios of Skorpion ore : alternative oxides feeds.

Zinc production from the zinc dross is fairly consistent for all blend scenarios, with an increase of only roughly 30 000 t per year in production across the range of blends tested. Considering the increase in the amount of oxide that will need to be brought in to blend in higher ratios, it would probably be best to keep the blending ratios for this particular sample below 30% to save on purchasing and freight costs for this oxide, relative to the zinc production obtained from it. This will become clearer in the financial feasibility section, which follows.

EAFD has very low overall zinc recoveries at high blending ratios (exceeding 30% oxide in the blend. This is partially due to high impurity contents, but also due to the lower zinc content (relative to the other two tested samples). Thus, the optimum zinc production takes place at 20% bleed, before impurity accumulation starts limiting the maximum total throughput to the refinery,

Essentially, from the mass balance, it is evident that the zinc fume provides the highest overall zinc production potential. For each of the oxides, there is a scenario which provides the maximum potential zinc production. For EAFD, a blending ratio of 20% oxides with ore is ideal, while the dross should be blended in a 10% ratio. Zinc fume provides the highest theoretical zinc production at a 50% bend with the Skorpion ore.

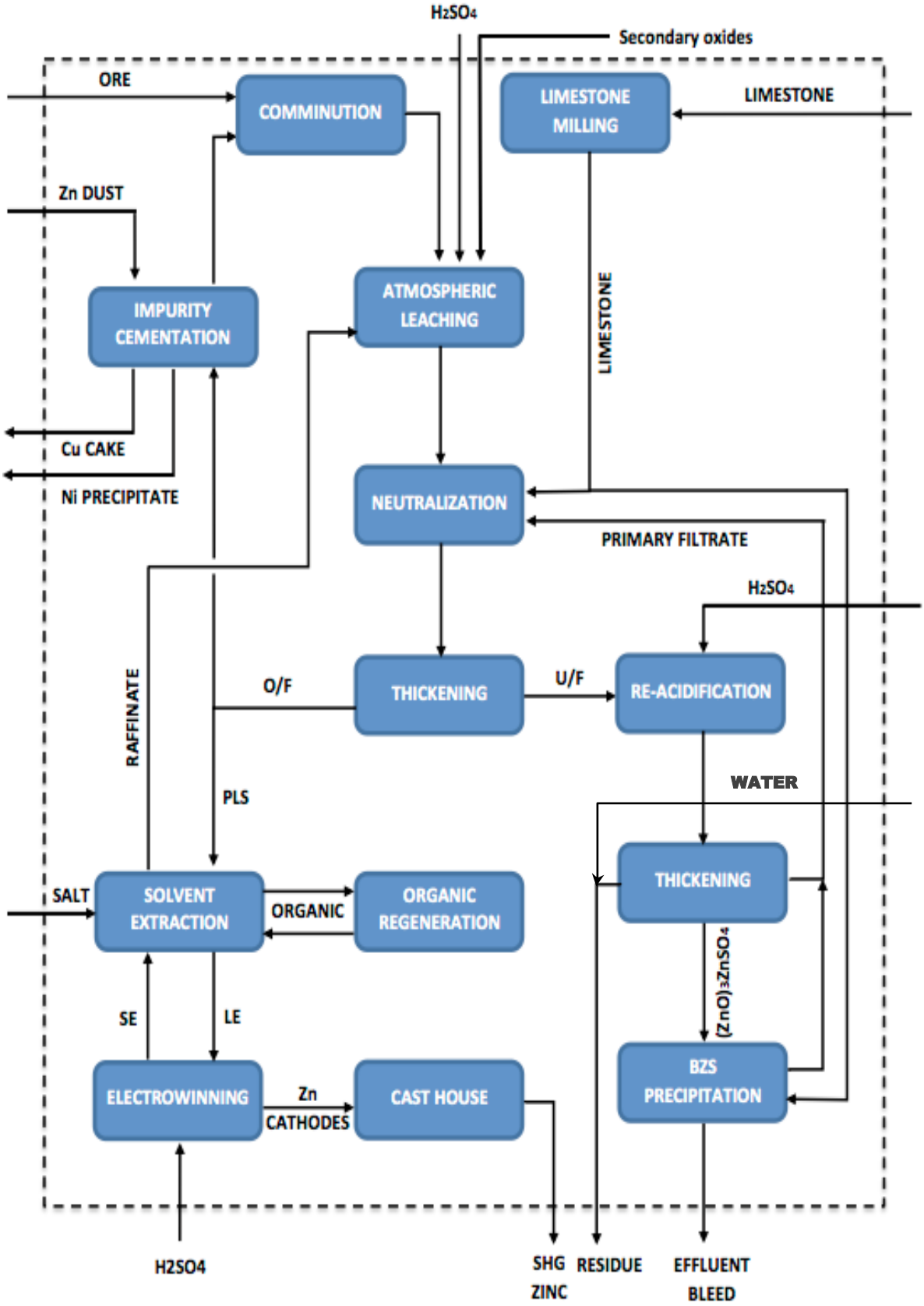

Figure 34. Flow sheet of the Skorpion Zinc process (Redrawn from Gnoinski, 2007).

6. Financial feasibility

Using an assumed LME (London Metal Exchange) zinc price, with an assumed fixed premium, the potential profit that Skorpion could make from processing each oxide, for the different blending ratios, was calculated. The assumed zinc price and premium were scaled to be 100, and all calculations were performed relative to this scaling. Since there is no standard price for the purchase of alternative zinc oxides, it was not possible to determine the exact purchase price. Instead, an assumption which stated that a certain % of the LME zinc price would be paid for the zinc contained in the alternative oxides was used.

Two different scenarios were investigated to determine the profitability of the different oxides. First, a purchase price of 20% of LME zinc price was used. Then this percentage was increased to 30%. It should be noted that this financial feasibility study included only the oxide portion of the production – zinc produced from the Skorpion ore was completely excluded. In each scenario, Skorpion's potential revenue from each oxide was calculated, using the total theoretical zinc production for a particular blend, as determined by the mass balance. Thus, the revenue from the sale of zinc produced from the oxide was calculated as (Equation 9):

$$Revenue = Zinc\ produced \cdot (Zinc\ price + Premium) \quad \text{Equation 9}$$

Next, the cost of producing the zinc was calculated, using the actual costs from the Skorpion refinery and adjusting the costs for the volumes of oxide that would be fed. Adjustments were also made to the mining and comminution costs (these were 0, as no mining or comminution was required for these feed sources. The total cost of production was then calculated as (Equation 10):

$$Cost\ of\ production = Operating\ costs + Fixed\ costs + Variable\ costs \quad \text{Equation 10}$$

Finally, the last cost element on the Skorpion side, the cost of purchasing the oxide, was calculated, using the assumed LME % (Equation 11):

$$Cost\ of\ purchasing\ oxide = Assumed\ \%\ LME \cdot LME\ zinc\ price \quad \text{Equation 11}$$

Next, the EBITDA (Earnings Before Interest Tax Deductions and Amortization) was calculated (Equation 12):

$$EBITDA = Revenue - Cost\ of\ production - Cost\ of\ purchasing\ oxide \quad \text{Equation 12}$$

It was important to ensure that the offer price assumed was reasonable. To determine this, the supplier's profit was also calculated. It is important to note that it was assumed that the supplier would be responsible for paying the freight costs to get the alternative oxide to the Skorpion refinery. Thus, this expense had to be taken into account for the supplier. The supplier's profit was then calculated as (Equation 13):

$$Supplier\ profit = Income\ from\ sale\ of\ oxide - Freight\ costs \quad \text{Equation 13}$$

Situations which resulted in a profit for both the supplier and Skorpion were considered plausible. The results are summarized in Table 24.

Table 24.Summary of revenue and costs relative to one another for Skorpion and the various oxide suppliers

	EAFD	Fume	Dross	EAFD	Fume	Dross
SKORPION ZINC						
Revenue from oxides	100	100	100	100	100	100
Cost of production	50.8	43.2	47.6	50.8	43.2	47.6
% LME for zinc in oxide	30.00%	30.00%	30.00%	20.00%	20.00%	20.00%
Purchase cost	28.4	28.4	28.4	18.9	18.9	18.9
Zn profit	17.5	27.1	22.5	28.1	37.0	32.5
SUPPLIER						
Income from oxide sale	28.4	28.4	28.4	18.9	18.9	18.9
FREIGHT COST						
Unit rate	6.8	6.8	15.8	6.8	6.8	15.8
Total freight	24.6	8.9	26.8	24.6	8.89	26.8
Supplier profit	6.6	20.5	3.0	-3.2	10.8	-6.8

Due to the confidential nature of the plant's processing costs, detailed financial data are omitted; the financial data presented have been scaled relative to oxide revenue, which was assigned a value of 100.

The relative values, in terms of total revenue and cost per ton are the same for all scenarios and are shown in Table 24. It is evident here that at 20% of LME zinc price, the suppliers for EAF dust and zinc dross will not make a profit. Skorpion will however. The zinc fume oxides supplier will make a profit, as will Skorpion, but this seems to be the only plausible sample for the 20% LME zinc price scenario.

At 30% of LME zinc price, all three suppliers will make a profit, as will Skorpion. However, Skorpion's profit per ton is significantly reduced (30-40%, depending on the source).

As the blending ratio is increased, the total income and profit for each source increase, although the per ton values do not change. A summary of the scaled total profit for the supplier and Skorpion are shown in Table 25.

It is clear from these results that the zinc fume oxide is the most profitable oxide option for Skorpion zinc. This is because of the large zinc production volumes that can be generated. EAF dust and zinc dross can be profitable and feasible if a purchase price of 30% of LME zinc price is agreed upon. EAFD dross provides the second highest supplier profit at 30% of LME price. This is due to the high zinc dross transport cost, relative to the transport costs of the other two oxides. EAFD also has the second highest overall income for Skorpion at blends of 30 oxide with ore, or less, due to the larger amounts of zinc that can be manufactured at this blending ratio (relative to the zinc dross zinc production, which is limited by impurities).

In summary, the zinc fume sample has the highest potential to be profitably processed, with both the supplier and Skorpion making a profit from the exchange. If 30% of LME zinc price is offered as the purchase price, both dross and EAFD can also be manufactured profitably, and the supplier will make a profit. In this case, dross will be more profitable to Skorpion than the EAFD, with a scaled profit of 22.5 versus the EAFD profit of 17.5 per ton of zinc.

Table 25. Summary of the annual overall scaled income and expenditure for each blending scenario.

Mass % oxide blended	Oxide source	% LME for zinc in oxide	EBITDA	Supplier profit
10%	EAFD	20.00%	1.4	-0.2
	Fume	20.00%	4.6	1.4
	Dross	20.00%	2.4	-0.5
20%	EAFD	20.00%	2.7	-0.3
	Fume	20.00%	9.3	2.7
	Dross	20.00%	3.1	-0.7
30%	EAFD	20.00%	3.4	-0.4
	Fume	20.00%	12.2	3.6
	Dross	20.00%	3.5	-0.7
40%	EAFD	20.00%	0.3	0.0
	Fume	20.00%	13.9	4.1
	Dross	20.00%	1.2	-0.3
50%	EAFD	20.00%	0.1	0.0
	Fume	20.00%	15.2	4.5
	Dross	20.00%	3.9	-0.8
10%	EAFD	30.00%	0.8	0.3
	Fume	30.00%	3.4	2.6
	Dross	30.00%	1.6	0.2
20%	EAFD	30.00%	1.7	0.7
	Fume	30.00%	6.8	5.2
	Dross	30.00%	2.2	0.3
30%	EAFD	30.00%	2.1	0.9
	Fume	30.00%	8.9	6.9
	Dross	30.00%	2.4	0.3
40%	EAFD	30.00%	0.2	0.1
	Fume	30.00%	10.2	7.8
	Dross	30.00%	0.9	0.1
50%	EAFD	30.00%	0.1	0.0
	Fume	30.00%	11.2	8.6
	Dross	30.00%	2.7	0.4

7. Conclusions and recommendations

7.1. Conclusions

Based on the experimental data it was concluded that it would be possible to leach zinc from any of the three alternative zinc oxide sources tested, using Skorpion's current process and operating conditions. Using the current conditions it was found that a zinc recovery of 93% could be obtained from the EAF dust, and 96.9% from the zinc dross, while a 98% recovery was attainable from the zinc fume oxide source.

EAFD zinc dissolution did not appear to be affected by variations in the pH and temperature. No clear relationship between temperature and pH and zinc dissolution kinetics was observed for the other two samples. Similar overall zinc recovery was not for all the temperature and pH conditions (less than a 5% variance between the final recoveries obtained for all the test runs). Although the zinc dross sample experienced the fastest zinc dissolution at a pH of 1.2-1.25 at 40°C and 60°C, a pH of 1.8-1.85 provide faster dissolution at 50 and 70°C. The zinc fume oxide, on the other hand experiences little change in the leaching kinetics between pH values of 1.2 and 1.5 at 40°C, and between pH values of 1.2, 1.5 and 1.8 at 50 °C. All four pH set points have similar kinetics at 70°C. However, at 60°C, the kinetics differ significantly with the fastest kinetics occurring at a pH of 1.2, then 2.1, 1.5 and the slowest at a pH of 1.8.

Although these results do not follow the trends expected from literature (due to the variable nature of the samples tested, versus the fixed composition of the samples tested in literature),they are significant in that they show that it should be possible to leach zinc from all three of the oxide sources, without making significant changes to Skorpion's processing parameters.

Acid consumption measured for these three sources was 1.02 t/t of zinc for the EAFD, 1.34 t/t of zinc on the zinc dross and 0.11 t/t Zn for the zinc fume oxides. Based on the Skorpion feasibility limit of 1.5 t/t of zinc leached, all three samples are below the target acid consumption. Based on the impurities leached from each of these samples, it seems that the calcium is the major acid consumer in the EAFD, while iron and aluminium consume most of the acid when leaching the zinc dross/ash sample. Iron seemed to be the major impurity in the zinc fume, but it was not prevalent in concentrations as high as in the dross and EAFD samples.

From the mass balance it was determined that the zinc fume sample would consistently provide the highest zinc production of the three samples, regardless of the blending ratio used. This sample can theoretically lead to an annual zinc production of 495kt, when blended in a 50% ratio with the Skorpion ore. This is approximately 125% of the maximum production from EAF dust (220 kt/y at a 20% blending ratio) and 170% of the maximum zinc dross zinc production (183 kt/y at a ratio of 10%). This was due, in part, to its high zinc concentration and because of its low impurity content, which meant that impurity accumulation was not a concern. In addition, because of its low acid consumption levels, relative to the other two samples, it would be the cheapest to process from an operational point of view.

On the other hand, because of its low zinc content, EAFD generally provided the lowest zinc production. However, under the right circumstances (i.e. blended in a ratio of less than 20%

alternative oxides with the ore); this source could provide more zinc production than the zinc dross. The dross was limited to a large extent by its impurity levels – specifically the nickel content, which was higher than the nickel content in either of the other two samples. Impurity levels in the leach residue liquid produced from each of these samples may be a cause for concern. The Skorpion circuit was designed to deal with a maximum aluminium and iron content in PLS of 1450 and 240 ppm respectively. While the zinc fume leach residue liquid does have lower impurity levels than this, the EAFD and zinc dross samples' iron content is in excess of 1800 ppm. The aluminium in the zinc dross residue liquid is also 3 times higher than the Skorpion circuit has been designed to deal with, at a concentration of 3800 ppm. As a result, there is a possibility that the neutralization circuit could be overloaded.

The financial feasibility study performed using the mass balance results showed that the zinc fume oxide would be the most profitable option of the three alternative oxide options. Of the three options, this was the only source that was profitable for both the supplier and Skorpion at a 20% LME zinc purchase price for the zinc contained in the oxide. At the 20% of LME cost, this sample allowed for a scaled profit of 37 on Skorpion's end, with a scaled profit to the supplier of 10.8. Increasing the proposed purchase price to 30% of LME zinc price to make the purchase price more attractive to the supplier resulted in a decrease in Skorpion's profit of 27% to 27.1. The supplier would then make a profit of 20.5.

7.2. Recommendations

To determine the effect of the impurities contained in each of these alternative feed stock samples, the samples should be sent for external analysis to fully define the elemental composition. Some elements cannot be analysed by the Skorpion Zinc on site laboratory, and may cause problems in the downstream processes, if proper measures are not put in place to prevent the transfer of these elements (e.g. antimony, fluorides, chlorides and arsenic). In addition, neutralization tests should be performed to determine whether the neutralization section will be capable of dealing with the increased quantities of iron and aluminium being fed to the circuit, particularly for the EAF dust and zinc dross/fly ash samples.

The high iron and aluminium contents in the leach residue liquid generated from the EAFD and zinc dross samples should be further investigated if the decision is made to use these samples as supplementary feed. Neutralization tests should be performed to determine whether the Skorpion circuit would be overloaded, or if it would be capable of handling these impurities.

Copper and nickel plant have never been operated at 100% of their theoretical design capacities, as the Skorpion had not required such high throughput in the past. It is recommended that these plants be tested to see whether maximum throughput is practically achievable before alternative oxides are fed to the plant.

Neutralizing the resultant PLS from the leaching circuit will cause some of the zinc to precipitate out of the solution. Skorpion's BZS circuit has been designed to provide a solution to this problem. However, it will be necessary to determine whether this process will work as effectively for the

alternative oxide sources as it does for the current Skorpion ore. To this end, BZS tests should be performed as a follow-up to the neutralizations tests.

Careful consideration will have to be given to the accounting of the feed of these alternative oxides. Attention will need to be given to determining how to account for the feed to the circuit, and how to account for the recoveries obtained from this material, if it needs to be accounted for separately.

Some additional studies can be done on the possibility of blending these alternative oxides with the stockpiled marginal zinc ore from Skorpion's pit. This material contains less than 4% zinc and high (>7%) calcium with large amounts of copper. It will therefore need to be carefully studied to ensure that the acid costs will not be beyond economically feasible limits, and to ensure that the additional copper will not overload the circuit.

The zinc content in the residue liquid for each of these samples exceeds the design maximum PLS tenor for the Skorpion circuit. Depending on which sample is chosen, and what blending ratios are used for feeding the sample to the refinery, some adjustments to the operating philosophy in SX may be required. This study should be done in detail. In addition, to establish the composition residue solution from the ore-oxide blends, leaching tests should be done using the different blends discussed in this report.

The potentially hazardous nature of the EAF dust and zinc dross is an important factor to consider when it comes to disposal of the tailings generated by leaching these solids. Literature indicates that the harmful lead, chromium and cobalt are generally leached together with the zinc (Oustadakis, *et al.*, 2010). Most of these impurities will, in Skorpion's case, be removed together with the copper or nickel in their respective plants.

Further studies to determine the exact composition of the residue, and the potential environmental impacts, should be done before processing of either of these sources commences. If stable ferric matrices or acid-generating wastes are formed at any point during neutralization, there may be environmental impacts associated with this that will also have to be considered. It is therefore important to take this into account when performing the more in-depth test work, and to ensure that proper testing is done on all waste before the oxides are fed to the refinery. Specialized waste management procedures and additional environmental permits may be required, which may have an economic impact on the feasibility of using the oxides.

8. References

1. Ahmed, I.M., Nayl, A.A., Daoud, J.A., 2012, Leaching and recovery of zinc and copper from brass slag by sulphuric acid, Journal of Saudi Chemical Society, pp. 1-5
2. Bahram, B., Babaeidehkordi, A., Moghadam, J., 2013, Determination of the optimum conditions for leaching of zinc cathode melting furnace slag in ammonium chloride media, Metallurgical and materials transactions, Vol. 45B, pp. 562-567
3. Barrett, E.C., Nenniger, E.H., Dziewinski, J., 1992, A hydrometallurgical process to treat carbon steel electric arc furnace dust, Hydrometallurgy, Vol. 30 (1-3), pp. 59-68
4. Crundwell, F., 2003, Principles and practice of leaching, Unpublished presentation for Skorpion Zinc operators, Johannesburg: CM solutions, pp. 1-10
5. Cruells, M., Roca, A., Nunez, C., 1992, Electric arc furnace flue dusts: Characterization and leaching with sulphuric acid, Hydrometallurgy, Vol. 31, pp. 213-231
6. De Walens, J., 2002, Cast house functional specification, Unpublished functional specification for the Skorpion Zinc joint venture, pp. 1-16
7. De Wet, J.R, 2000, Sulphuric acid consumption model, Unpublished technical report for Skorpion Zinc base metals, Anglo base metals: Johannesburg, pp. 1-15
8. Dreissinger, D.B., Peters, E., Morgan, G., 1990, The hydrometallurgical treatment of carbon steel electric arc furnace dust by the UBC-Chaparral process, Hydrometallurgy, Vol. 25, pp. 137-152
9. Duyvesteyn, W.P.C., Jha, M.C., 1986, Two stage leaching process for steel plant dusts, United States Patent, Patent number: 4 610 721, pp. 1-7
10. Dvořák, P., Jandová, J., 2005, Hydrometallurgical recovery of zinc from hot dip galvanizing ash, Hydrometallurgy, Vol. 77, pp. 29-33
11. Elgersma, F., Kamst, G.F., Witkamp, G.J, van Rosmalen, G.M., 1992, Acidic dissolution of zinc ferrite, Hydrometallurgy, Vol. 29, pp. 173-189
12. European Waste Catalogue and Hazardous Waste List, Published by the environmental Protection Agency, Ireland, Valid from 1 January 2002, pp. 1-49
13. Fukubayashi, H., 1972, The effect of impurities and additives on the electrowinning of zinc, Unpublished thesis, Missouri: Missouri university of science and technology, pp. 1-72
14. Gnoinski, J., 2007, Skorpion Zinc: Optimisation and innovation, The Southern African Institute of Mining and Metallurgy, The Fourth South African Conference on Base Metals, pp. 329-342
15. Green, D.W., Perry, R.H., 2008, Perry's chemical engineers' handbook, 8th edition, McGraw-Hill companies, pp. 18.59-18.61
16. Guspiel, J., Riesenkampf, W., 1993, Kinetics of dissolution of ZnO, MgO and their solid solutions in aqueous sulphuric acid solutions, Hydrometallurgy, Vol. 34, pp. 203-220
17. Havlik, T., Friedrich, B., Stopić, S., 2004, Pressure leaching of EAF dust with sulphuric acid, World of Metallurgy, ERZMETALL, Vol. 57 (2), pp. 113-120
18. Havlik, T., Turzakova, M., Stopić, S., Friedrich, B., 2005, Atmospheric leaching of EAF dust with diluted sulphuric acid, Hydrometallurgy, Vol. 77, pp. 41-50
19. Havlik, T., Souza, B.V., Bernardes, A.M., Schneider, I.A.H., Miškufová, 2006, Hydrometallurgical processing of carbon steel EAF dust, Journal of Hazardous materials, Vol. 153 (1-3), pp. 311-318
20. Herrero, D., Arias, P.L., Güemez, B., Barrio, V.L., Cambra, J.F., Requies, J., 2010, Hydrometallurgical process development for the production of a zinc sulphate liquor suitable for electrowinning, Minerals engineering, Vol. 23, pp. 511-517
21. Hoang Trung, Z., Havlik, T., I.A.H., Miškufová, 2007, Processes for steelmaking dust treatment, Unpublished technical paper, Technical University of Košice, pp. 1-6

22. Jandová, J., Prošek, T., Maixner, J., 1999, Leaching of zinc oxide in aqueous sulphuric acid solutions, Prague Institute of Chemical Technology, pp. 1-9
23. Jandová, J., Dvořák, P., Hong, V., 2002, Recovery of magnetite and zinc from steel-making dust by H_2SO_4 leaching, Proceedings of The Minerals, Metal and Materials Society FALL, pp. 252-259
24. Jha, M.K., Kumar, V, Singh, R.J., 2001, Review of hydrometallurgical recovery of zinc from industrial wastes, Resources, Conservation and recycling, Vol. 33 (1), pp. 1-22
25. Koutsaris, C., 2011, Metallic foam formation during continuous hot-dip galvanizing of steel sheet, Unpublished thesis, Montréal: Université de Montréal, pp. 1-122
26. Kukurugya, F., Vindt, T., Havlik, T., 2015, Behaviour of zinc, iron and calcium from electric arc furnace dust in hydrometallurgical processing in sulphuric acid solutions: Thermodynamic and kinetic aspects, Hydrometallurgy, Vol. 154, pp. 20-32
27. Langová, S., Riplová, J., Vallová, S., 2007, Atmospheric leaching of steel-making wastes and the precipitation of goethite from the ferric sulphate solution, Hydrometallurgy, Vol. 87 (3-4), pp. 157-162
28. Leaching and adsorption resource book, 2012, [online], Available: http://rsteyn.files.wordpress.com/2010/07/leaching-adsorption-basics-and-example.pdf, [2012, May 5]
29. Leclerc, N., Meux, E., Lecuire, J-M., 2003, Hydrometallurgical extraction of zinc from zinc ferrites, Hydrometallurgy, Vol. 70, pp. 175-183
30. Li, Z., Li, J., Zhang, L., Peng, J., Wang, S., Ma, A., Wang, B., 2015, Response surface optimization of process parameters for removal of F and Cl from zinc oxide fume by microwave roasting, Transactions of nonferrous metals society of China, Vol. 25, pp. 973-980
31. Lupi, C., Pilone, D., Cavallini, M., 1996, Hydrometallurgical processing of EAF steelmaking fumes, Proceedings of the second international symposium on extraction and processing for the treatment and minimization of wastes, The Minerals, Metal and Materials Society/AIME, pp. 711-718
32. Miller, G., 2005, Analysis of agitation leaching data – methods and interpretation, First extractive metallurgy operators' conference, pp. 1-6
33. Moradi, S., Monhemius, A.J., 2011, Mixed sulphide-oxide lead and zinc ores: problems and solutions, Minerals engineering, Vol. 24, pp. 1062-1076
34. Nagib, S., Inoue, K., 2000, Recovery of lead and zinc from fly ash generated from municipal incineration plants by means of acid and or alkaline leaching, Hydrometallurgy, Vol. 56, pp. 269-292
35. Nyirenda, R.L., 1991, Processing steelmaking flue dust, Minerals engineering, Vol. 4, pp. 1003-1025
36. Oustadakis, P., Tsakiridis, P.E., Katsiapi, A., Agatzini-Leonardou, S., 2010, Hydrometallurgical process for zinc recovery from electric arc furnace dust (EAFD), Part I: Characterization and leaching by diluted sulphuric acid, Journal of hazardous materials, Vol. 179, pp. 1-7
37. Pecina, T., Franco, T., Castillo, P., Orrantia, E., 2008, Leaching of a zinc concentrate in H2SO4 solutions containing H2O2 and complexing agents, Minerals engineering, Vol. 21, pp. 23-30
38. Pereira, C.F., Galiano, Y.L., Rodríguez-Piñero, M.A., Parapar, J.V., Long- and short-term performance of a stabilized/solidified electric arc furnace dust, 2007, Journal of hazardous materials, Vol. 148 (3), pp. 701-707
39. Rabah, M.A., El-Sayeh, A.S., 1995, Recovery of zinc and some of its valuable salts from secondary resources and wastes, Hydrometallurgy, Vol. 37, pp. 23-32

40. Ramachandra Sarma, V.N., Deo, K., Biswas, A.K., 1976, Dissolution of zinc ferrite samples in acids, Hydrometallurgy, Vol. 2, pp. 171-184
41. Ruşen, A., Sunkar, A.S., Topkaya, Y.A., 2008, Zinc and lead extraction from Çinkur leach residues by using hydrometallurgical methods, Hydrometallurgy, Vol. 93, pp. 45-50
42. Safari, V., Arzpeyma, G., Rashchi, F., Mostoufi, N., 2009, A shrinking particle-shrinking core model for leaching of a zinc ore containing silica, International Journal of Mineral Processing, Vol. 93, pp. 79-83
43. San Lorenzo, D.M., Nogueira, G.D., Leon, M.A.G., 2005, Process for the continuous production of high purity electrolytic zinc or zinc compounds from zinc primary or secondary raw materials, United States Patent, Patent number: US 6 869 520 B1, pp. 1-10
44. Shawabkeh, R.A., 2010, Hydrometallurgical extraction of zinc from Jordanian electric arc furnace dust, Hydrometallurgy, Vol. 104, pp. 61-65
45. Shitov, A.V., Klimushkin, A.N., Stoyarskii, O.A., Agapeev, E.N., 2005, Recycling of the dross formed in hot galvanizing, Metallurgist, Vol. 49 Nos. 7-8, pp.296-298
46. Sinclair, R.J., 2005, The extractive metallurgy of zinc, The Australian institute of mining and metallurgy, Spectrum series volume 13, First edition, pp. 105-112
47. Skorpion Zinc Solvent Extraction Operational Manual, 2003, Skorpion Zinc Project Joint Venture documentation [confidential internal communication], pp. 1-36
48. Sofilic, T., Rastovcan-Mioc, A., Cerjan-Stefanovic, S., Novosel-Radovic, V., Jenko, M., 2004, Characterization of steel mill electric arc furnace dust, Journal of hazardous materials, Vol. 109, pp. 59-70
49. Souza, A.D., Pina, P.S, Lima, E.V.O., da Silva, C.A., Leão, V.A., 2007, Kinetics of sulphuric acid leaching of a zinc silicate calcine, Hydrometallurgy, Vol. 89, pp. 337-345
50. Su, C., Shen, Y., 2009, Deflocculation and classification of electric arc furnace dust in aqueous solutions, Separation science and technology, Vol. 44, pp. 1816-1828
51. Suetens, T., Guo, M., Van Acker, K., Blanpain, B., 2015, Formation of the $ZnFe_2O_4$ phase in an electric arc furnace off-gas treatment system, Journal of hazardous materials, Vol. 287, pp. 180-187
52. Trpčevská, J., Hlucháňová, B., Vindt, T., Zorawski, W., Jakubéczyová, D., 2010, Characterization of the bottom dross formed during batch hot-dip galvanizing and its refining, Acta Metallurgica Slovaca, Vol. 16, No. 3, pp. 151-156
53. Turan, M.D., Altundoğan, H.S., Tümen, F., 2004, Recovery of zinc and lead from zinc plant residue, Hydrometallurgy, Vol. 75 (1-4), pp. 169-176
54. Web book in hydrometallurgy, 2012, [online], Available: www.biomine.skelleftea.se/biomine/leaching/letheo_11.htm, [2012, April 29]
55. Xu, H., Wei, C., Li, C., Fan, G., Deng, Z., Li, M., Li, X., 2010, Sulphuric acid leaching of zinc silicate ore under pressure, Hydrometallurgy, Vol. 105 (1-2), pp. 186-190
56. Yoshida, T., 2003, Leaching of zinc oxide in acidic solution, Materials transactions, Vol. 44, No. 12, pp. 2489-2493

Appendix A: Nomenclature and glossary

Symbol	Definition	UOM	Definition
A	Area	m^2/m^3	The amount of space taken up by a two dimensional region per unit volume
C	Concentration	g/l, mg/l, ppm	The amount of a substance present in a given unit volume
D	Diffusion constant	m^2/s	The amount of a substance diffusing from one region to another per unit area per second, with a concentration gradient of one
dC/dx	Concentration gradient	-	The gradual difference in concentration of a substance per unit distance in a solution
dn/dt	Moles diffusing per time	mol/s	Rate of diffusion of the moles of a substance
E_a	Activation energy	kJ/mol	Minimum energy required for a certain chemical reaction to take place
Demin	Demineralized water	-	Water purified using a reverse osmosis process to remove the majority of all dissolved salts
ETP	Effluent treatment plant	-	Portion of the refinery dedicated to treating all liquid process waste from all areas of the plant; serves as an impurity bleed for elements that would otherwise build up in the process solution
EW	Electrowinning	-	The term used to refer to the plating of metals onto a cathode by passing direct current through an ionic solution
J	Rate of diffusion	mol/s	Amount of substance that diffuses through a surface per unit time
K	Solubility constant	mol/dm^3	A compound in solid state in equilibrium with the same compound in solution
k	Rate constant	-	The relationship between chemical reaction at a specific temperature to the concentration of the reactants, when the concentration of each of each of the reactants is one
K_{SP}	Solubility product	mol^3/L^3	Concentration of dissolved ions in a solution raised to the power of the stoichiometric coefficients of the specific ions
kt/y	Kilotons per year	-	Production per annum
LFS	Leach feed solids	g	Zinc-rich solids fed to the leaching process and from which zinc is recovered by leaching
LRL	Leach residue liquid	ml/L	Zinc-rich solution generated by leaching of the feed solids
LRS	Leach residue solids	g	Zinc-poor solids remaining after leaching has been completed (from which zinc has been leached)

Symbol	Definition	UOM	Definition
M	Metal, e.g. Zn, Fe, Al	-	Used in reactions to represent a metal
MIC	Metal in concentrate	t	Expression of the mass of the metal of interest contained in concentrate; in this case, concentrate refers to the oxide sources under investigation
MT	Metric tonne	-	Unit of mass
M_w	Molecular weight	g/mol	Mass of 1 mole of a substance
N	Avogadro's number	mol^-	Amount of atoms or molecules contained in one mole of a substance
η	Viscosity	cP	The resistance of a fluid substance to deformation by a shear or tensile force
PLS	Pregnant leach solution	-	Solution obtained after leaching of solid substance with a lixiviant; contains the ion of interest in high concentration
R	Gas constant	Pa/mol·K	Also called the universal gas constant
R	Radius	mm	Radius of the diffusing molecule
r_A or r_i	Rate of reaction	s^{-1}	Rate of formation or consumption of a specific species
RAF	Raffinate	-	High acid, low zinc content solution which is used as a leachant in the Skorpion process; the return solution from SX after zinc has been extracted from PLS
RH	D2EHPA molecule	-	Representation of the extractant molecule used by Skorpion, where the H refers to the acid proton and the R to the rest of the molecule (organophosphorous portion)
rpm	Revolutions per minute	-	Unit of speed; used to refer to agitation rate
S_0	Specific surface area	m^2/kg	Surface area expressed per unit of mass of a substance
SX	Solvent extraction	-	An ion exchange process in which two solutions of different densities are contacted, one containing an extractant, to transfer only the ion of interest to the alternate solution phase
T	Temperature	°C	Measure of the degree of the intensity of the heat of a substance
t	Residence time	minutes	The amount of time over which a chemical reaction is allowed to take place
US$ mn	Million US dollars	-	Total profit for a specified amount of oxide
W	Weight	g, mg, kg	The force exerted upon a body by gravity
x	Diffusion layer thickness	mm	Thickness of the layer through which the lixiviant and dissolved substance must travel during leaching

Appendix B: Alternative zinc oxide assays

Table 26, below shows the elemental compositions of the various oxide samples selected for experimental test work. These compositions are based on the average assays obtained for these sources from a host of samples submitted to the Skorpion analytical laboratory.

Moisture results are based on the moisture in the as-received sample. This may be subject to change for bulk samples to the refinery, as shipping methods will differ for large quantities.

Table 26. Average elemental composition of each of the different types of samples used for experimental test work.

Element	Zinc dross	EAF dust	Zinc fume
Moisture (%)	0.12	<0.1	7
Zinc (%)	40-70	25-35	70-90
Aluminium (%)	5.0-7.0	0.4-1.5	0.06-0.15
Calcium (%)	0.1-0.2	1.0-2.5	0.1-0.2
Copper (%)	0.05-0.15	0.1-0.2	0.10-0.15
Iron (%)	1.0-3.0	8-13	0.5-0.8
Cadmium (%)	0.00-0.02	0.04-0.07	0.03-0.05
Cobalt (%)	0.00-0.01	0.001-0.01	0.05-0.08
Potassium (%)	0.3-0.5	1.0-2.5	0.15-0.25
Magnesium (%)	0.1-0.2	1.0-1.25	0.05-0.10
Manganese (%)	0.0-0.2	0.8-1.0	0.00-0.02
Nickel (%)	0.1-0.2	0.01-0.02	0.00-0.02
Lead (%)	0.01-0.03	0.1-2.0	4.5-5.5
Silica (%)	1.0-1.5	1.5-1.8	1.5-1.8

The particle size distributions for the three oxide samples selected are displayed in Table 27 below. These particle size analyses were performed on the samples based on the state in which they were received – no processing was performed before PSD analysis.

Table 27. Particle size distribution of the different samples used for this study.

	Zinc dross	EAF dust	Zinc fume
P10 (µm)	11	1	9
P50 (µm)	209	24	603
P80 (µm)	586	379	1074
P90 (µm)	851	671	1336

Appendix C: Experimental procedure

Equipment required for this experimental preparation included:
2x 1000ml Glass beaker
2x 1000ml volumetric flask
1x 250ml Measuring cylinder
1x Magnetic stirrer with built in hotplate, and stirrer bar
1x Electronic balance (0.1 grams accuracy)
1x pH meter
1x Thermometer
1x Rotary splitter

In addition, a set of reagents was required to prepare the solutions. These include the following:
98% Industrial grade sulphuric acid concentrate
Analytical grade zinc sulphate
Demineralised water

The ore sample required was sieved to -180 µm and a 136 g sample was extracted from the bulk sample for each experiment.

Zinc and sulphuric acid solution preparation

This solution was used to emulate the role of the raffinate in the refinery leaching circuit, and was therefore used as the leaching solution for the experiments. The presence of the zinc in the solution mimics the raffinate solution used for leaching on the plant, which contains some zinc. The amount of this solution used for each experiment varied depending on the pH of the experiment, and the composition of the solid sample. This solution consisted of 34g/l zinc and 72g/l sulphuric acid. The procedure for the preparation of 1 litre of this solution is as follows:

1. Place 149.5g of pure $ZnSO_4.7H_2O$ into a 1000ml glass beaker containing 500ml demineralised water
2. Measure out 41.22ml sulphuric acid and gently pour this into the water/zinc sulphate mixture while stirring with the magnetic stirrer (to avoid boiling)
3. Rinse the measuring cylinder used for the sulphuric acid 3 times with a small amount (100ml) of demineralised water (to remove all the acid) and add this to the solution
4. Transfer the solution to a 1000ml volumetric flask
5. Rinse the beaker with a 50ml demineralised water 3 times, adding this water to the volumetric flask
6. Allow the acid solution to cool to ambient temperature
7. Add demineralised water to the volumetric flask to increase the total volume to 1000ml
8. Mix the solution thoroughly by inverting the flask 10 times and allowing the air bubble to reach the top or bottom of the flask after each inversion
9. Allow the solution to cool to room temperature again and then top up the volume to 1000 ml again, if necessary
10. Take a 50ml sample of this solution and submit it for zinc and free acid analysis

Sulphuric acid solution preparation

For the leaching of the solid sample, this solution was required to maintain the pH at the desired set point. To make 1 litre of this solution, the following procedure should be used. This solution contains 500g/l sulphuric acid.

1. Measure 274.7 ml concentrated sulphuric acid out
2. Add this sulphuric acid to a 1 litre beaker containing 250ml demineralised water while stirring constantly with a magnetic stirrer
3. Rinse the measuring cylinder 3 times with a small amount (100ml) of demineralised water, adding this water to the beaker
4. Transfer the solution to a 1000ml volumetric flask and rinse the beaker with three 50ml measures of demineralised water, adding the rinse water to the volumetric flask
5. Allow the solution to cool to room temperature before topping the volume up to 1000ml and mixing thoroughly
6. Allow the solution to cool again and then top up, if necessary
7. Send a 50ml sample for free acid analysis

Washing solutions preparation

In addition to the leaching solutions, a washing solution is required for solid sample preparation. This solution is prepared by adding sulphuric acid to demineralised water until the pH has decreased to 2. The pH of this solution is adjusted by adding some of the 500g/l sulphuric acid solution. This washing solution is then heated to 80˚C and maintained at this temperature by using a water bath set to this temperature. A total of 1000 ml of this solution will be required for each experiment.

A second washing solution is also prepared. This solution is simply pure demineralized water, which is heated to 80˚C using the heating function on the magnetic stirrer. Only 500 ml of this sample is required.

Solid sample preparation

1. Dry the entire bulk sample at 70˚C for 24 hours to determine the moisture content
2. Weigh the dried sample and calculate moisture content
3. Sieve the samples using a 180 µm sieve, and grind the oversize fraction
4. Homogenise the samples by rotary splitting and combining three times
5. Split the sample into equal parts of roughly 150g each, and submit one of these samples for the following analyses:
    - Elemental analysis
    - PSD analysis (determine the -180µm fraction accurately)
6. Ensure that the samples used for the leaching tests are accurately weighed to 136g each

Experimental procedure

The Anaconda Leach test procedure used by Skorpion Zinc requires the following equipment:
1x pH meter
1x Water bath, with submersible circulation heater
1x Stopwatch
1x 5000ml Glass beaker for leaching vessel
1x Electrical agitator with Teflon coated stirring blades
1x 2000ml Class A measuring cylinder

In addition, the following reagents will be required for the experiments:
Zinc and sulphuric acid solution
Sulphuric acid solution
136 g solids of the desired sample
Approximately 500 ml room temperature demineralised water (to ensure slurry density of 1.4 g/l)

Leaching tests

1. Place the 5000ml leach vessel into a water bath heated to 50˚C
2. Pour 500ml demineralised water into the leaching vessel and heat to 50˚C and maintain this temperature throughout the course of the test with the help of the water bath
3. Position the agitator and stirring rod so that the stirring rod does not make contact with the vessel
4. Set the agitation speed to 300 rpm to ensure that a well-mixed slurry is formed
5. While stirring, add the 136 g solid sample
6. Using the portable pH meter, monitor the temperature and pH
7. Once the temperature of the slurry has reached 50˚C , record the pH
8. Now increase the agitation rate to approximately 700 rpm
9. Now start the stopwatch and start adding the leaching solution
   NOTE: The addition of this solution should be done slowly, ensuring that the pH never falls below the desired set point. Once the pH is essentially at set point, the 500g/l sulphuric acid solution can be added. In total, the addition of the leaching solution should not take longer than 15 minutes. It should also be noted that the pH should be varying only slightly around the set point when the change to sulphuric acid solution is made, otherwise acid consumption will be over-estimated.
10. Ensure that a vortex does not form, as a result of the agitation speed being too high
11. When the leaching solution has been added, and it is time to start adding the sulphuric acid solution, reset the stopwatch to time zero
12. Add small amounts of the sulphuric acid solution, to maintain the pH between 1.80 and 1.85
13. Continue stirring for another 120 minutes
14. During this time, ensure that the pH is maintained between 1.8 and 1.85 by adding small amounts of the sulphuric acid solution- the exact amount of this solution should be measured by adding it with a burette
15. For the duration of the test, the amount of acid added and the pH should be measured and recorded every 10 minutes
16. For the duration of the test, samples should also be taken at the following time intervals: 0, 10, 20, 30, 40, 50, 60, 80, 100, 120 minutes
17. Once the 120 minutes has elapsed, stop the agitator and filter the solution using the filter pot, as described in the next section

Filtration and washing

Equipment required for this final stage of the experiment is as shown:
1x Filter pot
1x Filter paper
1x Vacuum pump
2x 2000ml Class A measuring cylinder

The reagents required for this phase of the experiment are:
1000 ml pH 2 washing solution
500 ml heated demineralized water washing solution

After the full leaching time of 120 minutes has passed, the solids and liquids should be separated by vacuum filtration according to the procedure shown below.

1. Place the filter paper in the filter pot and ensure that the filter pot is properly affixed to its base
2. Place one 2000 l measuring cylinder below the output of the filter pot
3. Pour the slurry slowly onto the filter paper, through the top of the filter pot
4. Once all the slurry has been placed into the filter pot, place the lid onto the pot and secure the lid with the lid clamp
5. Next, connect the compressed air line to the filter pot lid
6. Open the ball valve of the compressed air line and allow all the solution to drain out of the filter pot into the measuring cylinder below
7. When no more solution is coming out of the pot, close the compressed air valve and open the vent valve on the lid of the filter pot
8. After all the compressed air has been vented from the pot, open the clamp and remove the pot lid
9. Record the volume and mass of the leach residue filtrate and send the filtrate for ICP and free acid analysis
10. Wash the leach residue solids with an accurately measured volume of 1 litre of pH 2 wash solution, heated to 80˚C by pouring the wash solution over the filter cake and then filtering it through the vacuum pot, according to the same procedure used for the leach residue slurry
11. Keep 100 ml of the washing filtrate and for analysis, after recording the filtrate mass and volume
12. Wash the cake again by using 500 ml of heated demineralised water
13. Weigh this filtrate and record both the mass and filtrate volume, before removing 100 ml of sample for analysis
14. Combine 100ml of each of the two washing filtrates and submit this combined sample for full ICP elemental analysis and free acid analysis
15. Weigh the wet filter cake
16. Dry the solid filter cake at a maximum temperature of 70˚C until the weight remains constant (approximately 24 hours)
17. Determine the weight of the dried filter cake and calculate the moisture content of the wet cake
18. Submit a portion of the solid filter cake for acid digestion and full elemental ICP analysis

Appendix D: Repeatability tests

Figure 35 shows the repeatability trends for the zinc from each oxide, using three experiments performed at 50°C, a pH of 1.8-1.85, with a solids content of 20% and at an agitation rate of 600 rpm.

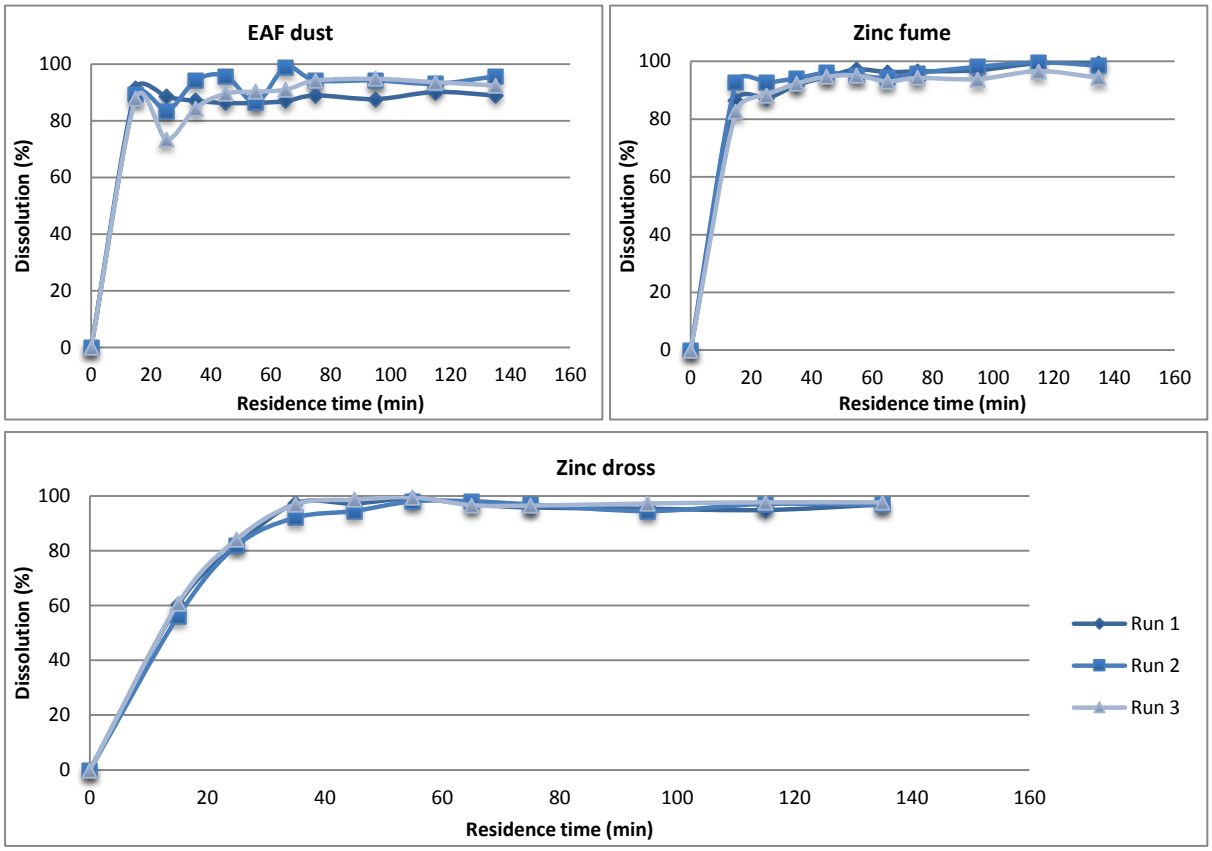

Figure 35. Zinc repeatability at Skorpion process conditions.

Table 28, below shows the standard deviation for each sample at each time, as well as the overall standard deviation for the sample, over the entire experimental period.

Table 28. Repeatability and standard deviation of zinc dissolution for each zinc oxide sample.

	Zinc dross				EAFD				Zinc fume			
Time	Repeat 1	Repeat 2	Repeat 3	Standard deviation	Repeat 1	Repeat 2	Repeat 3	Standard deviation	Repeat 1	Repeat 2	Repeat 3	Standard deviation
0	0.00	0.00	0.00	0.0	0.00	0.00	0.00	0.0	0.00	0.00	0.00	0.0
15	60.25	56.07	60.75	2.6	91.34	87.99	89.13	1.7	86.33	92.68	82.55	5.1
25	81.84	81.86	84.25	1.4	88.41	73.39	83.21	7.6	87.09	92.68	88.30	2.9
35	97.29	92.12	96.99	2.9	86.98	84.55	94.28	5.1	91.78	94.17	92.32	1.3
45	97.29	94.53	98.65	2.1	86.28	89.58	95.76	4.8	94.65	96.03	94.70	0.8
55	99.16	98.08	99.54	0.8	86.28	90.27	86.50	2.2	97.22	95.13	95.12	1.2
65	97.02	98.08	96.66	0.7	86.96	90.94	98.86	6.1	96.31	94.26	93.08	1.6
75	95.83	96.95	96.50	0.6	88.93	94.17	94.25	3.0	96.53	95.95	94.26	1.2
95	95.35	94.49	97.27	1.4	87.64	94.79	94.25	4.0	96.96	98.12	93.88	2.2
115	94.89	97.11	97.70	1.5	90.16	93.60	93.04	1.8	99.42	99.70	96.64	1.7
135	96.91	96.70	97.70	0.5	88.93	92.46	95.65	3.4	99.42	98.52	94.34	2.7
				1.3				3.6				1.9

Appendix E: Mass balance data

Base case

Figure 36, below is a simplified flow sheet representing the major flows for the base case situation in the mass balance, where only Skorpion zinc ore was fed to the circuit. Following the flow sheet is the stream table for this scenario (Table 29).

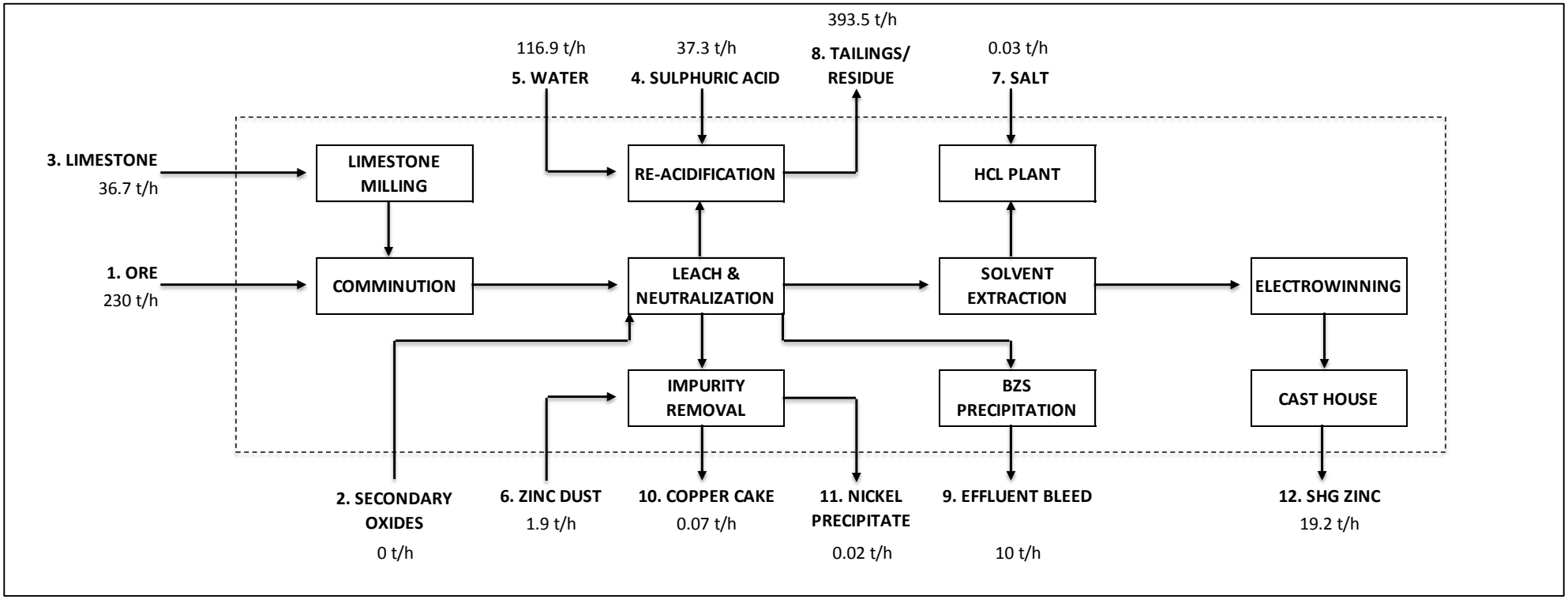

Figure 36. Flow sheet for the base case situation, feeding only Skorpion Zinc ore.

Table 29. Stream table for the base case situation involving only Skorpion ore being fed to the circuit.

		INPUT								OUTPUT					
Stream number		**1**	**2**	**3**	**4**	**5**	**6**	**7**		**8**	**9**	**10**	**11**	**12**	
Stream ID		**Ore**	**Secondary**	**Limestone**	**Sulphuric**	**Water**	**Zinc dust**	**Salt**	**TOTAL**	**Residue**	**Effluent**	**Copper**	**Nickel**	**SHG Zinc**	**TOTAL**
Total mass flow	t/h	230.00	0.00	36.71	37.29	116.87	1.90	0.03	422.80	393.52	10.00	0.07	0.02	19.19	422.80
Solid throughput	t/h	218.50	0.00	34.96	0.00	0.00	1.90	0.03	255.39	236.11	0.00	0.073	0.02	19.19	255.39
Liquid throughput	t/h	11.50	0.00	1.75	37.29	116.87	0.00	0.00	167.41	157.41	10.00	0.00	0.00	0.00	167.41
Solids content	%	95.00%	95.00%	95.00%	0.00%	0.00%	100.00%	100.00%	60.41%	60.00%	0.00%	100.00%	100.00%	100.00%	60.41%
Solids composition															
Zn	%	9.00%	0.00%	0.20%	0.00%	0.00%	100.00%	0.00%	-	0.99%	0.00%	0.00%	0.00%	100.00%	-
Fe	%	2.00%	0.00%	0.80%	0.00%	0.00%	0.00%	0.00%	-	1.97%	0.00%	0.00%	0.00%	0.00%	-
Al	%	5.50%	0.00%	1.60%	0.00%	0.00%	0.00%	0.00%	-	5.31%	0.00%	0.00%	0.00%	0.00%	-
Ca	%	4.00%	0.00%	29.00%	0.00%	0.00%	0.00%	0.00%	-	7.99%	0.00%	0.00%	0.00%	0.00%	-
Cu	%	0.05%	0.00%	0.00%	0.00%	0.00%	0.00%	0.00%	-	0.02%	0.00%	100.00%	0.00%	0.00%	-
Ni	%	0.01%	0.00%	0.00%	0.00%	0.00%	0.00%	0.00%	-	0.00%	0.00%	0.00%	100.00%	0.00%	-
Si	%	26.00%	0.00%	10.98%	0.00%	0.00%	0.00%	0.00%	-	25.68%	0.00%	0.00%	0.00%	0.00%	-
Mn	%	0.32%	0.00%	0.04%	0.00%	0.00%	0.00%	0.00%	-	0.30%	0.00%	0.00%	0.00%	0.00%	-
Mg	%	0.61%	0.00%	0.17%	0.00%	0.00%	0.00%	0.00%	-	0.59%	0.00%	0.00%	0.00%	0.00%	-
Acid	%	0.00%	0.00%	0.00%	0.00%	0.00%	0.00%	0.00%	-	0.00%	0.00%	0.00%	0.00%	0.00%	-
Liquid composition															
Zn	g/l	0.00	0.00	0.00	0.00	0.00	0.00	0.00	-	0.70	0.03	0.00	0.00	0.00	-
Fe	g/l	0.00	0.00	0.00	0.25	0.00	0.00	0.00	-	0.01	0.0005	0.00	0.00	0.00	-
Al	g/l	0.00	0.00	0.00	0.00	0.00	0.00	0.00	-	0.30	0.06	0.00	0.00	0.00	-
Ca	g/l	0.00	0.00	0.00	0.00	0.00	0.00	0.00	-	0.00	0.6	0.00	0.00	0.00	-
Cu	g/l	0.00	0.00	0.00	0.05	0.00	0.00	0.00	-	0.00	0.0005	0.00	0.00	0.00	-
Ni	g/l	0.00	0.00	0.00	0.00	0.00	0.00	0.00	-	0.00	0.01	0.00	0.00	0.00	-
Si	g/l	0.00	0.00	0.00	0.00	0.00	0.00	0.00	-	0.04	0.01	0.00	0.00	0.00	-
Mn	g/l	0.00	0.00	0.00	0.00	0.00	0.00	0.00	-	0.00	0.00	0.00	0.00	0.00	-
Mg	g/l	0.00	0.00	0.00	0.00	0.00	0.00	0.00	-	0.00	0.00	0.00	0.00	0.00	-
Acid	g/l	0.00	0.00	0.00	98.00%	0.00	0.00	0.00	-	10.00	2.00	0.00	0.00	0.00	-
Total elemental flow															
Zn	t/h	19.67	0.00	0.07	0.00	0.00	1.90	0.00	21.63	2.44	0.00	0.00	0.00	19.19	21.64
Fe	t/h	4.37	0.00	0.28	0.01	0.00	0.00	0.00	4.66	4.66	0.00	0.00	0.00	0.00	4.66
Al	t/h	12.02	0.00	0.56	0.00	0.00	0.00	0.00	12.58	12.58	0.00	0.00	0.00	0.00	12.58
Ca	t/h	8.74	0.00	10.14	0.00	0.00	0.00	0.00	18.88	18.87	0.01	0.00	0.00	0.00	18.88
Cu	t/h	0.12	0.00	0.00	0.00	0.00	0.00	0.00	0.12	0.05	0.00	0.07	0.00	0.00	0.12
Ni	t/h	0.03	0.00	0.00	0.00	0.00	0.00	0.00	0.03	0.01	0.00	0.00	0.02	0.00	0.03
Si	t/h	56.81	0.00	3.84	0.00	0.00	0.00	0.00	60.65	60.65	0.00	0.00	0.00	0.00	60.65
Mn	t/h	0.70	0.00	0.01	0.00	0.00	0.00	0.00	0.71	0.71	0.00	0.00	0.00	0.00	0.71
Mg	t/h	1.33	0.00	0.06	0.00	0.00	0.00	0.00	1.39	1.39	0.00	0.00	0.00	0.00	1.39
Acid	t/h	0.00	0.00	0.00	36.54	0.00	0.00	0.00	36.54	1.57	0.02	0.00	0.00	0.00	1.59
Annual production	t/y	**1 814 562**	**0**	**289 604**	**294 186**	**922 040**	**14 990**	**256**		**3 104 627**	**78 894**	**573**	**123**	**151 420**	

Zinc dross

Figure 37 and Table 30 show the details for the major streams in the mass balance for the zinc dross scenario which allowed for maximum zinc production from this oxide source.

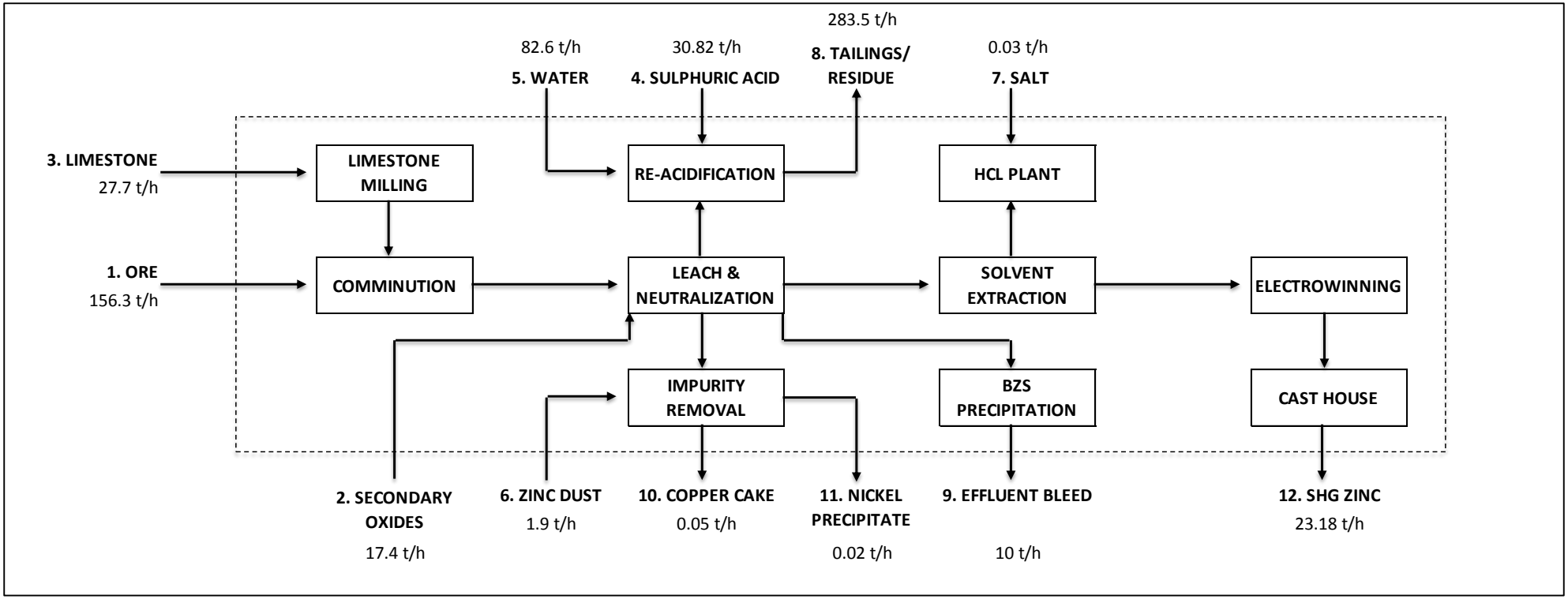

Figure 37. Flow sheet for the zinc dross blend scenario which allowed for the greatest zinc production.

Table 30. Stream table for the zinc dross scenario, which resulted in maximum zinc production from this source.

		INPUT								OUTPUT					
Stream number		**1**	**2**	**3**	**4**	**5**	**6**	**7**		**8**	**9**	**10**	**11**	**12**	
Stream ID		**Ore**	**Secondary oxide**	**Limestone**	**Sulphuric acid**	**Water**	**Zinc dust**	**Salt**	**TOTAL**	**Residue**	**Effluent bleed**	**Copper cake**	**Nickel precipitate**	**SHG Zinc**	**TOTAL**
Total mass flow	t/h	156.33	17.37	27.72	30.82	82.62	1.90	0.03	316.79	283.49	10.00	0.05	0.02	23.18	316.74
Solid throughput	t/h	148.51	16.50	26.40	0.00	0.00	1.90	0.03	193.35	170.09	0.00	0.051	0.02	23.18	193.35
Liquid throughput	t/h	7.82	0.83	1.32	30.82	82.62	0.00	0.00	123.40	113.40	10.00	0.00	0.00	0.00	123.40
Solids content	%	95.00%	95.00%	95.00%	0.00%	0.00%	100.00%	100.00%	61.03%	60.00%	0.00%	100.00%	100.00%	100.00%	61.04%
Solids composition															
Zn	%	9.00%	60.00%	0.20%	0.00%	0.00%	100.00%	0.00%	-	1.15%	0.00%	0.00%	0.00%	100.00%	-
Fe	%	2.00%	2.50%	0.80%	0.00%	0.00%	0.00%	0.00%	-	2.12%	0.00%	0.00%	0.00%	0.00%	-
Al	%	5.50%	6.60%	1.60%	0.00%	0.00%	0.00%	0.00%	-	5.67%	0.00%	0.00%	0.00%	0.00%	-
Ca	%	4.00%	1.00%	29.00%	0.00%	0.00%	0.00%	0.00%	-	8.09%	0.00%	0.00%	0.00%	0.00%	-
Cu	%	0.05%	0.10%	0.00%	0.00%	0.00%	0.00%	0.00%	-	0.03%	0.00%	100.00%	0.00%	0.00%	-
Ni	%	0.01%	0.15%	0.00%	0.00%	0.00%	0.00%	0.00%	-	0.01%	0.00%	0.00%	100.00%	0.00%	-
Si	%	26.00%	0.90%	10.98%	0.00%	0.00%	0.00%	0.00%	-	24.49%	0.00%	0.00%	0.00%	0.00%	-
Mn	%	0.32%	0.10%	0.04%	0.00%	0.00%	0.00%	0.00%	-	0.29%	0.00%	0.00%	0.00%	0.00%	-
Mg	%	0.61%	0.17%	0.17%	0.00%	0.00%	0.00%	0.00%	-	0.57%	0.00%	0.00%	0.00%	0.00%	-
Acid	%	0.00%	0.00%	0.00%	0.00%	0.00%	0.00%	0.00%	-	0.00%	0.00%	0.00%	0.00%	0.00%	-
Liquid composition															
Zn	g/l	0.00	0.00	0.00	0.00	0.00	0.00	0.00	-	0.70	0.03	0.00	0.00	0.00	-
Fe	g/l	0.00	0.00	0.00	0.25	0.00	0.00	0.00	-	0.01	0.0005	0.00	0.00	0.00	-
Al	g/l	0.00	0.00	0.00	0.00	0.00	0.00	0.00	-	0.30	0.06	0.00	0.00	0.00	-
Ca	g/l	0.00	0.00	0.00	0.00	0.00	0.00	0.00	-	0.00	0.6	0.00	0.00	0.00	-
Cu	g/l	0.00	0.00	0.00	0.05	0.00	0.00	0.00	-	0.00	0.0005	0.00	0.00	0.00	-
Ni	g/l	0.00	0.00	0.00	0.00	0.00	0.00	0.00	-	0.00	0.01	0.00	0.00	0.00	-
Si	g/l	0.00	0.00	0.00	0.00	0.00	0.00	0.00	-	0.04	0.01	0.00	0.00	0.00	-
Mn	g/l	0.00	0.00	0.00	0.00	0.00	0.00	0.00	-	0.00	0.20	0.00	0.00	0.00	-
Mg	g/l	0.00	0.00	0.00	0.00	0.00	0.00	0.00	-	0.00	0.20	0.00	0.00	0.00	-
Acid	g/l	0.00	0.00	0.00	98.00%	0.00	0.00	0.00	-	10.00	2.00	0.00	0.00	0.00	-
Total elemental flow															
Zn	t/h	13.37	9.90	0.05	0.00	0.00	1.90	0.00	25.22	2.04	0.00	0.00	0.00	23.18	25.22
Fe	t/h	2.97	0.41	0.21	0.01	0.00	0.00	0.00	3.60	3.60	0.00	0.00	0.00	0.00	3.60
Al	t/h	8.17	1.09	0.42	0.00	0.00	0.00	0.00	9.68	9.68	0.00	0.00	0.00	0.00	9.68
Ca	t/h	5.94	0.17	7.66	0.00	0.00	0.00	0.00	13.76	13.76	0.01	0.00	0.00	0.00	13.76
Cu	t/h	0.08	0.02	0.00	0.00	0.00	0.00	0.00	0.10	0.05	0.00	0.05	0.00	0.00	0.10
Ni	t/h	0.02	0.02	0.00	0.00	0.00	0.00	0.00	0.04	0.02	0.00	0.00	0.02	0.00	0.04
Si	t/h	38.61	0.15	2.90	0.00	0.00	0.00	0.00	41.66	41.66	0.00	0.00	0.00	0.00	41.66
Mn	t/h	0.48	0.02	0.01	0.00	0.00	0.00	0.00	0.50	0.50	0.00	0.00	0.00	0.00	0.50
Mg	t/h	0.91	0.03	0.04	0.00	0.00	0.00	0.00	0.98	0.98	0.00	0.00	0.00	0.00	0.98
Acid	t/h	0.00	0.00	0.00	30.20	0.00	0.00	0.00	30.20	1.13	0.02	0.00	0.00	0.00	1.15
Annual production	t/y	**1 233 350**	**137 039**	**218 714**	**243 124**	**651 797**	**14 990**	**256**		**2 236 546**	**78 894**	**406**	**189**	**182 891**	

EAF dust

The stream table and flow sheet for the EAF dust mass balance scenario with the highest zinc production are shown in Table 31and Figure 38 respectively.

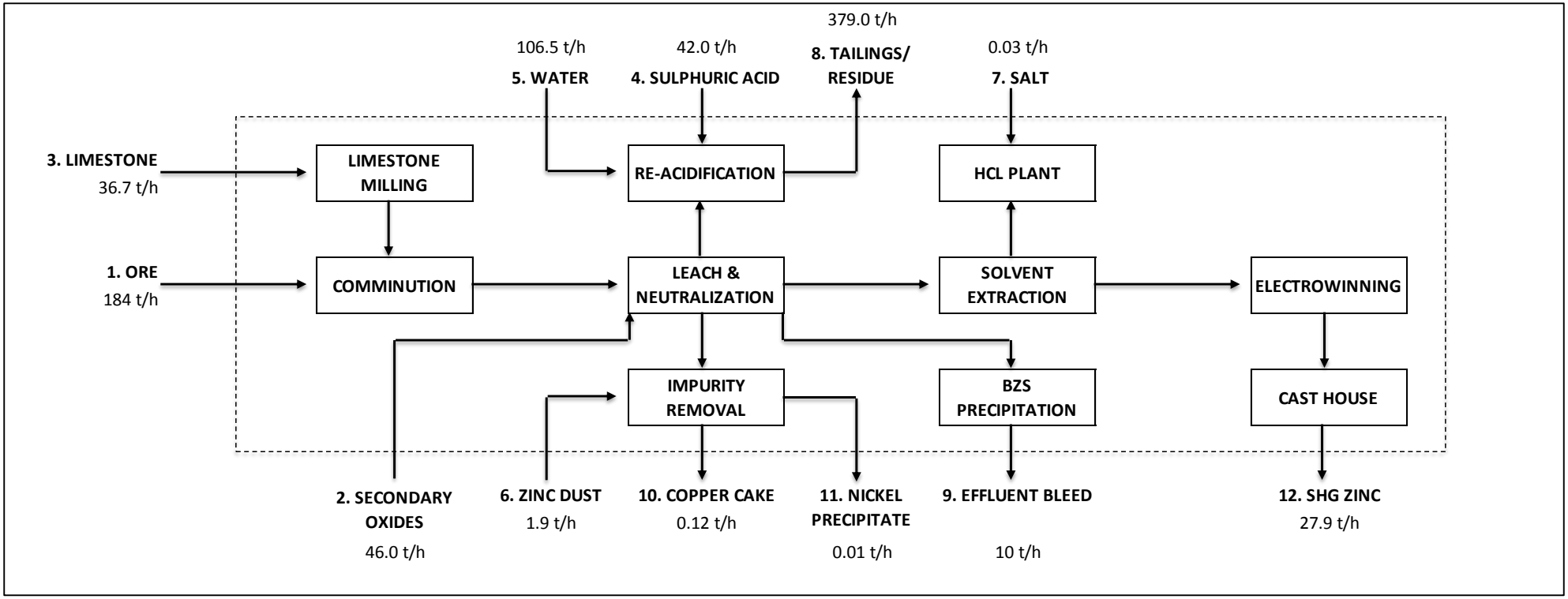

Figure 38. Flow sheet for the EAFD blend which resulted in the maximum zinc production.

Table 31. Stream table for the EAFD feed ratio, which resulted in the most zinc production from this source.

		INPUT								OUTPUT					
Stream number		**1**	**2**	**3**	**4**	**5**	**6**	**7**		**8**	**9**	**10**	**11**	**12**	
Stream ID		**Ore**	**Secondary oxide**	**Limestone**	**Sulphuric acid**	**Water**	**Zinc dust**	**Salt**	**TOTAL**	**Residue**	**Effluent bleed**	**Copper cake**	**Nickel precipitate**	**SHG Zinc**	**TOTAL**
Total mass flow	t/h	184.00	46.00	36.71	41.95	106.49	1.90	0.03	417.09	378.95	10.00	0.12	0.01	27.89	416.97
Solid throughput	t/h	174.80	43.70	34.96	0.00	0.00	1.90	0.03	255.39	227.37	0.00	0.125	0.01	27.89	255.39
Liquid throughput	t/h	9.20	2.19	1.75	41.95	106.49	0.00	0.00	161.58	151.58	10.00	0.00	0.00	0.00	161.58
Solids content	%	95.00%	95.00%	95.00%	0.00%	0.00%	100.00%	100.00%	61.23%	60.00%	0.00%	100.00%	100.00%	100.00%	61.25%
Solids composition															
Zn	%	9.00%	30.00%	0.20%	0.00%	0.00%	100.00%	0.00%	-	1.24%	0.00%	0.00%	0.00%	100.00%	-
Fe	%	2.00%	13.00%	0.80%	0.00%	0.00%	0.00%	0.00%	-	4.16%	0.00%	0.00%	0.00%	0.00%	-
Al	%	5.50%	1.50%	1.60%	0.00%	0.00%	0.00%	0.00%	-	4.74%	0.00%	0.00%	0.00%	0.00%	-
Ca	%	4.00%	2.50%	29.00%	0.00%	0.00%	0.00%	0.00%	-	8.01%	0.00%	0.00%	0.00%	0.00%	-
Cu	%	0.05%	0.20%	0.00%	0.00%	0.00%	0.00%	0.00%	-	0.03%	0.00%	100.00%	0.00%	0.00%	-
Ni	%	0.01%	0.02%	0.00%	0.00%	0.00%	0.00%	0.00%	-	0.01%	0.00%	0.00%	100.00%	0.00%	-
Si	%	26.00%	1.80%	10.98%	0.00%	0.00%	0.00%	0.00%	-	22.02%	0.00%	0.00%	0.00%	0.00%	-
Mn	%	0.32%	1.00%	0.04%	0.00%	0.00%	0.00%	0.00%	-	0.30%	0.00%	0.00%	0.00%	0.00%	-
Mg	%	0.61%	1.25%	0.17%	0.00%	0.00%	0.00%	0.00%	-	0.59%	0.00%	0.00%	0.00%	0.00%	-
Acid	%	0.00%	0.00%	0.00%	0.00%	0.00%	0.00%	0.00%	-	0.00%	0.00%	0.00%	0.00%	0.00%	-
Liquid composition															
Zn	g/l	0.00	0.00	0.00	0.00	0.00	0.00	0.00	-	0.70	0.03	0.00	0.00	0.00	-
Fe	g/l	0.00	0.00	0.00	0.25	0.00	0.00	0.00	-	0.01	0.0005	0.00	0.00	0.00	-
Al	g/l	0.00	0.00	0.00	0.00	0.00	0.00	0.00	-	0.30	0.06	0.00	0.00	0.00	-
Ca	g/l	0.00	0.00	0.00	0.00	0.00	0.00	0.00	-	0.00	0.6	0.00	0.00	0.00	-
Cu	g/l	0.00	0.00	0.00	0.05	0.00	0.00	0.00	-	0.00	0.0005	0.00	0.00	0.00	-
Ni	g/l	0.00	0.00	0.00	0.00	0.00	0.00	0.00	-	0.00	0.01	0.00	0.00	0.00	-
Si	g/l	0.00	0.00	0.00	0.00	0.00	0.00	0.00	-	0.04	0.01	0.00	0.00	0.00	-
Mn	g/l	0.00	0.00	0.00	0.00	0.00	0.00	0.00	-	2.12	0.20	0.00	0.00	0.00	-
Mg	g/l	0.00	0.00	0.00	0.00	0.00	0.00	0.00	-	2.17	0.20	0.00	0.00	0.00	-
Acid	g/l	0.00	0.00	0.00	98.00%	0.00	0.00	0.00	-	10.00	2.00	0.00	0.00	0.00	-
Total elemental flow															
Zn	t/h	15.73	13.11	0.07	0.00	0.00	1.90	0.00	30.81	2.93	0.00	0.00	0.00	27.89	30.81
Fe	t/h	3.50	5.68	0.28	0.01	0.00	0.00	0.00	9.47	9.47	0.00	0.00	0.00	0.00	9.47
Al	t/h	9.61	0.66	0.56	0.00	0.00	0.00	0.00	10.83	10.83	0.00	0.00	0.00	0.00	10.83
Ca	t/h	6.99	1.09	10.14	0.00	0.00	0.00	0.00	18.22	18.22	0.01	0.00	0.00	0.00	18.22
Cu	t/h	0.09	0.09	0.00	0.00	0.00	0.00	0.00	0.18	0.06	0.00	0.12	0.00	0.00	0.18
Ni	t/h	0.02	0.01	0.00	0.00	0.00	0.00	0.00	0.03	0.02	0.00	0.00	0.01	0.00	0.03
Si	t/h	45.45	0.79	3.84	0.00	0.00	0.00	0.00	50.07	50.07	0.00	0.00	0.00	0.00	50.07
Mn	t/h	0.56	0.44	0.01	0.00	0.00	0.00	0.00	1.01	1.01	0.00	0.00	0.00	0.00	1.01
Mg	t/h	1.07	0.55	0.06	0.00	0.00	0.00	0.00	1.67	1.67	0.00	0.00	0.00	0.00	1.67
Acid	t/h	0.00	0.00	0.00	41.11	0.00	0.00	0.00	41.11	1.52	0.02	0.00	0.00	0.00	1.54
Annual production	t/y	**1 451 650**	**362 912**	**289 604**	**330 976**	**840 168**	**14 990**	**256**		**2 989 654**	**78 894**	**983**	**113**	**220 005**	

Zinc fume oxide

The simplified flow sheet and stream table for the mass balance on the 50% zinc fume blend are shown in Figure 39 and Table 32 respectively. This blend resulted in the maximum theoretical zinc recovery from the zinc fume oxide, and the maximum zinc production overall for all the oxide samples.

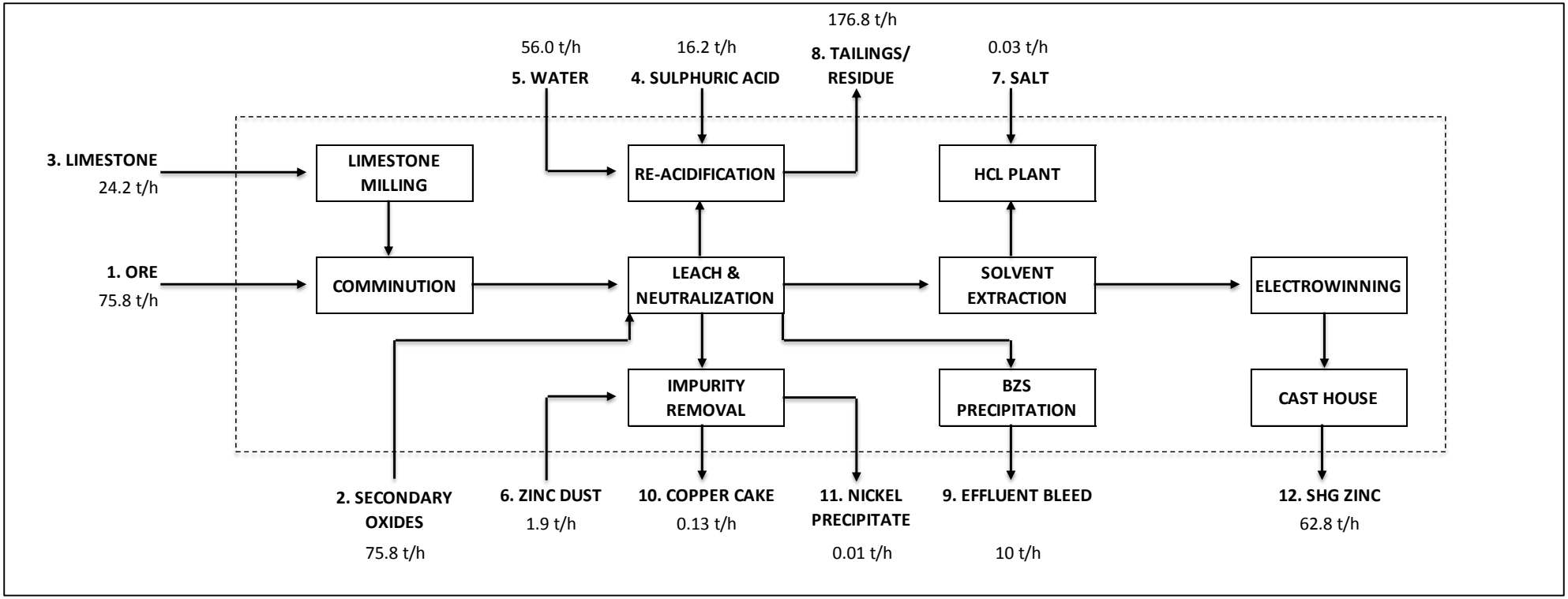

Figure 39. Flow sheet showing the major flows for the zinc fume blend which allowed for maximal zinc production.

Table 32. Stream table for the maximum zinc production scenario from the zinc fume oxide source.

		INPUT								OUTPUT					
Stream number		**1**	**2**	**3**	**4**	**5**	**6**	**7**		**8**	**9**	**10**	**11**	**12**	
Stream ID		**Ore**	**Secondary oxide**	**Limestone**	**Sulphuric acid**	**Water**	**Zinc dust**	**Salt**	**TOTAL**	**Residue**	**Effluent bleed**	**Copper cake**	**Nickel precipitate**	**SHG Zinc**	**TOTAL**
Total mass flow	t/h	75.80	75.80	24.20	16.22	55.95	1.90	0.03	249.90	176.78	10.00	0.13	0.01	62.80	249.71
Solid throughput	t/h	72.01	72.01	23.04	0.00	0.00	1.90	0.03	169.00	106.07	0.00	0.125	0.01	62.80	169.00
Liquid throughput	t/h	3.79	3.60	1.15	16.22	55.95	0.00	0.00	80.71	70.71	10.00	0.00	0.00	0.00	80.71
Solids content	%	95.00%	95.00%	95.00%	0.00%	0.00%	100.00%	100.00%	67.63%	60.00%	0.00%	100.00%	100.00%	100.00%	67.68%
Solids composition															
Zn	%	9.00%	78.00%	0.20%	0.00%	0.00%	100.00%	0.00%	-	1.65%	0.00%	0.00%	0.00%	100.00%	-
Fe	%	2.00%	0.70%	0.80%	0.00%	0.00%	0.00%	0.00%	-	2.01%	0.00%	0.00%	0.00%	0.00%	-
Al	%	5.50%	0.10%	1.60%	0.00%	0.00%	0.00%	0.00%	-	4.13%	0.00%	0.00%	0.00%	0.00%	-
Ca	%	4.00%	0.15%	29.00%	0.00%	0.00%	0.00%	0.00%	-	9.11%	0.00%	0.00%	0.00%	0.00%	-
Cu	%	0.05%	0.15%	0.00%	0.00%	0.00%	0.00%	0.00%	-	0.02%	0.00%	100.00%	0.00%	0.00%	-
Ni	%	0.01%	0.00%	0.00%	0.00%	0.00%	0.00%	0.00%	-	0.00%	0.00%	0.00%	100.00%	0.00%	-
Si	%	26.00%	1.70%	10.98%	0.00%	0.00%	0.00%	0.00%	-	21.19%	0.00%	0.00%	0.00%	0.00%	-
Mn	%	0.32%	0.06%	0.04%	0.00%	0.00%	0.00%	0.00%	-	0.26%	0.00%	0.00%	0.00%	0.00%	-
Mg	%	0.61%	0.01%	0.17%	0.00%	0.00%	0.00%	0.00%	-	0.46%	0.00%	0.00%	0.00%	0.00%	-
Acid	%	0.00%	0.00%	0.00%	0.00%	0.00%	0.00%	0.00%	-	0.00%	0.00%	0.00%	0.00%	0.00%	-
Liquid composition															
Zn	g/l	0.00	0.00	0.00	0.00	0.00	0.00	0.00	-	0.70	0.03	0.00	0.00	0.00	-
Fe	g/l	0.00	0.00	0.00	0.25	0.00	0.00	0.00	-	0.01	0.0005	0.00	0.00	0.00	-
Al	g/l	0.00	0.00	0.00	0.00	0.00	0.00	0.00	-	0.30	0.06	0.00	0.00	0.00	-
Ca	g/l	0.00	0.00	0.00	0.00	0.00	0.00	0.00	-	0.00	0.6	0.00	0.00	0.00	-
Cu	g/l	0.00	0.00	0.00	0.05	0.00	0.00	0.00	-	0.00	0.0005	0.00	0.00	0.00	-
Ni	g/l	0.00	0.00	0.00	0.00	0.00	0.00	0.00	-	0.00	0.01	0.00	0.00	0.00	-
Si	g/l	0.00	0.00	0.00	0.00	0.00	0.00	0.00	-	0.04	0.01	0.00	0.00	0.00	-
Mn	g/l	0.00	0.00	0.00	0.00	0.00	0.00	0.00	-	0.00	0.20	0.00	0.00	0.00	-
Mg	g/l	0.00	0.00	0.00	0.00	0.00	0.00	0.00	-	0.00	0.20	0.00	0.00	0.00	-
Acid	g/l	0.00	0.00	0.00	98.00%	0.00	0.00	0.00	-	10.00	2.00	0.00	0.00	0.00	-
Total elemental flow															
Zn	t/h	6.48	56.17	0.05	0.00	0.00	1.90	0.00	64.59	1.80	0.00	0.00	0.00	62.80	64.60
Fe	t/h	1.44	0.50	0.18	0.00	0.00	0.00	0.00	2.13	2.13	0.00	0.00	0.00	0.00	2.13
Al	t/h	3.96	0.07	0.37	0.00	0.00	0.00	0.00	4.40	4.40	0.00	0.00	0.00	0.00	4.40
Ca	t/h	2.88	0.11	6.68	0.00	0.00	0.00	0.00	9.67	9.66	0.01	0.00	0.00	0.00	9.67
Cu	t/h	0.04	0.11	0.00	0.00	0.00	0.00	0.00	0.15	0.02	0.00	0.13	0.00	0.00	0.15
Ni	t/h	0.01	0.00	0.00	0.00	0.00	0.00	0.00	0.01	0.00	0.00	0.00	0.01	0.00	0.01
Si	t/h	18.72	1.22	2.53	0.00	0.00	0.00	0.00	22.48	22.48	0.00	0.00	0.00	0.00	22.48
Mn	t/h	0.23	0.04	0.01	0.00	0.00	0.00	0.00	0.28	0.28	0.00	0.00	0.00	0.00	0.28
Mg	t/h	0.44	0.01	0.04	0.00	0.00	0.00	0.00	0.49	0.48	0.00	0.00	0.00	0.00	0.49
Acid	t/h	0.00	0.00	0.00	15.90	0.00	0.00	0.00	15.90	0.71	0.02	0.00	0.00	0.00	0.73
Annual production	t/y	**598 017**	**598 017**	**190 887**	**127 996**	**441 386**	**14 990**	**256**		**1 394 713**	**78 894**	**986**	**41**	**495 419**	

Appendix F: Sample calculations

Mass balance over the experimental system

Once the entire experiment has been completed, the experimental system can be represented as follows:

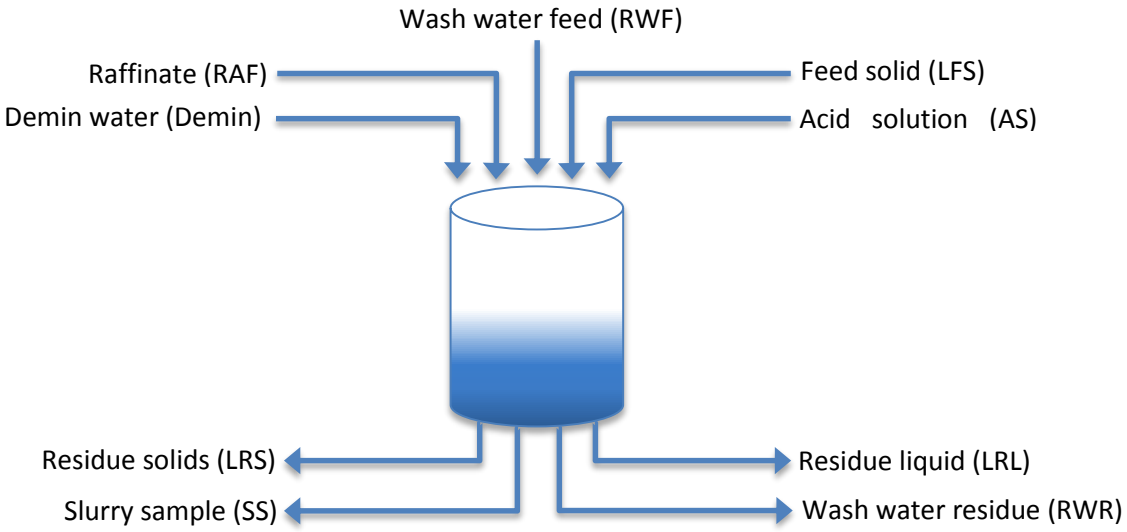

Thus, performing the mass balance on one specific element, M, at the end of the experiment would be done as follows:

$$M_{in} = M_{out}$$
$$M_{RAF} + M_{Demin} + M_{RWF} + M_{LFS} + M_{Acid\ solution} = M_{LRS} + M_{RWR} + M_{LRL} + M_{SS}$$

At any other time during the course of the experiment, the system would be represented like this:

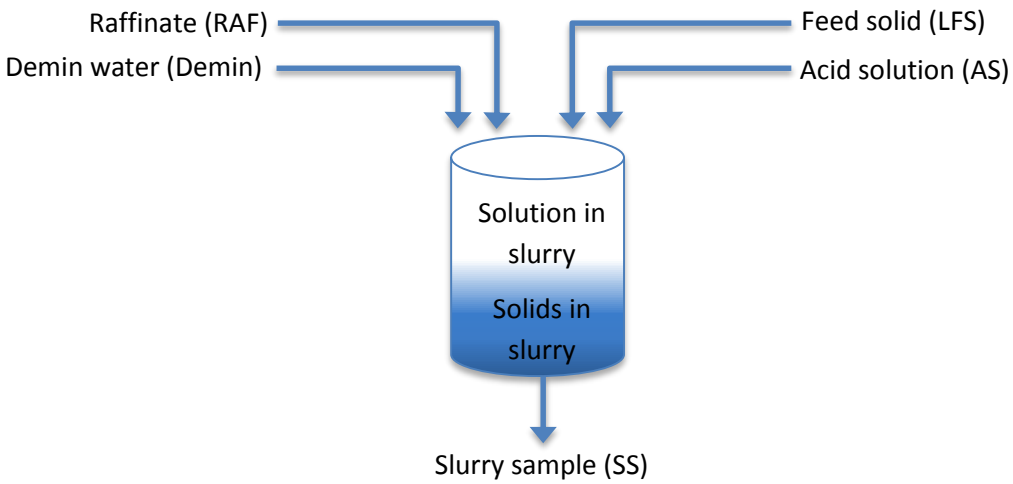

Thus, the mass balance for the system at time, t, would be as follows:

$$M_{in} = M_{out} - M_{generation} + M_{accumulation} + M_{consumption}$$

Since there is no generation or consumption in this system, the formula can be simplified as below:

$$M_{RAF} + M_{Demin} + M_{LFS} + M_{Acid\ solution} = M_{Slurry\ solids} + M_{Slurry\ solution} + M_{SS}$$

At any given time, it is assumed that the concentration of a particular element in the solution portion of the slurry sample is equal to the concentration of this element in the solution portion of the slurry remaining in the beaker.

Recalculated head grade

It is often very difficult to obtain a perfectly homogenous solid sample for the purpose of feed sample analysis. Thus, it is assumed that the solid sample used for feed sample analysis provides an approximation of the composition of the feed solids.

To provide a more accurate determination of the feed solids composition, all the residue solids are dissolved in an acid digestion process, and full elemental analysis is performed on this solution. These results, together with the results of the residue liquid and the wash water residue compositions are used to back-calculate the feed head grade, using mass balance principles. This is done by using the following calculation:

For a particular element, M:

$$M_{LFS,recalculated}(\%) = \frac{M_{LRL}(g) + M_{LRS}(g) + M_{RWR}(g) - M_{RAF}(g) - M_{RWF}(g)}{LFS_{Dry}(g)} \cdot 100$$

$$= \frac{(LRL \cdot [M]_{LRL} + V_{SS} \cdot [M]_{SS} + LRS \cdot [M]_{LRS} + RWR \cdot [M]_{RWR} - RAF \cdot [M]_{RAF} - RWF \cdot [M]_{RWF}) \cdot 100}{LFS_{Dry}}$$

Here, the residue liquids can be calculated to be the sum of the starting volume (demin water) and the raffinate added, if no samples were to be removed from the system.

For example the recalculated head grade of zinc for experiment RM5, the zinc dross sample run at 50 ˚C and a pH of 1.8-1.85, 20% solids, 600 rpm and with normal particle size distribution:

$$Zn_{LFS,recalculated} = \frac{(1.115 \cdot 71.5 + (40.11) + 16.6 \cdot 0.0393 + 1.45 \cdot 0.84 - 1.2 \cdot 33.6 - 1.5 \cdot 0)}{136/100}$$

$$Zn_{LFS,recalculated} = 59.84\ \%$$

Percentage dissolution

The amount of dissolution of a particular element that has taken place during leaching can be determined using the following formula:

$$Dissolution\ (\%) = \frac{M_{LRL} - M_{RAF} + M_{Slurry\ samples}}{M_{LFS}} \cdot 100$$

Once again, RM5 (50 ˚C, pH 1.8-1.85, 20% solids, 600 rpm agitation and normal PSD) is used to illustrate this calculation. After 25 minutes of residence time, the analysis on the liquid portion of the

slurry sample indicates that the zinc content in the sample is 64.5 g/l. Thus, the percentage zinc dissolution at this point is:

$$Zinc\ dissolution\ (\%) = \frac{1.57 \cdot 64.5 - 1.2 \cdot 33.6 + (0.065 \cdot 64.5 + 0.065 \cdot 52.8)}{136 \cdot 0.5984} \cdot 100 = 84.25\%$$

Recovery

The act of washing the residue solids with a pH 2 wash solution after the experiment has been completed is intended to mimic the role of the belt filters in Skorpion's process. These filters are washed with a low pH solution to flush any soluble zinc that may have precipitated in the residue out of the residue and into solution.

This maximises the recovery of the zinc. However, this does mean that the zinc dissolution and zinc recovery are not the same concept. Instead, the recovery refers to a combination of the dissolved zinc and the soluble zinc that is flushed out with the residue wash solution. Thus, the recovery is calculated in the following way:

$$Zinc\ recovery\ (\%) = \frac{Zn_{LFS} - Zn_{LRS}}{Zn_{LFS}} \cdot 100 = \frac{Zn_{LRL} + Zn_{RWR} - Zn_{RAF} - Zn_{RWF}}{Zn_{LFS}} \cdot 100$$

Using RM5 as an example (zinc dross sample run at 50 ˚C and pH of 1.8-1.85, 20% solids, 600 rpm agitation and normal PSD):

$$Zinc\ recovery\ (\%) = \frac{136 \cdot 0.6110 - 16.6 \cdot 0.0393}{136 \cdot 0.6110} \cdot 100 = 99.2\%$$

Alternatively, using the solution analyses:

$$Zinc\ recovery\ (\%) = \frac{1.7 \cdot 71.5 + 1.45 \cdot 0.84 - 1.2 \cdot 33.6 - 1.5 \cdot 0}{136 \cdot 0.6110} \cdot 100 = 99.2\%$$

Total acid consumption

Total acid consumption refers to the total mass of acid consumed per unit mass of feed material.

$$Total\ acid\ consumption = \frac{[Acid]_{RAF} \cdot V_{RAF} + [Acid]_{AS} \cdot V_{AS} - [Acid]_{LRL} \cdot V_{LRL} - [Acid]_{SS} \cdot V_{SS}}{M_{LFS}}$$

Once again, the RM5 sample run at 50°C and a pH of 1.8-1.85 with 20% solids in the feed slurry at 25 minutes residence time, the following total acid consumption calculation can be performed:

$$Total\ acid\ consumption = \frac{71.6 \cdot 1.2 + 500 \cdot 0.1 - 3.08 \cdot 1.57 - (2.43 \cdot 0.065 + 3.08 \cdot 0.065)}{136/1000}$$

$$Total\ acid\ consumption = 961.22\ kg/t\ ore$$

Gangue acid consumption

Gangue acid consumption (GAC) is the quantification of the amount of acid used to leach impurity elements, rather than the element of interest. It is displayed as total tons of gangue acid consumed in unit mass, but may also sometimes be expressed as total acid consumed per unit mass of feed material.

$$Gangue\ acid\ consumption = \frac{Total\ acid\ consumption - M_{Zn,leached} \cdot \frac{Mw_{Acid}}{Mw_{Zn}}}{M_{LFS}}$$

$$Gangue\ acid\ consumption = \frac{961.22 \cdot 136/1000 - 68.57 \cdot 98/65.4}{136/1000}$$

$$Gangue\ acid\ consumption = 205.7\ kg/t$$

Overall acid consumption

The overall acid consumption considers the gangue acid consumption, which is the only portion of the acid consumed, which is not regenerated in the solvent extraction circuit (during the zinc extraction process). Then, the acid losses experienced from the belt filters (acid contained in the moisture leaving with the residue) and the effluent treatment plant are added. This is then calculated as overall acid loss per t of zinc in the feed, as per the formula below:

$$Overall\ AC = \frac{(GAC + Free\ acid\ losses + Soluble\ Zn\ losses + Re - acid\ losses) \cdot M_{LFS}}{M_{Zn,LFS}}$$

The re-acidification and soluble zinc acid losses are based on assumptions made for the Skorpion process, from the Skorpion acid consumption model. Thus these losses are 9.4 and 8.6 kg/t ore respectively. Free acid losses are based on the free acid in the wash solution after washing has been completed.

For the RM5 example used so far, the calculation is shown below.

$$Overall\ acid\ consumption = \frac{(205.7 + 14.8 + 9.4 + 8.6)/1000 \cdot 136}{59.84/100 \cdot 136}$$

$$Overall\ acid\ consumption = 0.4\ t/t\ Zinc$$

Appendix G: Material safety data sheets

Sulphuric acid

Common name: Sulphuric acid

Synonyms: Oil of vitriol, sulphuric acid, hydrogen sulphate, vitriol brown oil, battery acid

Hazards identification:
Corrosive and harmful

First aid:
Inhalation: Corrosive and irritating, causing severe irritation of the respiratory tract leading to coughing, choking or shortness of breath. May also cause sore throat and delayed lung oedema, as well as burns to the respiratory tract. Remove to fresh air. Give AR, but not by direct mouth-to-mouth if victim inhaled or ingested substance. If breathing is difficult, give oxygen. Contact physician.

Skin Contact: May be absorbed and corrosiveness may cause redness, irritation, burning. Wash with large quantities of water for at least 15 minutes, removing contaminated clothing and cover the affected area with an emollient. Soap may be used for washing in the case of serious skin contact. Contact a physician immediately.

Eye contact: Causes severe eye burns and irritation with possible symptoms including redness, tearing, pain and conjunctivitis. May cause irreparable eye damage. Flush with water for 15 minutes, separating eyelids with fingers. Contact physician immediately.

Ingestion: This substance is corrosive and toxic. May cause severe burns and permanent damage to digestive system. Can cause nausea, vomiting, and abdominal pain. Do not induce vomiting, but if the victim is conscious, give 2-4 glasses of milk or water. Seek immediate medical assistance.

Flammability:
This substance is non-flammable, but decomposition when in the presence of fire (thermal decomposition) will cause the release of fumes of oxides of sulphur.

Accidental release:
Use dry earth or vermiculite (or another dry, non-combustible, inert material) to absorb the spill. Sodium carbonate or lime may be used to neutralize the residual acid. Dispose of in waste container. Remove ignition sources and release water spray to reduce vapour.

Storage:
Store away from ignition sources in moderately warm, dry place, with good ventilation, away from strong alkalis, acids, combustibles and oxidising agents. Ensure that there are no ignition sources nearby.

Zinc sulphate heptahydrate

Common name: Zinc sulphate heptahydrate

Synonyms: White vitriol, zinc vitriol, zinc salt heptahydrate

Hazards identification:
Harmful if inhaled or swallowed. Dust can cause irritation to affected areas. This substance is harmful to the environment.

First aid:
Inhalation: Inhalation can cause severe irritation of the respiratory tract. May cause coughing, sore throat, irritation of the mucous membranes, shortness of breath. If exposed, remove to fresh air and provide oxygen if the victim struggles to breath. Seek medical attention if any persistent symptoms.

Skin Contact: Can cause skin irritation after prolonged exposure. Redness, itching and pain may result after prolonged exposure. Wash the affected area with large amounts of water and non-abrasive soap. If symptoms persist, seek medical assistance.

Eye contact: Causes extreme irritation and possible lasting eye damage; symptoms include redness, tearing, pain and conjunctivitis. Flush with water for 15 minutes, separating eyelids with fingers. Contact physician immediately.

Ingestion: Substance is toxic. May cause nausea, vomiting and diarrhoea as well as irritation to the gastrointestinal tract. Do not induce vomiting, but victim should ingest milk, egg whites or water. Seek medical aid immediately.

Flammability:
The substance is not flammable, but thermal decomposition may occur when exposed to large amounts of heap. During thermal decomposition, toxic vapours (oxides of sulphur) may be released.

Accidental release:
Sweep the spillage and collect in a suitable container for disposal. Do not allow the substance to enter drains, sewers or waterways, as it is extremely toxic to the environment.

Storage:
Store in a cool, dry, well-ventilated area. Ideally, store material in a sealed plastic container.

EAFD dust

Common name: Electric arc furnace dust

Synonyms: EAFD, EAF bag house dust, EAF drop out box material

Hazards identification:
Toxic and harmful
First aid:
Inhalation: Toxic and irritating. May cause metal fume fever, irritation of the mucous membranes and respiratory system, weakness, headache, coughing, pneumonia, bronchitis, sinusitis, laryngitis, chest pain, cardiopulmonary arrest. Exposure to certain of the components contained in this product (lead, manganese and nickel) may lead to metabolic, gastrointestinal, reproductive, blood, kidney and central nervous system disorders. If exposed, remove to fresh air and seek medical attention.

Skin contact: May cause skin irritation, dermatitis and lesions. Wash thoroughly with warm water and non-abrasive soap.

Eye contact: May cause eye irritation, which could lead to conjunctivitis. Flush for 15 minutes with large amounts of lukewarm water. If irritation does not subside, seek medical attention.

Ingestion: Although unlikely to occur, if this does happen, watch for signs of intestinal blockage over the course of several days. In the event of a blockage, seek medical attention.

Flammability:
This product is not flammable and presents no fire or explosion risk.

Accidental release:
Sweep dust together and place in containers used for hazardous substance disposal. Do not allow the product to be discharged into sinks, drains, sewers, the air or the environment. This material must be disposed of at hazardous waste disposal facility.

Storage:
The material is stable, but should be stored away from calcium hypochlorite, performed acid, ethylene oxide, bromine pentafluoride and finely divided aluminium. Store in a dry area away from acids.

Zinc dross

Common name: Zinc dross

Synonyms: Zinc fine ash, hot-dip galvanizing zinc ash

Hazards identification:
Harmful if inhaled or swallowed

First aid:
Inhalation: May cause metal fume fever; headaches, coughing, fever, weakness, chest pain; can also cause shortness of breath, irritation of the mucous membranes and respiratory tract. Remove victim to fresh air and seek medical help if symptoms do not subside shortly.

Skin contact: May cause skin irritation. Wash thoroughly with warm water and non-abrasive soap.

Eye contact: May cause eye irritation, after excessive exposure. Flush for 15 minutes with large amounts of lukewarm water. If irritation does not subside, seek medical attention.

Ingestion: This is unlikely to occur, but is a health hazard if ingested. May cause abdominal pain, nausea, diarrhoea and gastrointestinal damage. Allow patient to ingest 2-4 cups of milk or water (if conscious) and seek immediate medical attention. Do not induce vomiting.

Flammability:
This product is flammable and may release toxic fumes or gas when burning. Smother the fire using dry sand or earth, but not water.

Accidental release:
Sweep dust together and place in containers for disposal. Do not allow the product to be discharged into sinks, drains, sewers, the air or the environment. This material must be disposed of at hazardous waste disposal facility.

Storage:
Store the substance in a cool, dry, well-ventilated area. Keep away from oxidizing agents, strong acids and alkalis, halogenated agents and alkali hydroxides.

Natural state zinc oxide powder

Common name: Zinc oxide

Synonyms: Calamine, zincite, zinc white

Hazards identification:
Harmful if inhaled or swallowed

First aid:
Inhalation: May cause shortness of breath, irritation of the mucous membranes and respiratory tract, with nasopharyngitis and laryngitis. Remove victim to fresh air and seek medical help if symptoms do not subside shortly.

Skin contact: May cause skin irritation. Remove contaminated clothing and brush the material off the affected skin. Wash thoroughly with warm water and non-abrasive soap.

Eye contact: May cause eye irritation. Flush for 15 minutes with large amounts of lukewarm water. If irritation does not subside, seek medical attention.

Ingestion: Moderately toxic if ingested. May cause abdominal pain, nausea and diarrhoea. Allow patient to ingest 1-2 cups of milk or water (if conscious) and seek immediate medical attention. Do not induce vomiting.

Flammability:
This product is non-flammable and non-combustible. However, thermal decomposition of this product during a fire may cause the release of toxic ZnO fumes.

Accidental release:
Sweep dust together and place in containers for disposal. Do not allow the product to be discharged into sinks, drains, sewers, the air or the environment.

Storage:
Store the substance in a cool, dry, well-ventilated area. Keep away from chlorinated rubber, linseed oil, magnesium, hydrogen fluoride, aluminium and hexachloroethane, zinc chloride, phosphoric acid and strong oxidizing agents.